3D BIOPRINTED HYDROGEL SCAFFOLDS LADEN WITH SCHWANN CELLS FOR USE AS NERVE REPAIR CONDUITS

A Thesis Submitted to the College of

Graduate Studies and Research

In Partial Fulfillment of the Requirements

For the Degree of Doctor of Philosophy

In the Division of Biomedical Engineering

University of Saskatchewan

Saskatoon

By

AJAY RAJARAM

PERMISSION TO USE

In presenting this thesis in partial fulfilment of the requirements for a Postgraduate degree from the University of Saskatchewan, I agree that the Libraries of this University may make it freely available for inspection. I further agree that permission for copying of this thesis in any manner, in whole or in part, for scholarly purposes may be granted by Prof. Daniel Chen and Prof. David Schreyer who supervised my thesis work or, in their absence, by the Head of the Division of Biomedical Engineering or the Dean of the College of Engineering in which my thesis work was done. It is understood that any copying or publication or use of this thesis or parts thereof for financial gain shall not be allowed without my written permission. It is also understood that due recognition shall be given to me and to the University of Saskatchewan in any scholarly use which may be made of any material in my thesis.

Requests for permission to copy or to make other use of material in this thesis in whole or part should be addressed to:

Head of the Division of Biomedical Engineering

Room 2B60, 57 Campus Drive

University of Saskatchewan

Saskatoon, Saskatchewan S7N 5A9

Canada

ABSTRACT

The goal of nerve tissue engineering is to promote and guide axon growth across a site of nerve injury without misdirection. Bioengineered tissue scaffolds have been shown to be promising for the regeneration of damaged peripheral nerves. Schwann cells play a pivotal role following nerve injury by forming aligned "bands of Büngner" that promote and guide axon regeneration into the distal nerve segment. The incorporation of living Schwann cells into various hydrogels has therefore been urged during the fabrication of tissue engineered nerve scaffolds. The aim of this research is to characterize biomaterials suitable for 3D bioplotting of nerve repair scaffolds. Here a novel technique of scaffold fabrication has been optimized to print alginate-based three-dimensional tissue scaffolds containing hyaluronic acid and living Schwann cells. Alginate/hyaluronic acid scaffolds were successfully fabricated with good printability and cell viability. Addition of the polycation polyethyleneimine (PEI) during the fabrication process stabilized the structure of alginate through the formation of a polyelectrolyte complex and had a significant influence on the degree of swelling, degradation rate, mechanical property, and release kinetics of incorporated protein within the scaffolds. A preliminary *in vivo* study showed the feasibility of implanting 3D printed alginate/hyaluronic acid scaffolds as nerve conduits in Sprague-Dawley (SD) rats with resected sciatic nerves. However alginate/hyaluronic acid scaffolds were found to be unsuitable for axonal regeneration. Further *in vitro* culture of Schwann cells was performed in collagen type-I, fibrin, fibrin/hyaluronic acid, and their combination with alginate. It was found that Schwann cells had more favorable cell morphology in fibrin/hyaluronic acid or collagen without alginate. Schwann cell proliferation and alignment were better in fibrin/hyaluronic acid. Therefore fibrin/hyaluronic acid is more ideal than most other hydrogel formulations for use in the bioprinting of nerve repair tissue engineering

scaffolds, which incorporate cellular elements. As Schwann cells also align along the long axis of the printed fibrin/hyaluronic acid strands, 3D bioprinting of multiple layers of crosslinked fibrin strands can be used to fabricate a nerve conduit mimicking the bands of Büngner.

ACKNOWLEDGMENTS

I would like to thank my supervisors, Dr. Daniel Chen and Dr. David Schreyer, for their exceptional guidance and tremendous support during my doctoral study at the University of Saskatchewan. I also extend my appreciation to my doctoral advisory committee; Dr. Assem Hedayat, Dr. Patrick Krone, Dr. Chris Zhang, and Dr. Fang Xiang Wu, Graduate Chair of Biomedical Engineering.

The financial support from the Saskatchewan Health Research Foundation (SHRF) (through the research grants to Dr. Chen and Dr. Schreyer) and the University of Saskatchewan (through the scholarship to me) is greatly acknowledged.

I appreciate the support from the Bio-Fabrication Lab at the University of Saskatchewan and the Cameco MS Neuroscience Research Center at Saskatoon City Hospital, where research presented in this thesis was performed. Specifically, I wish to thank Dr. Valerie Verge, Tangyne Berry, Shannon Berko, Dr. Ruiling Zhai, Jayne Johnston, Anita Givens, Doug Bitner, and Ning Cao for their valuable advice and technical support. My friends in the Tissue Engineering Research Group – Peng Zhai, Mindan Wang, Dr. Ning Zhu, Jingwen Li, Zohreh Izadifar, Mohammad Izadifar, Md. Aslam Sarker, Fu You, Adeola Olubamiji, Liqun Ning, and Xue Han, have helped enrich my intellect with their thought-provoking discussions. I also thank my friends at the City hospital, Dr. Vaigundaragavendran Jagadeesan, Mylene Tham, Joelle Nadeau, Nikki McLean, Dr. Zhengxin Ying, and Atiq Hassan, who have helped me elucidate concepts in molecular pathobiology of nerve regeneration. I thank Dr. Adam McInnes for his help with experiments involving the incorporation of ECM proteins in alginate. I specially thank Stephanie England for her assistance with research involving fibrin, and for her intriguing research queries.

I appreciate the assistance from all staff at the Lab Animal Service Unit (LASU), University of Saskatchewan and Dr. Melanie van der Loop's help with the treatment of animals used in this study.

I would like to acknowledge my friends, Dr. Amzad Hossain, Arun Thomas, Sushaal Sherman, Scott and Theresa Ziegler, Mark Haviland, and Jonathan and Rachelle Hutchinson.

I am grateful to my parents and my sister for their constant support, love, motivation, and for making my research endeavor possible. My brothers, Ashok, Manoj Dhanapal, Raghu Dhanapal, Kasi Rajan, and Rajesh Kannan have always been constant sources of support. I also extend my thanks to the rest of my family.

TABLE OF CONTENTS

LIST OF TABLES

LIST OF FIGURES

CHAPTER 1
INTRODUCTION

1.1 Peripheral Nerve Injury

Injury to peripheral nerves occurs commonly due to trauma, compression, excessive stretching, and iatrogenic injury during surgical or anesthetic procedures. Trauma is the most common etiology and injuries to the nerve occur as a result of motor vehicle accidents, lacerations, limb fractures, and crush injuries (Robinson, 2000). In a retrospective analysis (Noble *et al.*, 1998) of patients with nerve injury at the Sunnybrook Health Science Center (Toronto, ON, Canada) a decade ago, it was found that motor vehicles accidents was the predominant etiology. The radial nerve was the most frequently injured nerve in the upper extremity and the peroneal nerve in the lower extremity. Motor vehicle accidents was the predominating etiology in a more recent study completed at Turkey (Eser *et al.*, 2009). Although peripheral nerve injuries are common in limb trauma, the overall incidence rate is still low (Taylor *et al.*, 2008). Damage to peripheral nerves may also arise due to sprained joints (Nitz *et al.*, 1985) and nerve sheath tumors (Ducatman *et al.*, 1986). The endoneurium of the nerve is elastic due to its high collagen content; but excessive traction forces may induce avulsion of the nerve. Local infiltration of anesthetic agents can also inflict nerve damage (Cameron and Stewart, 1975); although the incidence of this serious complication after peripheral nerve blockade is not very common (Barrington *et al.*, 2009)

Injury to the peripheral nerve can affect either the axon or the myelin sheath. Crush or disruption of the axons lead to altered gene expression in the nerve cell body and degeneration of the distal segment and the axon terminal. Wallerian degeneration is the characteristic consequence at the distal end of the damaged nerve (Chaudhry *et al.*, 1992). The events, occurring during regeneration, guide the newly spouted axons as they innervate the target organs. There is an ‘initial delay’, before the appearance of new axonal sprouts from the distal end (Sunderland, 1978). Czaja *et al.*, (2008) had estimated this delay to be between 3–42 days. The initial axonal sprouts that are guided by Schwann cells are unmyelinated.

Schwann cells proliferate rapidly and by day 3 (Stoll *et al.*, 1989) rearrange themselves to form bands of Büngner, which form a vital guidance cue for the regenerating axon (Fawcett and Keynes, 1990). The elaborate arrangement of Schwann cells in the Büngner bands, serve as physical conduits, guiding axons to their targets. Son and Thompson, (1995) showed that axonal

regeneration is limited by the absence of processes from Schwann cells. Perry *et al.*, (1987) established that macrophages invade damaged peripheral nerves and are localized around the damaged axons. These macrophages are recruited to phagocytize myelin and other debris even before maximal Schwann cell proliferation (Goodrum *et al.*, 1994). Fernandez-Valle *et al.*, (1995) showed the ability of Schwann cells in clearing myelin debris, *in vitro*. Schwann cells also produce various neurotrophins like BDNF, NT-3, NT-4/5, and NGF (Funakoshi *et al.*, 1993). Pellitteri *et al.*, (2006) showed that Schwann cells enhanced the production of neurotrophins in cultures of neurons from rat embryonic cerebral cortex. Schwann cells have also been genetically modified, to overexpress BDNF and NT-3; thereby promoting spiral ganglion cell survival *in vitro* (Pettingill *et al.*, 2008).

Axonal advancement is also promoted by extracellular matrix components like laminin and fibronectin. Addition of anti-laminin-2 antibodies to a culture of embryonic chick sensory neurons reduced the growth and total length of the neurites (Agius and Cochard, 1998). The newly sprouted axons enlarge and attain close-to-normal diameters with a compensated increase in myelin sheath thickness, as they proceed towards the distal end (Sanders, 1948). There are many newly grown axonal fibers and that not in close proximity to the target are pruned away (McQuarrie, 1985). Thus extracellular matrix factors, Schwann cells and neurotrophins could be exploited and integrated into scaffolds for enhanced regenerative properties.

1.2 Current clinical repair of injured peripheral nerves

1.2.1 Epineural suturing

Tension-free coaptation of transected nerves using non-absorbable sutures at the epineurium is the standard surgical repair technique (Rowshan *et al.*, 2004). In a study by Murovic (2008), 25.7% of the patients with radial nerve injury at the Louisiana State University Health Sciences Center, between the years 1967 and 1997 were treated with sutures. Surgery is performed within a week to repair uncomplicated nerve injuries (Dvali and Mackinnon, 2003) or is delayed until 3-4 weeks in contusion or traction injuries. Coaptation could be epineural, fascicular, or grouped fascicular repair. In fascicular repair each individual fascicle is sutured to be continuous and in grouped fascicular repair, motor and sensory fascicular groups are identified and sutured separately. Although both fascicular and grouped fascicular repair lead to better alignment of the axons and reduce axonal misdirection (Brushart *et al.*, 1983), additional

dissection and suturing compared to epineural repair can compromise blood supply (Ogata and Naito, 1986) and increase fibrotic tissue. Despite the advances in surgical techniques, complete functional recovery is rarely achievable (Siemionow and Brzezicki, 2009).

1.2.2 Autografts

Autologous nerve grafts are still considered to be the gold standard in repairing injured peripheral nerves (Deumens *et al.*, 2010), as they provide a natural scaffold containing Schwann cells and their basal lamina. Schwann cells secrete various neurotrophic factors and the basal lamina contains many extracellular matrix proteins. It is known that the loss of Schwann cells in nerve conduits results in suppression of nerve regeneration (Hall, 1986). Therefore autografts provide an appropriate environment for regenerating axons. In a study by Murovic (2008), 33.9% of the patients with radial nerve injury at the Louisiana State University Health Sciences Center, between the years 1967 and 1997 were treated with grafts. 54 graft, 41 suture, 64 neurolysis. 159 total

Sensory cutaneous nerves such as the sural nerve, lateral antebrachial cutaneous nerve, medial antebrachial cutaneous nerve, dorsal cutaneous branch of ulnar nerve, and the superficial sensory branch of the radial nerve are commonly used donor nerves for autografting (Matsuyama *et al.*, 2000). Donor nerves are sensory nerves as their harvest results in acceptable donor-site sensory loss. A donor nerve is chosen based on the caliber of the nerve to be repaired, defect length, and donor site morbidity. About 20 cm of the sural nerve can be harvested (Ortigüela *et al.*, 1987).

However, the need for a second surgery to obtain the donor nerve, loss of donor-site function, mismatch between the injured and donor nerve size, and neuroma formation, are setbacks of autografts. Harvesting the sural nerve can result in sensory loss along the lateral aspect of the foot in nearly 50% of the patients (Staniforth and Fisher, 1978) and neuroma formation in up to 8% of the patients (Ortigüela *et al.*, 1987).

1.2.3 Allografts

Allografts have been successfully used as alternatives to autografts (Mackinnon *et al.*, 2001). However the implantation of fresh allografts can induce immune responses and immunosuppressive therapy may be needed for few years (Siemionow and Sonmez, 2007).

Patients on immunosuppressive therapy are susceptible to opportunistic infections. Allografts can be processed using various protocols to make them less immunogenic (Szynkaruk *et al.*, 2013).

1.2.4 Decellularized nerves

Isolated allograft nerves, processed with chemicals, result in decellularized nerves (Hudson, Liu, *et al.*, 2004). Though the cellular components are lost, the extracellular matrix scaffolding within the nerve is retained (Hudson, Zawko, *et al.*, 2004). This three-dimensional matrix is absent in other nerve guidance conduits. The chemical detergent technique to decellularized nerve is accepted clinically (Brooks *et al.*, 2012). More recently, detergent-free techniques have also been used (Vasudevan *et al.*, 2014). Detergent processed nerves were shown to be equivalent to autografts with respect to the nerve fiber count and the recovery of contractile force in the reinnervated muscles (Moore *et al.*, 2011).

Acellular grafts lack Schwann cells and they are not as successful as autografts when used to bridge larger gap distances (Nadim *et al.*, 1990). Decellularized nerve grafts are also limited by disrupted endoneurial tubes and damaged basal lamina (Whitlock *et al.*, 2009). The absence of Schwann cells make decellularized grafts lack the functional characteristics of normal peripheral nerves.

1.2.5 Nerve transfer

Nerve transfers involve the repair of an injured nerve by connecting the proximal end of another nerve or its fascicle to the distal aspect of the injured nerve. The function of the donor nerve is sacrificed so that the more important damaged nerve reinnervates more quickly (Narakas and Hentz, 1988). In this technique, unlike with autografts, the donor nerve would have reasonable amount of motor nerve fibers (Midha, 2004). Reinnervation of the injured nerve is done close to its target muscle for better outcome (Nath *et al.*, 1997). The need for excision of a nerve graft from another site is not required as nerves in close proximity are used. However as the use of additional nerve grafts decrease functional outcome (Waikakul *et al.*, 1999), the donor nerve has to be very close in proximity to the recipient nerve. This makes nerve transfer applicable only at certain anatomical sites as the area innervated by the donor nerve, loses function after the procedure.

1.3 Tissue repair scaffolds and scaffold materials

Since each of the nerve-repair strategies discussed above has its own drawbacks, other novel nerve grafts have been constantly developed and investigated. Tissue repair scaffolds serve as supportive constructs to help with cell growth, migration and differentiation. They are fabricated using a wide selection of biomaterials, ranging from naturally occurring hydrogels to synthetic polymers. Agarose (Lee *et al.*, 2009a), hyaluronic acid (Suri and Schmidt, 2010), alginate (Dhoot *et al.*, 2004), hydroxylethyl methacrylate (Yu and Shoichet, 2005) and other hydrogel materials have been used to fabricate scaffolds in nerve tissue engineering. Bioactive poly (L-lactic acid) conduits have been seeded with Schwann cells (Evans *et al.*, 2002), while the same material has also been spun into aligned nanofibers (Yang *et al.*, 2005). Tissue engineered scaffolds for peripheral nerve regeneration should have similar diameter as the nerve being repaired, be biodegradable, and easily implantable using currently available surgical techniques (Chalfoun *et al.*, 2006). The scaffolds must also have appropriate surface chemistry favoring cellular attachment and have adequate mechanical properties (Hutmacher, 2001). Few common biomaterials used in the fabrication of scaffolds for peripheral nerve tissue engineering are briefly reviewed below.

1.3.1 Alginate

Alginate is a naturally occurring polysaccharide and has a promising role in the realm of tissue engineering. The proclivity of alginate in tissue engineering is attributed to the ability of including living cells within them. Other unique properties of alginate include an inert environment with adequate porosity allowing good diffusion rates of macromolecules and biodegradation of the system under normal physiological conditions (Gombotz and Wee, 1998).

Alginate is commonly isolated from brown algae (kelp), found in the sea (Smidsrød and Skjak-Braek, 1990). A few of the sources of alginate include *Laminaria hyperborea*, *Ascophyllum nodosum*, and *Macrocystis pyrifera*. Alginate is a polysaccharide, composed of (1-4) β-D-mannuronic acid (M) and α-L-guluronic acid (G). Both the M and G blocks are linked either randomly or as homopolymers (Johnson *et al.*, 1997). The architecture of the blocks depends on the origin of the alginate. Having randomly arranged blocks, the molecular weight of alginate could vary and so would the viscosity, being dependent on the molecular weight (Kong *et al.*, 2002). Alginate gels easily on binding of divalent cations to the G-units. This binding

causes a unique transition of the structure of alginate into the so-called ‘egg-box’ model (Sikorski *et al.*, 2007).

In general, alginates rich in G-blocks are stronger and more brittle than those with more M-blocks. The elastic modulus of alginate depends on the length of the chains and strength of the crosslinking (Draget *et al.*, 1997). The concentration and type of the crosslinking agent also have a vital role. Other crosslinking agents, besides divalent calcium ions include adipic dihydrazide, methyl ester L-lysine, and PEG-diamines (Lee et al., 2000). The use of divalent ions could lead to the loss of 60% of mechanical strength within 15 hours of exposure to the physiological environment. Thus the use of non-ionic crosslinking agents could regulate the mechanical properties and swelling indices of alginate (Lee, Bouhadir, *et al.*, 2000). Increasing the content of G-blocks could increase the mechanical properties and porosity of alginate (Thu *et al.*, 1996). While being crosslinked, alginate moves from the inner to the gelling zone and thus most of the gel at the center is ‘shifted’ (Draget *et al.*, 1997). This leads to inhomogeneity in the gel and occurs when divalent ions are used in the crosslinking process. Controlled release of calcium (or other divalent ions) by using calcium carbonate or D-glucono-δ-lactone (GDL), solves this inhomogeneity issue (Kuo and Ma, 2001). Homogeneity of hydrogel is a major advantage for the encapsulation of cells.

Certain sterilization techniques can compromise the viscosity of alginate. Autoclaving alginate results in the reduction of its viscosity by 64% (Vandenbossche and Remon, 1993). Similar losses in viscosity are also observed with ethylene oxide. γ-irradiation, on the hand induces free oxygen radical formation in alginate (Draget *et al.*, 1997). Neural cells, in particular are very sensitive to free radicals or oxygen species (Raps *et al.*, 1989). Membrane filtration does not confer a compromise to the viscosity and molecular weight (Vandenbossche and Remon, 1993).

Native or unmodified alginate is a poor substrate for the adhesion of mammalian cells. These cells have no receptors to adhere to alginate, making the growth of process from cells unfeasible, without the modification of alginate (Augst *et al.*, 2006). Schwann cells cultured in 2% low viscosity alginate resulted in reduction of neurite growth (Mosahebi *et al.*, 2001). The culture of ovine intervertebral disc nucleus pulposes cells in 0.14% alginate beads, resulted in good viability but a poor cellular morphology.(Pattison *et al.*, 2001).

Naturally occurring substances such as collagen (Sang *et al.*, 2011), laminin (Yamada *et al.*, 2010) and fibronectin (Mosahebi *et al.*, 2003b) can however be added to enhance cellular adhesion. Laminin induces potent neurite outgrowth and promotes nerve regeneration over unusually long distances (Malinda and Kleinman, 1996). Laminin consists of three peptide chains, namely A, B1 and B2. The functional domains on the laminin chain define its interaction between various other cell surface receptors (Mecham, 1991a). Few laminin-based synthetic peptides have similar biological activity like laminin (Massias *et al.*, 1993). The pentapeptide Tyr-Ile-Gly-Ser-Arg (YIGSR) and Cys-Asp-Pro-Gly-Tyr-Ile-Gly-Ser-Arg (CDPGYIGSR) on the B1 chain of laminin are involved with cell adhesion and migration (Graf *et al.*, 1987). The Ile-Lys-Val-Ala-Va (IKVAV) sequence is found on the long arm of the A chain. This sequence is particularly known to aid the growth of neurites (Tashiro *et al.*, 1989). The Arg-Gly-Asp (RGD) sequence in laminin is found in the short arm of the A chain (Tashiro *et al.*, 1991). This sequence is pivotal in cellular attachment and is also the primary integrin-dependent cell-binding site on fibronectin. Fibronectin is a multimer protein in the extracellular matrix and exists as a soluble disulphide-linked dimer in plasma (Potts and Campbell, 1996). The fibronectin monomers consist of three different protein modules, namely F1, F2 and F3. In fibronectin, the RGD sequence of peptides is inserted in a loop between the two β-strands of module F3 (Bork *et al.*, 1996). Therefore modifying alginate with the addition of fibronectin, laminin, or cell adhesive peptides, is a mandate when culturing neural cells.

1.3.2 Fibrin

Fibrinogen, a glycoprotein is present in human blood plasma at a concentration of about 2.5 mg/ml (Iwanaga *et al.*, 2008). It is essential for hemostasis, angiogenesis, wound healing, and inflammation. Fibrinogen is soluble, but it forms a gel on interaction with the serine proteolytic enzyme thrombin. However the resulting fibrin filaments are not crosslinked until the addition of the transglutaminase, activated factor XIII (Kanaide and Shainoff, 1975). Fibrin is currently used clinically to plug bleeding vessels and as a replacement to sutures (Albala and Lawson, 2006). Using fibrin glue instead of sutures or staples enhances healing, minimizes scarring, and eases application. It has surgical applications in polymeric mesh fixation during inguinal hernia repair (Canonico *et al.*, 2013), and skin graft adhesion (Branski *et al.*, 2011). Fibrin sealant has also been successful at the coaptation of severed sciatic nerves in rats (Martins *et al.*, 2005).

Few extracellular components interact with fibrin and can alter the structure and properties of fibrin clots. Fibronectin can covalently bind to fibrin (Kanaide and Shainoff, 1975). Fibrin also binds with hyaluronic acid and von Willebrand factor (Weisel, 2005). Fibrin has RGD sites and a pair of AGDV sites through which it can interact with integrins on Schwann cells (Chernousov and Carey, 2003). Binding of fibronectin with fibrin, would be an added advantage for Schwann cells as their proliferation is augmented by fibronectin (Baron-Van Evercooren *et al.*, 1982).

After injury to a peripheral nerve, fibrinogen from the plasma is activated into fibrin and is incorporated as an additional extracellular matrix protein of the nerve (Akassoglou *et al.*, 2000). Fibrin gel has been used as a vehicle to deliver nerve growth factor (Sakiyama-Elbert and Hubbell, 2000). Fibrin containing Schwann cells has been used as a luminal filler to promote axonal regeneration (Galla *et al.*, 2004). The addition of neurotrophins along with Schwann cells into fibrin has also been used for the regeneration of rat sciatic nerves (Ma *et al.*, 2013). Inkjet printing has enabled layers of neural cells and fibrin to be stacked over each other to form a 3D structure (Xu *et al.*, 2006). Fibrin is also an effective scaffold for cartilage and cardiovascular tissue engineering.

1.3.3 Collagen

There are many types of collagen and only a few of these form most of the extracellular matrix of peripheral nerves (Thomas and Olsson, 1984). Collagen plays an important role in the development and maintenance of the nerve (Hubert *et al.*, 2009) and is present in all its three layers of connective tissue. Type-I, type-III and type-V collagens are the most common collagens in the nerve connective tissue. Type-IV collagen forms the basement membrane and it integrates laminin, perlacan, nidogen, and other ECM proteins into complex basement membrane aggregates (Hudson, Reeders, & Tryggvason, 1993). Collagens type-I and III provide mechanical support to the regenerating axons after nerve injury.

Collagen provides good support for cell growth and it can enhance the differentiation of many cell types (Kleinman *et al.*, 1981). Collagen conduits are used to bridge the gap between injured nerve stumps and can direct axonal sprouting from the proximal end of the nerve (Waitayawinyu *et al.*, 2007). They are permeable, unlike other synthetic conduits and permit the

diffusion of nutrients between the conduit lumen and surrounding tissue. There are commercially available type-I collagen conduits available for clinical use–Neurawrap™, NeuroMatrix™, NeuroFlex™, and Neuragen®.

Collagen gel, when used as an *in vivo* luminal filler in nerve conduit channels, increases axonal length and results in improved sensory function (Jin *et al.*, 2013). Rolled sheets of collagen gels with cultured Schwann cells have been proposed as promising nerve repair conduits (Goto *et al.*, 2010). 3D collagen scaffolds have been printed using a cryogenic direct-plotting system, where the extruded collagen is immediately frozen to retain its structure (Kim *et al.*, 2009).

1.4 Incorporating cells in hydrogel scaffolds

Neurite extension and migration within nerve scaffolds is augmented in the presence of neuroglia cells (Struzyna *et al.*, 2014). Various living cells such as Schwann cells, olfactory ensheathing cells (Imaizumi *et al.*, 2000), and neural stem cells (Guo and Dong, 2009) have been incorporated into scaffolds to support peripheral nerve regeneration. Living cells can be either seeded over scaffolds after their fabrication or incorporated during the scaffold fabrication process.

Olfactory ensheathing cells are a type of macroglia exclusively located in the olfactory nerve and they produce neurotrophic factors to mediate neuronal survival and axonal elongation (Ramón-Cueto and Avila, 1998). In addition to enhancing axonal regeneration (Radtke *et al.*, 2009), they produce myelin (Devon and Doucette, 1992) and have better migratory potential to penetrate glial scars. Axonal regeneration was more pronounced in presence of olfactory ensheathing cells included into a laminin filled silicone tube (Verdu *et al.*, 1999). Olfactory ensheathing cells have also been examined for spinal cord regeneration due their ability to promote growth of axons across the central and peripheral nervous system interface (Li *et al.*, 1997a), (Ramón-Cueto *et al.*, 1998).

Macrophages have a pivotal role in clearing the myelin and cellular debris during Wallerian degeneration of distal nerve tissue, thereby facilitating axon regeneration through this tissue (Perry *et al.*, 1987). There is *in vivo* evidence that macrophage recruitment could be important for the increase in nerve growth factor synthesis following nerve injury (Brown *et al.*,

1991). Enhanced recruitment of macrophages can be achieved by efforts to improve the vascularization of peripheral nerve scaffolds (Griffin *et al.*, 1993).

Following peripheral nerve injury, activated migratory Schwann cells stimulate the elongation of axons (Torigoe *et al.*, 1996). The guidance of axons is also influenced by the basal lamina of Schwann cells (Nguyen *et al.*, 2002). They are the glial cells of the peripheral nervous system and produce neurotrophic factors, extracellular matrix, and adhesion proteins. Schwann cells of the distal nerve stump align themselves into 'bands of Büngner' (Fawcett and Keynes, 1990) and the importance of this arrangement in promoting axonal growth is well documented (Taniuchi *et al.*, 1986). During regeneration, Schwann cells migrate ahead of the extending axonal growth cones to guide axons (Torigoe *et al.*, 1996). Regenerating axons do not elongate profoundly through acellular nerve grafts (Hall, 1986). Thus incorporation of Schwann cells into tissue-engineered scaffolds is beneficial.

1.5 Fabrication of hydrogel scaffolds using dispensing techniques

By employing various fabrication techniques, hydrogels can be used to achieve the inclusion of Schwann cells into scaffolds. Among these techniques, rapid-prototyping (RP) methods have greater advantages in the fabrication of tissue-engineered scaffolds than the conventional techniques. RP enables greater pore inter-connectivity and higher porosity scaffolds, versatile control over the scaffold architecture, and discrete placement of different biomaterials. RP techniques such as fused-deposition modeling, selective laser sintering and stereolithography either require high temperatures or use resin in the fabrication of scaffolds, making them incompatible with most biomaterials. 3D printing and 3D bioplotting are examples of dispensing-based RP techniques that are compatible with the use of natural biomaterials and can be carried out under physiologically mild conditions, making incorporation of most cell types within scaffold biomaterials practical (Peltola *et al.*, 2008). This approach allows incorporation of cells in the deeper layers of scaffolds, which is difficult to achieve by seeding live cells on pre-formed scaffolds.

3D bioplotting, as the name suggests, ‘plots’ scaffolds in three dimensions. 3D bioplotting is more accurate and requires less biomaterial than 3D inkjet printing (Pfister *et al.*, 2004). It is versatile, and can be used to dispense different materials including compatible polymers, resins and biopolymeric hydrogel solutions such as agar and gelatin (Glicklis *et al.*,

2000). Structural rigidity of scaffolds is achieved by using thermoreversible hydrogels. Rat embryonic neurons, included in collagen and gelatin gels were printed into 3D scaffolds by maintaining the temperature of the gelling medium below the gelation temperature of the gels (Lee *et al.*, 2009). In order to prevent collapse of the forming 3D structure prior to gelation of the hydrogel, dispensing can also be done into a liquid medium with approximately similar density as the plotting material, allowing buoyancy to counteract gravity (Landers, Pfister, *et al.*, 2002). This enables better structural integrity of the scaffold as it is printed layer-by-layer. Bioplotting hydrogels into appropriate solutions (similar viscosity and density as the hydrogel) may also prevent excessive spreading of hydrogel on extrusion. Using a crosslinking solution (with the right physical and biological parameters) can also prevent the plotted scaffold from drying and could help with the fabrication of scaffolds with high cell viability.

1.6 Research objectives

The aim of this research is to characterize biomaterials suitable for 3D bioplotting of nerve repair scaffolds.

Bioplotting, a freeform scaffold fabrication technique can be used for creating artificial tissue scaffolds containing living cells. However, simultaneous maintenance of scaffold structural integrity and cell viability is a challenging task. Schwann cells incorporated in the scaffolds must retain their viability, morphology, and also align themselves along the plotted strands for successful axonal guidance. Therefore a comparison of the suitability of alginate, collagen type-I, fibrin, and their mixtures for 3D bioprinting of hydrogel scaffolds containing Schwann cells is desired.

Therefore the specific objectives of this research are as follows.

- Fabricating a tissue engineered scaffold containing living Schwann cells for the repair of peripheral nerves. Bioplotting will be used to achieve scaffold fabrication, using a suitable crosslinker as the plotting solution.
- Comparing Schwann cell viability in scaffolds strands that are printed into a crosslinking solution and printed in air.
- Comparing Schwann cell viability and morphology in ‘printable’ hydrogels such as alginate, fibrin, and collagen type-I. The print fidelity of each hydrogel will be assessed by measuring scaffold strand width and interstrand spacing.

- Conducting a preliminary *in vivo* study using scaffolds with incorporated Schwann cells as nerve conduits in a rat sciatic nerve model. Functional outcome of the study will be assessed by behavioral studies and axonal regeneration will be assessed using immunohistochemistry techniques.

1.7 Organization of the dissertation

The dissertation is organized into 7 chapters. Besides this introduction, it includes five manuscripts, followed by the conclusions drawn from this research.

A literature review on scaffold design and recent advances in biofabrication of scaffolds for use in peripheral nerve repair is presented in chapter 2. The review focuses on the biological events following nerve injury, recent techniques used in the fabrication of biocompatible scaffolds, and strategic tissue scaffold designs for nerve injury repair.

Chapters 3 and 4 focus on the fabrication of alginate-hyaluronic acid scaffolds containing Schwann cells. A novel technique, which helps with attaining good scaffold architecture, as well as viability of the contained Schwann cells is discussed. Chapter 4 illustrates the effect of a polycation on the physical properties of an alginate-hyaluronic acid scaffold.

A preliminary *in vivo* experiment using alginate-hyaluronic acid scaffolds as a nerve conduit is presented in chapter 5. In chapter 6, the biological and fabrication of more biomaterials suitable for nerve regeneration are compared.

Finally, chapter 7 presents the conclusions drawn from this research. This is followed by suggestions and recommendations for possible future research.

1.8 Contributions of the primary investigator

The manuscripts included in this thesis are co-authored; however it is the mutual understanding of all authors that Ajay Rajaram, as the first author, is the primary investigator of the research work. The contributions of other authors are greatly appreciated and acknowledged in this thesis.

CHAPTER 2
STRATEGIC DESIGN AND RECENT FABRICATION TECHNIQUES FOR BIOENGINEERED TISSUE SCAFFOLDS TO IMPROVE PERIPHERAL NERVE REGENERATION[*]

[*]This chapter has been published as "Rajaram A, Chen XB, Schreyer DJ. (2012) Strategic design and recent fabrication techniques for bioengineered tissue scaffolds to improve peripheral nerve regeneration. *Tissue Engineering Part B: Reviews*. 18(6): 454-467". According to the Copyright Agreement, "the authors retain the right to include the journal article, in full or in part, in a thesis or dissertation".

2.1 Introduction

Peripheral nerve injuries can entail partial or complete transection of the nerve. At the cellular level, there can be transection of individual axons, possible neuronal death, and damage to the supporting Schwann cells and the myelin sheaths that they produce. Nerve injuries are described clinically using Seddon's classification (Seddon, 1943). Some injuries allow the proximal and distal portions of the nerve to maintain continuity, allowing easy regrowth of transected axons, while others produce a gap that is difficult to bridge. One immediate goal of nerve tissue engineering is to create artificial, biomimetic scaffolds that can be used to bridge gaps and improve the ability of axons to regenerate back toward their peripheral innervation targets. This review focuses on the biological events that occur following nerve injury, recently developed techniques for fabrication of biocompatible scaffolds, and the strategic design of biomimetic tissue scaffolds for nerve injury repair.

2.2 Peripheral nerve injury

2.2.1 Incidence and etiology

Noble *et al.*, (1998) compiled the incidence and prevalence rates of peripheral nerve injuries over the preceding decade. Their study illustrated that almost 46% of nerve injuries were due to road traffic incidents. The radial nerve, a nerve in the posterior compartment of the forearm, was injured most frequently. Nerve injuries also commonly occur as complications of regional anesthesia (Jeng *et al.*, 2010). In a retrospective study by Taylor *et al.*, (2008), the total

incidence of peripheral nerve injuries due to upper- or lower-limb trauma was 1.64%, with crush trauma having the highest rate of associated nerve injury. Grade-III ankle sprains, arising mostly from sporting activities, lead to a significant incidence of nerve injury to the nerves in the leg, causing prolonged rehabilitation time (Nitz *et al.*, 1985). Compression neuropathies, such as carpel tunnel syndrome, can also induce chronic peripheral nerve injury. Moreover, some neuropathic disorders and tumors of the peripheral nerve require excision of part of the nerve.

2.2.2 Events in nerve repair

Functional losses following peripheral nerve injuries arise primarily from interruption of the integrity of sensory, motor and autonomic axons. Crush or transection of the axon leads to reactive biological events in the neuronal cell bodies, the proximal segment of the injured nerve, the distal segment, and the peripheral innervation targets.

Axon transection separates distal lengths of axon from their parent cell bodies and results in a set of events in the distal peripheral nerve called Wallerian degeneration (Chaudhry *et al.*, 1992). The lengths of axon in the distal nerve that have been disconnected from the neuronal cell body degenerate, although the remaining proximal lengths of axon remain largely viable. Wallerian degeneration entails a set of histological changes in the distal nerve that include disintegration of severed axons and their myelin sheaths, and invasion of macrophages to clear degenerating cellular debris (Eto *et al.*, 2003). Beirowski *et al.*, (2005) showed that in mice, distal fragmentation of damaged nerves occurs within a short time frame of 40-44 hours. Resident Schwann cells also phagocytize the myelin debris (Goodrum *et al.*, 1994); a phenomenon which has also been demonstrated *in vitro* (Fernandez-Valle *et al.*, 1995). It is thought that timely clearance of degenerating debris is necessary in order for peripheral axons to regenerate properly (Chen and Bisby, 1993). Disintegration of disconnected axons also appears to require activation of the intrinsic ubiquitin-proteasome system which causes cytoskeletal disintegration (Fernyhough *et al.*, 2005). The ubiquitin-proteasome cascade helps in the targeted degradation of proteins.

Three to four days after injury, Schwann cells throughout the distal stump and at the tip of the proximal stump increase their rate of division (Hall, 2005) and elaborately rearrange themselves to form bands of Büngner, the vital guidance cue for the regenerating axon (Fawcett and Keynes, 1990). Schwann cells help to guide the regrowth of axons toward peripheral targets

to restore nerve function (Stoll and Müller, 2006). Son and Thompson, (1995) show that axonal regeneration is limited if Schwann cells are prevented from extending processes. Schwann cells also produce various neurotrophins, such as brain-derived neurotrophic factor (BDNF), neurotrophin (NT)-3, NT-4/5, and nerve growth factor (NGF) (Funakoshi *et al.*, 1993), (Pellitteri *et al.*, 2006) which can promote neuronal survival and/or axonal growth.

In addition to events that occur near the damage site in peripheral nerves, axonal growth also depends on the type of neuron, age and inherent regenerative capacity (Chierzi *et al.*, 2005). Injured neurons must switch from a metabolic state that supports the function of mature, stable axons to one that supports the formation of a motile 'growth cone' expansion of the axon tip. Nerve injury results in the upregulation of various growth-associated proteins including transcription factors, signaling proteins, cytoskeletal proteins (Skene, 1989) and neurotrophic factors and their receptors. One example is the growth-associated protein-43 (GAP-43), a neuron specific protein which undergoes elevated expression during nerve regeneration (Skene and Willard, 1981). Partial depletion of GAP-43 in growth cones using antibodies (Shen *et al.*, 2002) or antisense oligonucleotides (Aigner and Caroni, 1993) results in the reduction of F-actin, thereby impairing the motility function of growth cones. The synthesis of cytoskeletal proteins required for axonal reconstruction is also increased during regeneration (Fornaro *et al.*, 2008). Lund *et al.*, (2002) used *in situ* hybridization to show an increase in the β-actin mRNA levels, suggesting the importance of β-actin during axon regrowth.

Important extrinsic growth factors include the neurotrophins, insulin-like growth factors (Fernyhough *et al.*, 1993), hematopoietic cytokines such as leukemia inhibitory factor (McKay Hart *et al.*, 2003) and interleukins (Bourde *et al.*, 1996), fibroblast growth factor (Grothe and Nikkhah, 2001), and transforming growth factor (Chalazonitis *et al.*, 1992). Extracellular matrix proteins such as laminin, fibronectin, collagen, matrix metalloproteinases and cell adhesion molecules also support and regulate nerve regeneration through specific interactions with the cell surfaces. These matrix components can also interact with the growth factors and promote axonal advancement. Addition of anti-laminin-2 antibodies to a culture of embryonic chick sensory neurons reduces the growth and total length of the neurites (Agius and Cochard, 1998). Thus, extracellular matrix factors, Schwann cells, and neurotrophins could potentially be exploited and integrated into scaffolds as biological factors that enhance regenerative success.

Newly sprouted axons enlarge and attain close-to-normal diameters with greater myelin sheath thickness as they proceed towards the distal end (Sanders, 1948). Quan and Bird, (1999) report that remyelination of injured peripheral nerves takes between 2–12 weeks, depending on the extent of the injury. Although the mechanism isn't completely elucidated, it is known that many new axonal fibers grow and those that do not achieve close proximity to the target are pruned away. This specificity of reinnervation, produced by selective pruning of axon collaterals, could be influenced by relative levels of target-derived trophic support (Robinson and Madison, 2004) and by molecular cues on Schwann cells (Martini *et al.*, 1992).

Fugleholm *et al.*, (1994) assessed axonal growth in cats by using implanted electrodes and found the regenerative growth rate to be 3-4 mm/day after crushing a nerve, but lowered to 2.5 mm/day in animals with sectioned nerves. Hoffman and Lasek, (1980) tagged rat cytoskeletal proteins with radioactive isotopes and found the actin in lesioned nerves to move distally at a rate of 2-5 mm/day. Buchthal and Kuhl, (1979) studied the sensory potential, evoked by stimuli to the digits, in patients treated for complete section of the median nerve. They found the rate of sensory axonal growth to be 1.5-2 mm/day. The rate of regeneration of peripheral axons is slower in humans than in rodents (Höke, 2006). Studies on *in vivo* nerve regeneration have usually been done on acute models of injury. However it is known that chronic denervation impedes the success of nerve regeneration (Fu and Gordon, 1997), suggesting that delayed treatment is likely to lead to a poorer clinical outcome. Better understanding of the molecular mechanisms that impede or delay nerve regeneration would be beneficial in designing tissue repair scaffolds that are implanted at variable post-injury intervals to support axon regeneration.

2.3 Fabrication of tissue scaffolds

The emerging field of tissue engineering offers a new prospect for treatment strategies to foster regeneration of injured nerves and thereby promote restoration of sensory, motor and autonomic function. Tissue scaffolds are designed to serve as templates that support the regeneration of a tissue, organ or specific structure. These scaffolds can be fabricated using a wide selection of biomaterials, ranging from hydrogels to composite polymers. Rapid-prototyping (RP) methods have advantages in the fabrication of tissue-engineered scaffolds over conventional techniques (Park *et al.*, 2009). RP enables fabrication of scaffolds with greater pore inter-connectivity and higher porosity, versatile control over the scaffold architecture, and

discrete placement of different biomaterials. However, RP techniques such as fused-deposition modeling, selective laser sintering, and stereolithography require either high temperatures or the use of resin in the fabrication of scaffolds, making them incompatible with most biomaterials. Three dimensional printing and three dimensional bioplotting are examples of dispensing-based RP techniques that are more compatible with natural biomaterials and could be carried out under physiologically mild conditions, making the incorporation of biological materials, even living cells, within scaffold biomaterials more practical (Peltola *et al.*, 2008). Indeed, this approach can allow specific and directed incorporation of living cells anywhere within the scaffold, which would be difficult to achieve by seeding living cells onto the surfaces of pre-formed scaffolds.

2.4 CAD-based tissue engineering

Computer-aided design (CAD) is used extensively in the medical realm. Surgical reconstructions of large bone defects, especially cranial bones, are heavily dependent on CAD-based reconstruction. Using CAD techniques and stereolithography with computed tomography guidance enables the fabrication of implants with good results in the reconstruction of complex skull defects (Saringer *et al.*, 2002). Similarly, CAD techniques are useful in the fabrication of joint prostheses; for example, Jiankang *et al.*, (2006) report the use of CAD techniques in fabricating and successfully implanting a customized tibial hemi-knee joint prosthesis in a 14-year old girl. With increasing demands for biomimetic tissue scaffold designs, CAD techniques have been utilized in a number of recent fabrication methods (Table 2.1).

2.4.1 Three dimensional bioplotting

As the name suggests, this technique ‘plots’ scaffolds in three dimensions, by which a viscous biomaterial is dispensed through a nozzle into a liquid medium, thereby retaining its shape without any temporary supportive structures. (Landers, Hübner, *et al.*, 2002) describe a procedure for effective dispensing of hydrogels using the three dimensional bioplotting technique. In order to prevent the collapsing of the scaffold layers prior to gelation, the material is dispensed into a liquid medium with approximately the same density as the plotted material, allowing buoyancy to counteract gravity. Structural rigidity of thermoreversible hydrogels is achieved if the temperature of the receiving medium is below the gelation temperature of the

hydrogel. They also suggest the use of roughened surfaces as substrates for the first hydrogel layer dispensed; for example, the use of sandblasted metal plates as receiving surfaces. Lee *et al.*, (2009) included rat embryonic (day 18) neurons in collagen and gelatin gels and then printed them into three dimensional scaffolds. Low pneumatic pressures (< 5 psi) and nebulization of the hydrogel crosslinker over each layer (once deposited) helped in achieving a good construct.

Table 2.1. CAD-based fabrication techniques.

Technique	Description	Advantages	Reference
3D bioplotting	Viscous biomaterial plotted into a liquid with similar density	3-D scaffolds, wide variety of materials could be dispensed	(Pfister *et al.*, 2004)
Matrix-assisted pulsed-laser evaporation direct-write	Laser-guided dispensing of cells	Better resolution and no dispensing nozzle	(Wu *et al.*, 2003)
Lased-induced forward transfer	Laser activates a metal film that indirectly dispenses cells	Less thermal damage to cells and better resolution	(Ringeisen *et al.*, 2010)
Two-photon photopolymerization	Infrared laser is focused onto a photosensitive biomaterial and polymerization is initiated by two-photon absorption	High spatial resolution	(Lee *et al.*, 2008)

(Pfister *et al.*, 2004) compare three dimensional bioplotting with three dimensional printing, finding the former to be more accurate and requiring less quantity of the dispensed biomaterial. Three dimensional bioplotting is versatile and can be used to dispense different materials including polymers, resins, and biopolymeric hydrogel solutions such as agar and gelatin (Glicklis *et al.*, 2000). Although plotting of most synthetic polymers using dispensing techniques could be challenging, polymeric formulations such as TEEX-29b (copolymer of L-lactide and D,L-lactide dissolved in trichloroethylene and tetrachloroethane) and TEEX-31b (poly-l-lactide-caprolactone in trichloroethylene and tetrachloroethane) may be used due to their bioabsorbability, ability to be ink-jet printed, and cellular adhesion properties (Silva *et al.*, 2007). However the ability to print patterns with an adequate and controlled density of living cells or

biologically active molecules would be precluded by the use of organic solvents in the fabrication process.

2.4.2. Laser-based fabrication techniques

Laser-based techniques accurately deploy scaffold materials without the use of orifice- or nozzle-based dispensing. Thus, the process is immune to polymer adhesion and nozzle blockades. This approach also tolerates variations in the viscosity of the polymer or biomaterial solution. Laser-based methods are fast and can be more accurately controlled than most other techniques. Material deposition speeds are influenced by the laser pulse rate, stage control accuracy, and the nature of the receiving substrate.

2.4.2.1 Two-photon polymerization

In two-photon polymerization (2PP), a beam of infrared laser is focused onto a photosensitive biomaterial and polymerization is initiated by two-photon absorption. The greatest advantage of two-photon polymerization is that the absorption of photons from the laser by the material occurs only in the immediate vicinity of the focal point (Belfield *et al.*, 2000). Using this approach, selective focusing of the laser within a three-dimensional space can bring about the fabrication of three dimensional structures with high spatial resolution (Sun and Kawata, 2004). Biodegradable triblock copolymer scaffolds of poly(ε-caprolactone-co-trimethylenecarbonate)-b-poly(ethyleneglycol)-b-poly(ε-caprolactone-co-trimethylenecarbonate) have been made using 4,4'-bis(diethylamino)benzophenone as the photoinitiator with 4-μm resolution (Claeyssens *et al.*, 2009). Two-photon polymerization of photosensitive materials are used to fabricate scaffolds with 100-nm resolution (Koroleva *et al.*, 2010). (Lee *et al.*, (2008) reported micro-patterning of a cell adhesive ligand (peptide RGDS) in poly(ethylene glycol-co-peptide) diacrylate hydrogels using a two-photon polymerization technique. Human dermal fibroblasts seeded into these hydrogels underwent migration selectively into the RGDS-patterned regions of the hydrogels. Livnat *et al.*, (2009) used multi-photon ablative laser to pattern fibrinogen hydrogel containing polyethylene glycol. Neurons could display motility within these constructs and their processes elongated in specific directions, aligning themselves to the patterns made on the gel. Thus, similar techniques might be used in peripheral nerve engineering

to guide migration of Schwann cells along bioadhesive pathways to form artificial bands of Büngner. Unfortunately, certain photoinitiators used in the polymerization technique can be cytotoxic. For example, acetophenone is toxic to cultured HepG2 cells at amounts greater than 0.9 mg/mL (Liu and Bhatia, 2002). Thus, caution is needed during the initial selection of hydrogels, photoresists, or photoinitiators used in this technique.

2.4.2.2. Laser-induced forward transfer (LIFT)

Laser-induced forward transfer (Fig. 2.1) is a method that harnesses energy from nanosecond pulses of laser light and induces forward transfer of material. When used specifically to transfer living cells from cultures, this technique is known as biological laser printing (BioLP) (Ringeisen *et al.*, 2010). BioLP is a nozzle-free technique that minimizes cellular damage and maintains cellular phenotype (Othon *et al.*, 2008). No direct laser interaction with the substrate occurs and this technique is highly controllable and reproducible. Chen *et al.*, (2006) show that bovine aortic endothelial cells are almost 100% viable with minimal effects from heat or shear stress when they are included during the BioLP process.

Laser absorption onto any material causes an increase in temperature, leading to volatilization or even material expulsion. These material changes occur due to the thermo-acoustical mechanisms initiated by photoabsorption of incident laser energy. BioLP utilizes an energy conversion layer consisting of a thin film of titanium oxide (TiO_2), which absorbs most of the energy, thus preventing cellular damage. The cells to be transferred are maintained in a hydrogel material known as 'bioink', positioned immediately below the TiO_2 layer. Upon laser irradiation, the TiO_2 layer absorbs most of the energy and the heat induces displacement of cells from the bioink layer. Barron *et al.*, (2004) exposed the TiO_2 layer to laser beams with a wavelength of 266 nm and estimated that 99.9% of the incident laser energy was absorbed by the TiO_2 absorption layer. Materials printed from the bioink by this technique are therefore exposed to substantially less heat (Barron *et al.*, 2005). The absorption material must have a thickness greater than the penetration depth of the laser, but the transfer of heat through the laser absorption layer is independent of the absorption material thickness.

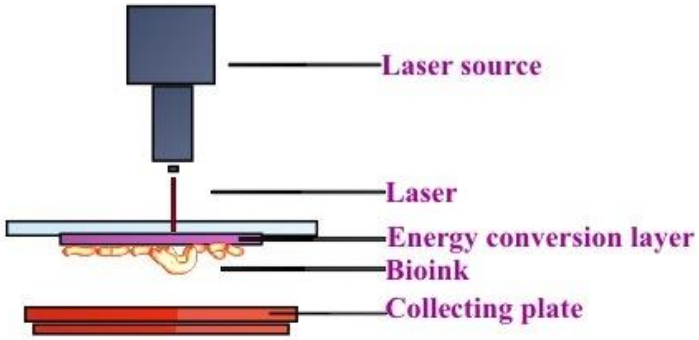

Figure 2.1 Laser-induced forward transfer (LIFT).

Ringeisen *et al.*, (2010) show good viability of olfactory ensheathing cells transferred onto a layer of Matrigel (a commercial mixture of extracellular matrix proteins) and success with the co-printing of olfactory ensheathing cells with rat cortical neurons. Othon *et al.*, (2008) also demonstrate the capability of BioLP to print three-dimensional tissue scaffolds containing olfactory ensheathing cells, where the cells retain their phenotype and cell-cell interactions. This technique can transfer a volume of cells or other biomolecules at the pico-scale. Barron *et al.*, (2005) demonstrate transfers as small as 0.5 pL and a droplet diameter as low as 30 μm. Dinca *et al.*, (2011) used BioLP to dispense SH-SY5Y human neuroblastoma cells and show the ability of these cells to orient, migrate, and produce organized cellular arrangements on patterns generated on polyethyleneimine. Hopp *et al.*, (2010) were unable to obtain 100% survival rates of transferred cells using BioLP (which they referred to as absorbing-film assisted LIFT). This may have been due to their use of femtosecond lasers instead of nanosecond lasers for the transfer of cells. Although ultra-short laser pulses reduce the thermal effects on the cells, they likely cause greater mechanical damage induced by the energetic plasma.

2.4.2.3 Matrix-assisted pulsed-laser evaporation direct-write (MAPLE DW)

The MAPLE DW technique (Wu *et al.*, 2003) is a micro-printing tool that could help in the deposition of living cells within a scaffold biomaterial after fabrication of three-dimensional scaffold constructs. MAPLE DW is used to create micro-channels, micro-patterns, or networks within scaffolds. The micro-architectures created this way can be exploited for alignment of cells as most cells have a tendency to align themselves along certain cues, such as the presence of

extracellular matrix proteins (Zhu *et al.*, 2010) or fields of electric current (Borgens, 1999) or also along the direction of small channels or patterns (Wilkinson *et al.*, 2002). Harris *et al.*, (2008) created channels of various depths in gelled agarose by altering the aperture of the laser. A431 human epithelial carcinoma cells and B35 neuroblast-like cells grown on these agarose scaffolds were subsequently found to align themselves in the direction of the micro-channels. Laser direct-write has also been used to pattern mouse embryonic stem cell distribution within gelatin (Raof *et al.*, 2011); these cells maintained their stem cell pluripotency as evidenced by persistent expression of Oct-4. Creation of micro-channels in scaffolds for peripheral nerve regeneration therefore constitutes another method that could be used to produce alignment of Schwann cells in a pattern akin to the bands of Büngner. Indeed, sculpting patterns into scaffolds using the MAPLE DW technique could be of general value in the production of biomimetic cellular architecture to solve various problems in tissue engineering.

2.5 Strategic design of scaffolds for nerve regeneration

The architecture, material, and even the fabrication process used to create a tissue engineering scaffold must be chosen with reference to, and with optimization for, the organ or tissue system being engineered. The unique structure and biological pathology of the peripheral nervous system imposes certain constraints. Biomimetic approaches that seek to duplicate or enhance the normally favorable aspects of peripheral nerve regeneration are likely to be successful (Winter and Schmidt, 2002). These include strategies to recreate endogenous healing mechanisms and appropriate mechanical environments within the engineered tissue (Willie *et al.*, 2010). Some strategies discussed here in the context of peripheral nerve regeneration might also prove applicable to other tissue engineering applications, such as the repair of central nervous system injuries. Some of the fabrication techniques discussed previously have already been implemented for the development of tissue engineering strategies in other organs.

2.5.1 Incorporation of cells within scaffolds

Previous studies have reported the incorporation of a variety of living cell types into scaffolds to support peripheral nerve regeneration, including Schwann cells, olfactory ensheathing cells (Imaizumi *et al.*, 2000) or neural stem cells (Guo and Dong, 2009). Living cells

can either be seeded into scaffolds upon completion of fabrication or incorporated during the scaffold manufacturing process, provided that harsh conditions are avoided.

As described earlier, Schwann cells of the distal nerve stump align themselves into bands of Büngner (Fawcett and Keynes, 1990) and the importance of this arrangement in promoting axonal growth is well documented (Taniuchi *et al.*, 1986). Since activated Schwann cells stimulate axon elongation (Torigoe *et al.*, 1996) following peripheral nerve injury, the incorporation of Schwann cells into tissue-engineered scaffolds is likely to be a beneficial strategy. Hall, (1986) shows that regenerating axons do not elongate through acellular nerve grafts in which the migration of Schwann cells is impeded. (Li, Yan, *et al.*, 2009) included Schwann cells and neural cells from the cortex of rats in composite scaffolds fabricated using alginate and gelatin. They found the cells to be viable for a week and also succeeded in seeding them in a gradient pattern. (Dewitt *et al.*, 2009) incorporated Schwann cells into composite scaffolds of Matrigel® and collagen. Although Schwann cells have a spherical morphology in collagen type I scaffolds, the addition of Matrigel resulted in increased elongation of Schwann cell processes (by 4.2 times), better survival of the cells, and superior mechanical properties.

Olfactory ensheathing cells are a type of macroglia exclusively located in the olfactory nerve that can continuously produce neurotrophic factors to mediate neuronal survival and axonal elongation (Ramón-Cueto *et al.*, 1998). In addition to enhancing axonal regeneration Radtke *et al.*, (2009), they can produce myelin under certain circumstances (Devon and Doucette, 1992) and have better migratory potential to penetrate glial scars. (Verdu *et al.*, 1999) show that bridging proximal and distal nerve stumps with a laminin-filled silicone tube does not repair resected rat sciatic nerves, but axonal regeneration is observed when olfactory ensheathing cells are seeded along with laminin. Olfactory ensheathing cells have also been examined for their potential use to promote spinal cord regeneration due their ability to promote growth of axons across the central/peripheral nervous system interface (Ramón-Cueto *et al.*, 1998), (Li *et al.*, 1997b).

Macrophages have a pivotal role in clearing the myelin and cellular debris during Wallerian degeneration of distal nerve tissue, thereby facilitating axon regeneration through this tissue (Perry *et al.*, 1987). There is *in vivo* evidence that macrophage recruitment could be important for the increase in NGF synthesis seen following nerve injury (Brown *et al.*, 1991). The peripheral nervous system receives ample infiltration by phagocytic cells (compared with

the central nervous system) and these are not usually included in peripheral nerve tissue engineering (Winter and Schmidt, 2002). However, enhanced recruitment of macrophages could be achieved by improving the vascularization of peripheral nerve scaffolds (Griffin *et al.*, 1993).

Besides the addition of supportive cells, their orientation in scaffolds is also necessary for the maintenance of adequate function. Alignment of myocytes in muscle repair scaffolds is pivotal for triggering adequate and forceful contractions along a specific direction (Shimizu *et al.*, 2009). Working with bone repair scaffolds, Kerschnitzki *et al.*, (2011) concluded that formation of oriented collagen matrices in bone, and in turn better mechanical strength, requires specific alignment of osteoblasts. In peripheral nerve repair, Seggio *et al.*, (2010) show that even in the absence of secondary guidance cues, a positive correlation exists between neurite outgrowth and orientation of the Schwann cells.

Random seeding of cells into scaffolds may be insufficient to permit subtle tracking of cell migration and reproduce biologically important cell–cell interactions. Also, close confinement of cells at high density may result in regulation of specific cell signaling, resulting in reduced cell motility and proliferation. Advanced scaffold fabrication techniques such as laser-based deposition and bioprinting could help achieve precise cell-deposition in tissue scaffolds, applicable to peripheral nerve regeneration. Othon *et al.*, (2008) showed that BioLP could be used to create three-dimensional hydrogel constructs with olfactory ensheathing cells confined in certain directions of the construct strands. This oriented arrangement significantly promoted the migration of the cells in the hydrogel, reaching up to 400 μm from their original printed position within 24 hours. Bioprinting also helps regulate the spatial arrangement of cells during fabrication and it could be exploited for the simultaneous use of different materials, thereby enabling construction of composite scaffolds. This may not be possible by means of conventional methods. With the bioprinting method, Schuurman *et al.*, (2011) fabricated composite scaffolds using cell-laden alginate and polycaprolactone. They showed that these composite scaffolds had better mechanical properties and also had the advantage of specific placement of various cell types in chosen patterns.

2.5.2 Incorporation of bioactive peptides within scaffold materials

Naturally occurring proteins, such as laminin (Yamada *et al.*, 2010), fibronectin (Mosahebi *et al.*, 2003a), and collagen (Sang *et al.*, 2011) or peptides derived from them can be

added to scaffold materials to enhance cellular activities. Laminin induces potent neurite outgrowth and thus promotes nerve regeneration over long distances (Malinda and Kleinman, 1996). Laminin is a heteromer composed of three protein subunits (A, B1 and B2) that each contain functional domains mediating interaction with various cell surface receptors (Mecham, 1991b). Synthetic peptides based on laminin sequences have been shown to have biological activity (Massia *et al.*, 1993). The peptides Tyr-Ile-Gly-Ser-Arg (YIGSR) and Cys-Asp-Pro-Gly-Tyr-Ile-Gly-Ser-Arg (CDPGYIGSR) on the B1 chain of laminin are involved in cell adhesion and migration (Graf *et al.*, 1987). YIGSR also prevents tumor metastasis (Witkowska *et al.*, 2004). The Ile-Lys-Val-Ala-Va (IKVAV) peptide sequence is found on the long arm of the A chain. This sequence is known to aid the growth of neurites (Tashiro *et al.*, 1989). The Arg-Gly-Asp (RGD) sequence in laminin is found in the short arm of the A chain (Tashiro *et al.*, 1991). This sequence is pivotal in cellular attachment through integrin receptors and is also a key sequence in another extracellular matrix protein, fibronectin.

Fibronectin is also a multimeric protein that is present in the extracellular matrix, but also exists as a soluble disulphide-linked dimer in plasma (Potts and Campbell, 1996). The fibronectin monomers consist of three different domains (F1, F2 and F3). In fibronectin, the RGD peptide sequence is found in a loop between the two β-strands of the domain F3 (Bork *et al.*, 1996). The RGD sequence is the primary integrin-dependent cell-binding site on fibronectin and is associated with cell adhesion.

Specific peptide sequences from other extracellular matrix proteins also can aid in neuronal regeneration. (Kajiwara *et al.*, 2005) investigated fetal hippocampal-derived neurospheres cultured on alginate gel. They observed adhesion and neurite outgrowth only when peptide sequences from the tumor necrosis factor receptor-1 protein were included in the alginate. The efficacy of peptides as growth-enhancing components depends on the expression of associated receptors in neural tissue (Meiners and Mercado, 2003; Yu and Shoichet, 2005).

Itoh *et al.*, (1999) show that axonal growth cones and Schwann cells have a high affinity towards laminin but may not recognize RGD sequences. However the YIGSR sequence of laminin enhances the adhesiveness of Schwann cells. Successful bridging of transected sciatic nerves was seen in rats when these transected nerves were grafted with silicone tubes filled with either Type I collagen fibers coated with laminin or the YIGSR sequence. The YIGSR sequence is thought to be recognized by receptors present on the growth cone or Schwann cell, promoting

their attachment and migration. Recently, laser transfer fabrication techniques have been employed in the transfer of peptide sequences to enhance cell adhesion. Spots of REDV peptide spots were transferred onto polyethylene terephthalate (PET) surfaces using LIFT. Human endothelial cells were layered over these peptide spots, and the patterned peptide was found to secure better attachment (Guillemot *et al.*, 2008). Similarly, Zouani *et al.*, (2009) deposited RGD peptides onto PET surfaces using the LIFT technique.

2.5.3 Incorporation of neurotrophic factors

The neurotrophin family of signaling molecules, including NGF, BDNF, NT-3, and NT-4/5, were initially thought to act primarily as regulators of neuronal survival. It is now clear that these neurotrophins are required for a variety of signaling functions in the regulation of development, maintenance, and function of the nervous system. They also control cellular differentiation, axonal growth, dendrite pruning and as well as the expression of various neural proteins and neurotransmitters (Huang and Reichardt, 2001). Since the acknowledgement of their diverse functions and mechanisms of action, many studies have incorporated the use of neurotrophins in peripheral nerve tissue engineering.

Artificial polysulfone nerve conduit tubes incorporating NGF and the extracellular matrix adhesion protein laminin promote successful nerve repair on par with autologous nerve implants (Yu and Bellamkonda, 2003). Synthetic polymeric scaffolds made of poly(lactide-co-glycolide) (PLGA) and coated with another neurotrophic protein, ciliary neurotrophic factor (CNTF), can repair 25-mm long canine tibial nerve defects (Shen *et al.*, 2010). Lee *et al.*, (2009) used copolymers of N-hydroxyl succinimidyl ester pyrrole and pyrrole and found that the addition of NGF to the copolymers favored neurite extension in neuron-like PC12 cells.

The use of hydrogels in the delivery of neurotrophins is advantageous due to their sustained-release behavior. Katz and Burdick, (2009) studied nerve conduits filled with the hydrogel poly(2-hydroxyethyl methacrylate-co-methyl methacrylate) along with NGF-loaded poly(D,L-lactide-co-glycolide) microspheres. The result was more sustained release of NGF compared to conduits without microspheres. The effective role of hydrogels as carriers of microspheres or other delivery methods is the subject of continuing study (Piotrowicz and Shoichet, 2006).

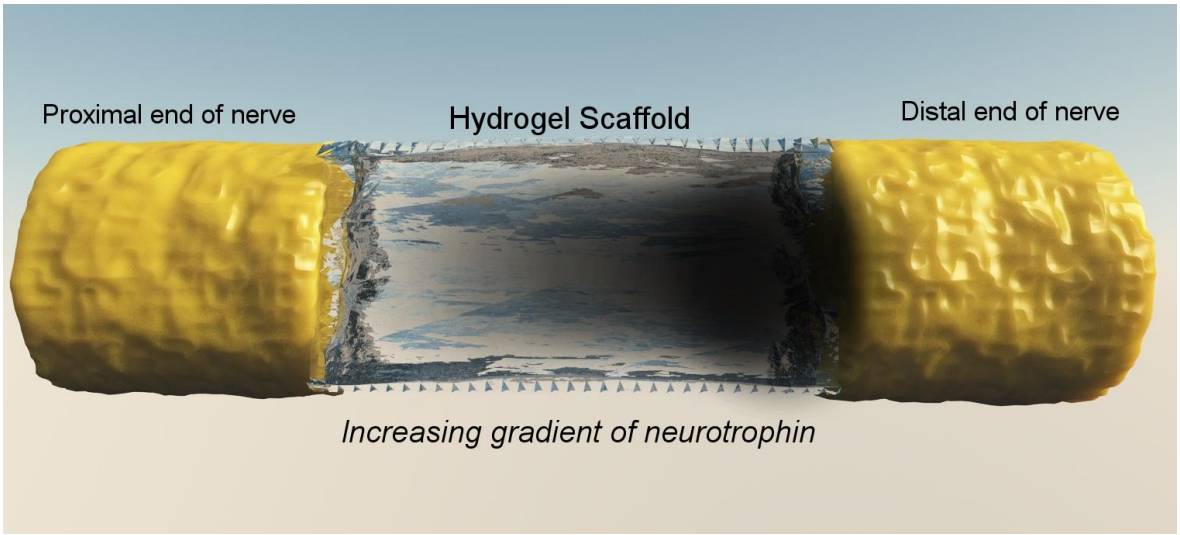

Figure 2.2 Schematic of a scaffold with a neurotrophic factor gradient.

Neurotrophins have also been encapsulated in microspheres made of various polymers such as chitosan, alginate, poly(lactic acid), poly(glycolic acid), poly(lactic-co-glycolic acid), and poly(caprolactone) (Maysinger *et al.*, 1996; Cao and Shoichet, 2003). Viral vectors have also been used to transfect genes that code for expression of neurotrophins (Berry *et al.*, 2001). Non-viral methods, such as transfection via lipoplexes, have also been used to introduce genetic material into cells (Whittlesey and Shea, 2006). Although a positive role of neurotrophins in peripheral nerve regeneration is widely recognized, a few studies indicate a potential 'dark-side' of these proteins and their receptors. Specifically, NT-4/5 may exacerbate free radical-induced necrosis of neurons both *in vitro* and *in vivo*. For example, neuronal death was accelerated upon addition of 10-100 ng/mL of NT-4/5 in neurons exposed to Fe^{2+} or L-buthionine-[*S, R*]-sulfoximine (Won *et al.*, 2000). Park *et al.*, (1998) report similar effects with 100 ng/mL BDNF or NGF, with the damage dependent on the level of neurotrophins. Prolonged activation of TrkB, a receptor for BDNF, may have some detrimental consequences for neuronal survival (Kim *et al.*, 2003). Thus, the optimal quantity and temporal profile of release of neurotrophins from the scaffold for efficient neuronal re-growth has yet to be established.

Higher concentrations of neurotrophins could saturate cell surface receptors and lead to receptor down-regulation (Zigmond, 1981). Hence controlled and graduated concentrations of neurotrophins (Fig. 2.2) could help as guidance cues to the growth cones of axons (Gundersen and Barrett, 1979). The axons are guided to their targets by a combination of contact mediated and diffusible cues, either attractive or repulsive (Paves and Saarma, 1997). Cao and Shoichet,

(2001) devised a model to estimate the minimal and maximal effective concentration gradients of NGF in a custom-designed diffusion chamber. The minimum concentration required to guide neurite outgrowth from PC12 cells was assessed and found to be 133 ng/mL per mm. Dodla and Bellamkonda, (2008) describe a polysulfone nerve conduit filled with agarose hydrogel imbued with different concentrations of laminin and NGF. The concentration varied between 8 and 33 µg/mL across four increasing step-gradients for laminin, and between 1.2 and 4.8 x 10^8 liposomal microtubules (containing NGF)/mL across similar increasing step-gradients. Regenerating axons were observed in rats implanted with these anisotropic scaffolds but were absent in those implanted with scaffolds without gradients (isotropic). Moore *et al.*, (2006) created a gradient hydrogel scaffold using a gradient maker with two inter-connected chambers; both were filled with p(HEMA) while only one chamber contained NGF. Spin bars blended both chambers as a peristaltic pump drove NGF-containing p(HEMA) into the p(HEMA) alone chamber, followed by extrusion of a hydrogel containing an increasing gradient of NGF. Although this system is capable of establishing a general global gradient, use of more recent fabrication techniques, such as bioplotting, permit better control over the configuration of gradients. Bioprinting techniques have been used to print spatially varying concentrations of neurotrophins by adjusting the printing resolution or number of dispensed droplets in a given area. Ilkhanizadeh *et al.*, (2007) printed a gradient of increasing levels of ciliary neurotrophic factor (CNTF) on poly-acrylamide-based hydrogel and found a linear increase in the expression of the astrocyte marker glial fibrillary acidic protein (GFAP) by neural stem cells cultured on the surface.

2.5.4 Electrical stimulation of scaffolds

Artificially applied electrical stimulation can enhance peripheral nerve regeneration (Al-Majed *et al.*, 2000; Brushart *et al.*, 2005; Geremia *et al.*, 2007). A strategy of electrical stimulation might usefully be incorporated into the design of nerve repair scaffolds. Conductive polymers are a subgroup of materials with electronic and ionic conductivity, such as polyaniline, polypyrrole, polythiophene, and polyacetylene. The conductive property of these polymers is the result of certain dopant ions that help carry charges as electrical current (Ravichandran *et al.*, 2010). These polymers have been used in the synthesis of biosensors, bioactuators (Otero and Cortés, 2003) and neural prosthetics (Abidian *et al.*, 2010). Polyaniline and poly(D,L-lactide)

electrospun at a ratio of 3:1 is electroconductive and cells seeded over these scaffolds are able to proliferate (McKeon *et al.*, 2010).

Weak electrical currents can accelerate axonal growth *in vitro*. For example, PC-12 cells grown on oxidized polypyrrole films show a two-fold increase in neurite outgrowth when subjected to weak electrical stimulation (Schmidt *et al.*, 1997). The growth of axons in a constant electrical field *in vitro* is dependent on the charge of the substratum: axons move towards the cathode on negatively charged laminin surfaces and towards the anode on positively charged poly-L-lysine coated surfaces (Rajnicek *et al.*, 1998).

Induction of weak direct currents by implanting an electric circuit in rats enhances nerve regeneration and increases blood supply, as seen by an increased in number and diameter of the vasa nervorum (Mendonça *et al.*, 2003) in association with enhanced axon regeneration. Thus, enhancement of vascular function (see below) may be a second beneficial outcome of electrical stimulation in nerve tissue engineering.

The beneficial effect of electrical stimulation on axon regeneration *in vivo* is greater if electrical stimulation is initiated rapidly following injury. Conversely, Yeh *et al.*, (2010) found better myelination in rat sciatic nerves stimulated two weeks post-injury than those immediately treated with weak currents. However the effects of electrical stimulation are not always positive. In a study involving nerve regeneration through silicone rubber chambers, electrical stimulation hindered the growth of axons across the gap, although it accelerated the maturation of regenerating nerves if applied later (Lu *et al.*, 2011). Moreover, McConnell *et al.*, (2009) report local, deleterious, inflammatory changes in tissue surrounding chronically implanted electrodes, akin to late-onset neurodegenerative diseases. Hence, electrical stimulation could have both positive and negative effects, depending on pattern, strength, and/or timing.

2.5.5 Addition of antioxidants

Oxidative stress can lead to apoptotic death of neurons (Greenlund *et al.*, 1995). Apoptotic death of cholinergic neurons can be induced by NGF withdrawal, but this is prevented by high concentrations (50 mM) of antioxidant ascorbic acid (Kew and Sofroniew, 1997). Rogério *et al.*, (2002) show that the antioxidant melatonin decreases neuronal death at doses of 1-50 mg/kg in rats. Acetyl-L-carnitine (ALCAR) also has inherent antioxidant properties and is involved in mitochondrial aerobic glycolysis (Tesco *et al.*, 1992). In a study by Wilson *et al.*,

(2007) long-term systemic administration of ALCAR at 50 mg/kg/day increased nerve regeneration after injury and also resulted in greater myelination, improving the innervation of target organs. Carnosine (beta-alanyl-L-histidine), also an antioxidant, is protective for PC12 cells subjected to excitotoxic stress caused by N-methyl-d-aspartate (NMDA) over-activation of glutamate receptors (Shen *et al.*, 2007). Kilmartin *et al.*, (2005) used NMR studies to evaluate the antioxidant properties of polyaniline and polypyrrole and observed that these substances could neutralize the damaging effects of 2,2-diphenyl-1-picrylhydrazyl (DPPH), a potent free radical. Thus, concurrent therapy with anti-oxidants, either administered systemically or included in nerve repair scaffolds, could be a useful strategy for tissue engineering targeting peripheral nerve repair.

2.5.6 Enhancement of angiogenesis

Proximity of a nutrient source is pivotal in the regeneration or growth of any cell or tissue type. *In vivo*, most cells lie within one to three cell widths of a capillary (Freitas Jr, 1999). Vascular compromise is prominent in most peripheral nerve injuries, including either the intrinsic or the extrinsic system of local blood vessels, or both. Incorporation of blood vessels within silicon conduits bridging nerve defects as long as 2-3 cm has been successful in rats (Kakinoki *et al.*, 1997). 'Feeder' blood vessels within artificial nerve conduits also help axons regenerate for longer distances (Kakinoki *et al.*, 1995). In current practice, a "vascularized nerve graft", or one that has viable blood supply, is often used to bridge a gap between transected nerve stumps. This attempt to maintain blood supply can also help sustain the Schwann cell population and decrease fibroblast infiltration (El-Barrany *et al.*, 1999). Podhajsky and Myers, (1993) show an increase in the endothelial surface area of local small blood vessels one week following crush injury of the rat sciatic nerve, followed by a decrease at three weeks. However, the pattern was bimodal and endothelial surface area increased again six weeks after the injury. The initial increase was attributed to endothelial hypertrophy and the later increase to an increase in the number of blood vessels.

The importance of coexisting capillary growth in promoting nerve regeneration has been emphasized by others (Goligorsky *et al.*, 1999; Papavasiliou *et al.*, 2010), but has received limited direct examination. In a study comparing angiogenesis following peripheral nerve injury, endoneurial capillaries were observed to sprout 5 mm distal to a nerve crush, repaired

transection, or ischemic injury, but not following a resection injury that created a gap (Nukada, 1988). Neovascularization following nerve injury could be promoted by signals arising either as a consequence of nerve ischemia or as an inherent aspect of the regenerative process (Nukada and Dyck, 1984). Delayed vascularization in most tissue-engineered scaffolds is attributed to the absence of a preexisting vascular network. (Penkert *et al.*, 1988) show that Schwann cells can survive for only one week in a graft without blood supply.

Nitric oxide (NO) is a short-lived signaling molecule with multiple functions, including action as a potent modulator of vascular growth. Three isoforms of nitric oxide synthase (NOS) are expressed in peripheral nerve: neural NOS (nNOS) accumulating in growing axons of regenerating peripheral nerves, inducible NOS (iNOS) expressed in the invading macrophages, and endothelial NOS (eNOS) expressed by blood vessels in the vasa nervoram (González-Hernández and Rustioni, 1999). Nerve regeneration and vascularization are delayed in endothelial nitric oxide synthase (eNOS) knockout mice when compared with wild-type mice (Keilhoff *et al.*, 2002). Specific inhibition of eNOS using antisense oligodeoxynucleotides inhibits vascular remodeling (Goligorsky *et al.*, 1999). Thus, incorporating a source of NO in scaffolds could be useful for peripheral nerve engineering to promote simultaneous establishment of new capillaries concurrent with axon regeneration

Vascular endothelial growth factor (VEGF) is also a fundamental regulator of both normal and abnormal angiogenesis (Ferrara, 1999). VEGF induces endothelial sprouting from sources of endothelial tissue embedded in collagen gel (Nicosia *et al.*, 1994). Aizawa *et al.*, (2010) show that the movement of endothelial cells can be guided in three dimensional hydrogels by concentration gradients of VEGF. This could thus be a promising strategy to enhance blood vessel growth into artificial tissue scaffolds. Hobson *et al.*, (2000) assessed the effects of VEGF on the enhancement of vascularization and indirectly, on axonal regeneration in damaged nerve. VEGF and the synthetic extracellular matrix product Matrigel were enclosed in a nerve conduit and implanted into rats to bridge a sciatic nerve transection. After 180 days, the number of regenerated and myelinated axons was 78% greater when compared to control conduits lacking VEGF. In another study, Lee *et al.*, (2010) constructed three dimensional scaffolds incorporating murine neural stem cells, collagen, and VEGF-releasing fibrin gel. The neural stem cells in closest proximity to the VEGF-releasing fibrin gel demonstrated better morphological changes as

well as migratory responses. Thus, VEGF could have roles beyond angiogenesis in neural regeneration.

Novel delivery techniques for VEGF have also been explored. Kim and Kiick, (2010) propose the use of a specific polyethylene glycol-low molecular weight heparin (PEG-LMWH) hydrogel for carrying VEGF. VEGF was well contained in these hydrogels, due to its interaction with heparin, but was released for specific interaction with the VEGF receptor-2 (VEGFR-2). Similarly, Golub *et al.*, (2010) demonstrated sustained release of VEGF from poly(lactic-co-glycolic acid) (PLGA) nanoparticles, leading to enhanced blood vessel growth in mouse femoral artery ischemia models. Thus, patterned hydrogels could be synthesized to include bioactive substances enabling sustained delivery at specific sites. The benefits of vascular growth in parallel to nerve regeneration are apparent in many studies and bioengineering efforts to enhance peripheral nerve regeneration might include strategies that utilize factors and techniques that aid angiogenesis. With recent advances in fabrication techniques, supportive nerve cells and vascular endothelial cells could be printed simultaneously. Gaebel *et al.*, (2011) showed that LIFT-based seeding of cells enhanced cell survival and modified their growth characteristics leading to increased blood vessel formation. Better formation of vessel-like structures was attributed to the precise control of arrangement of endothelial cells using the LIFT technique. Khalil and Sun, (2009) used a bioprinting fabrication system to print alginate scaffolds with a cell suspension of rat heart endothelial cells. Besides endothelial cells, VEGF has also been incorporated in fibrin gels and printed into collagen scaffolds using a bioprinter, to enable sustained release of the growth factor (Lee *et al.*, 2010).

2.6 Conclusions and future perspectives

Much progress has been made since the earliest use of biomaterials as simple conduits in nerve regeneration. Techniques to incorporate neurotrophins, and control their release (Pfister *et al.*, 2008) or produce gradients (Kapur and Shoichet, 2004) have been achieved. Material modification with peptide sequences have made scaffolds more adhesive, aiding in accelerated neural repair. Methods to promote adjunct angiogenesis (Hobson *et al.*, 2000) are also of key interest. Recent advances in fabrication technology show great promise for even more sophisticated, precise and combinatorial strategies, thus generating synergy, in peripheral nerve repair.

Though techniques to fabricate scaffolds with precise resolution are constantly explored or improved, methods to assess and visualize tissue growth or axonal regeneration *in vivo* are in need of improvement. Particularly useful would be the improvement of two photon imaging, diffusion tensor imaging, and ultrasound-based techniques to enable better monitoring of cell distribution during the process of nerve repair. Two-photon excitation can be used to visualize autofluorescent cells seeded onto three dimensional scaffolds (Schade *et al.*, 2010), where most of the seeded cells remain close to the scaffold surface. This technique might also help assess cellular distribution in more sophisticated scaffolds where cell distribution is micropatterned during the fabrication process, as the scaffold need not be sectioned or manipulated for imaging. Diffusion tensor imaging (DTI) is a magnetic resonance-based technique that provides good imaging contrast and resolution to visualize nerve tracts (Le Bihan *et al.*, 2001). This technique could be used to monitor nerve fiber content within scaffolds and along distal pathways toward peripheral targets. Hence, nerve regeneration *in vivo* could be assessed non-invasively. Ultrasound elasticity imaging (UEI) is a technique that images objects based on the induction of distortions, which reflect the elastic properties of the object being investigated (Svensson and Amiras, 2006). Speckle tracking has been used extensively in echocardiography (Blessberger and Binder, 2010), and was recently used to non-invasively assess the degradation of poly (1,8-octanediol-co-citrate) scaffolds both *in vivo* and *in vitro* (Kim *et al.*, 2008). Further development of these techniques is needed for more effective monitoring and analysis of nerve regeneration *in vivo.*

The emerging fabrication techniques are themselves poised to be refined further for the advanced design of artificial scaffolds for applications such as peripheral nerve tissue engineering. Novel methods can be developed to simultaneously incorporate biomaterials such as growth factors or adhesive peptides along with living cells or other associated components that would closely mimic the natural environment and physiology of the tissue targeted for repair. Research aimed at understanding the cellular mechanisms of repair and further improving the engineering of biofabrication is likely to overcome some of the short-term impediments to the successful use of scaffolds to promote the improved repair of peripheral nerve injury.

CHAPTER 3

BIOPLOTTING ALGINATE/HYALURONIC ACID HYDROGEL SCAFFOLDS WITH STRUCTURAL INTEGRITY AND PRESERVED SCHWANN CELL VIABILITY*

*This chapter has been published as "Rajaram A, Schreyer D, Chen D. (2014) Bioplotting alginate/hyaluronic acid hydrogel scaffolds with structural integrity and preserved Schwann cell viability. *3D Printing and Additive Manufacturing*. 1(4): 194-203". According to the Copyright Agreement, "the authors retain the right to include the journal article, in full or in part, in a thesis or dissertation".

3.1 Introduction

Bioplotting entails the extrusion of a biomaterial mixed with living cells to create tissue scaffolds for repairing or replacing damaged tissues or organs in tissue engineering (Chien *et al.*, 2013). Since the biomaterial is extruded layer-by-layer, a mechanically-stable structure can be created with interconnected pores favorable for the transport of nutrients. Due to its ability to continuously deposit material(s), an extrusion-based system can be used to fabricate tissue scaffolds with more complicated, yet repeatable, structures than conventional methods, such as solvent casting, freeze-drying, and leaching (Yeo and Kim, 2014).

Compared to seeding cells over prefabricated scaffolds, incorporation of living cells during bioplotting allows better organization of the cellular components within scaffolds, including the uniformity in cell deposition and the ability to organize cell distributions to mimic the cellular organization of the intended tissue type (Nicodemus and Bryant, 2008). Bioplotting with living cells requires the use of a biomaterial that can be handled in aqueous and physiologically mild conditions. These materials are typically hydrogels made from natural carbohydrate or protein biopolymers and/or other synthetic polymers. Recently, the use of three dimensional (3D) biofabrication techniques has shown promise in the fabrication of hydrogel-based structures laden with various types of cells. Fedorovich *et al.*, (2008) used bioplotting to print various hydrogels with bone marrow stem cells. They showed good cell viability after the extrusion process and were also able to combine two distinct cell populations within a single scaffold. Schuurman *et al.*, (2011) constructed scaffolds by alternate deposition of polycaprolactone fibers and alginate hydrogel containing C20A4 cells, a chondrocyte cell line.

These studies illustrate that by using 3D biofabrication techniques, scaffolds with spatial variations of more than one lineage of cells or different biomaterials could be fabricated.

Hydrogels, either natural or synthetic, have been drawing considerable attention since they were first used to encapsulate pancreatic islet cells three decades ago (Lim and Sun, 1980). The high water content and tissue-like properties of most hydrogels make them ideal materials to encapsulate cells. Various hydrogels such as alginate, hyaluronic acid (HA), gelatin, type I collagen, fibrin, Extracel^{TM} hydrogel, methylcellulose, chitosan and polyethylene glycol have been used for 3D scaffold fabrication (Murphy *et al.,* 2013). Alginate is a polysaccharide hydrogel, which is ionically crosslinked either in the presence of divalent ions such as calcium or barium, or by covalent methods (Christensena, 2011). Chemical crosslinking could compromise cell viability due to the harsh reaction conditions or the production of toxic intermediate products. However, ionic crosslinking of alginate using calcium chloride occurs under biocompatible conditions (Drury *et al.*, 2004a; Khalil and Sun, 2009; Song *et al.*, 2011) allowing for the incorporation of living cells during the fabrication process.

HA is a glycosaminoglycan with repeating disaccharide units of glucuronic acid and N-acetylglucosamine residues (Fraser *et al.,* 1997a). It is a ubiquitous extracellular tissue matrix substance and has been known to promote peripheral nerve regeneration. HA prevents perineural scar formation during nerve repair and thereby improves peripheral nerve regeneration (Ozgenel, 2003).

Composite alginate/HA hydrogels have good mechanical properties, once crosslinked with calcium chloride (Wang *et al.*, 2013). The interaction of HA with water significantly decreases the rate of weight loss of alginate/HA beads (Oerther *et al.,* 1999), indicating improved stability. HA films containing vascular endothelial growth factor have been shown to improve electrophysiological and histological parameters in rats with transected sciatic nerves (Zor *et al.*, 2014).

Inspired by these studies, the present study was aimed to fabricate alginate/HA hydrogels containing Schwann cells for use in peripheral nerve repair. Schwann cells provide haptotactic cues to axons and axonal outgrowth across a tissue lesion is accelerated in the presence of Schwann cells in peripheral nerve (Son and Thompson, 1995b). Mosahebi *et al.*, (2002) have shown that including allogeneic Schwann cells in alginate-filled nerve repair conduits enhanced axonal regeneration without inducing an immune response. Schwann cell-filled nerve scaffolds

have also promoted functional recovery in rats with 2 cm long deficits in the median nerve (Sinis *et al.*, 2005).

The plotting of alginate and other composite hydrogels into scaffolds is a challenging task since many parameters, such as polymer concentration and viscosity, dispensing pressure, nozzle diameter, dispensing speed, and crosslinking, can affect the scaffold fabrication (Maher, Keatch, Donnelly, Mackay, *et al.*, 2009; Nair *et al.*, 2009). Ahn *et al.*, (2012) used a nebulization technique and sprayed aerosolized calcium chloride solution over the surface of alginate struts dispensed on to a dry surface. However, dispensing low volumes of less concentrated alginate solution onto a dry surface can eventually lead to drying of the hydrogel, thereby compromising the viability of incorporated cells. If dispensing scaffold materials in an aqueous medium, the crosslinking medium itself also needs to be biocompatible to ensure cell viability. Strand buoyancy must also be controlled in order to prevent newly dispensed strands from floating in the medium during scaffold production (Pfister *et al.*, 2004). Another important issue when bioplotting alginate is to ensure that the first layer of alginate adheres to the platform surface to prevent the collapse or disruption of the structure as more layers are stacked on it. The key factors for effective bioplotting include the enhancement of adhesion between the initial layer of hydrogel to the plotting surface and minimizing the density gradient between the hydrogel and the dispensing medium to achieve buoyancy compensation (Landers, Hübner, *et al.*, 2002).

In the present study, we addressed the preliminary requisites for bioplotting to enable effective fabrication of alginate-based scaffolds containing HA and living Schwann cells. We modified the platform for improved adhesion of the first scaffold layer and used a modified ionic crosslinking solution to improve structural control while retaining cell viability. We also characterized the bioplotting process in terms of scaffold strand width and interstrand spacing in single-layered scaffold patterns, and monitored the longer-term viability of incorporated cells after completion of scaffold fabrication.

3.2 Materials and methods

Alginate (sodium salt from brown algae), hyaluronic acid (HA) (sodium salt from *Streptoccous equi*), polyethyleneimine (PEI) (MW 750,000, 50% w/v in H_2O), poly-l-lysine (PLL), glycerol, calcium chloride and polyvinyl alcohol (PVA) (MW 85,000-124,000) were purchased from Sigma Aldrich, Canada. PEI (MW 60,000, 50% w/v in H_2O) was purchased

from Alfa Aesar, MA, USA. Calcein-AM and propidium iodide were purchased from Anaspec, CA, USA.

3.2.1 Cell culture

RSC96 cells (ATTC, VA, USA), an immortalized rat Schwann cell line, were cultured using Dulbecco's Modified Eagle's Medium (DMEM) (Sigma, Oakville, ON, Canada) supplemented with 10% fetal bovine serum (HyClone, Logan, UT, USA) in a 37°C humidified environment containing 5% CO_2.

Primary rat Schwann cells were isolated according to the D-valine selection method described by (Kaewkhaw *et al.*, 2012). These were also maintained in DMEM with 10% fetal bovine serum in a 37°C humidified environment containing 5% CO_2. Primary Schwann cells do not proliferate as quickly as RSC96 cells, thereby providing an advantage for culturing at longer time intervals.

3.2.2 Polycationic surface for improved alginate/hyaluronate adhesion

Alginate has an anionic charge at physiological pH, and the polycation PEI has been used as a coating over microfluidic devices to enable surface adhesion of alginate (Johann and Renaud, 2007). To promote adhesion of alginate to the plotting surface during the scaffold fabrication technique, tissue culture plates used as receiving platforms were coated with varying concentrations of sterile PEI (MW 60,000 and 750,000; in 10 mM phosphate buffered saline) and incubated overnight at 37°C. The plates were then washed with sterile water before use in scaffold fabrication.

To assess the biocompatibility of PEI-coated surfaces, RSC96 cells were cultured in PEI-coated 96-well plates for 12 hours. A 3-(4,5-dimethylthiazol-2-yl)-2,5-diphenyltetrazolium bromide (MTT) conversion assay was performed to confirm viability of the cells. MTT solution (5 mg/ml) was added to each well and the plate was incubated again for 5 hours. The medium was aspirated from all wells and dimethyl sulfoxide was added to solubilize the formazan reaction product. The absorbance of each well was measured at 560 nm using a micro-plate reader (Molecular Devices SpectraMax 340, California, USA). Control wells did not include PEI, but were coated with PLL, which is a commonly-used polycationic substrate for the culture of Schwann cells and dorsal root ganglion cells (Vleggeert-Lankamp *et al.*, 2004).

3.2.3 Bioplotting of alginate/hyaluronate scaffolds

Alginate/HA scaffolds were fabricated using a 3D-Bioplotter® (Envisiontec GmbH, Germany). The 3D-Bioplotter® is a pneumatic-based three-axis dispensing machine, which can be used to build scaffolds layer-by-layer. Scaffold designs were programed using CAD software to control the dispensing process. A solution containing alginate and HA (2.5% w/v alginate and 0.25% w/v HA) was dispensed and plotted into the crosslinking solution using a steel-tip dispensing needle (EFD Nordson, Westlake, OH, USA) with an inner diameter of 100 µm. The plotting head was programmed to move the dispensing needle horizontally along the X or Y-axis at a speed of 4 mm/s and the pneumatic pressure driving extrusion of alginate/HA was set to 1.2 bar (17.4 psi). In the present study, the scaffold was designed to have 16 layers, each having a height of approximately 125 µm, and an overall rectangular cuboid geometry of 10 × 3 × 2 mm (Fig. 3.1). Inter-strand spacing was set to 500 µm (measured between the centers of adjacent strands). The extrusion of biomaterial was continuous for each layer, but was interrupted and resumed for each subsequent layer. Strands dispensed in each layer were oriented perpendicular to those in the previous layer. The time elapsed for fabricating such a 3D scaffold was about 5 minutes.

The alginate/HA strands were plotted into a solution containing 100 mM calcium chloride, 25 mM HEPES buffer pH 7.4, 0.1% w/v PEI, and 0.95% w/v PVA. Low concentrations of PEI are known to increase the crosslinking of alginate (Devi *et al.*, 2007) and PVA was included to prevent the strands from floating as they were being plotted. In some experiments PEI and/or PVA were omitted for comparison.

To create single–layered hydrogel patterns (strands with width of approximately 110 µm printed in a 10 x 10 mm pattern) alginate/HA biomaterial of the same composition were plotted using the 3D-Bioplotter® with the same dispensing needle and plotting parameters, but onto a PEI-coated surface in the absence of the crosslinking solution (i.e. in air). To prevent the hydrogel from drying and to enable crosslinking, a nebulized solution of 100 mM calcium chloride and 25 mM HEPES was sprayed over the hydrogel patterns as they were plotted. Afterward, they were immersed into the crosslinking solution (100 mM calcium chloride and 0.95% PVA in 25 mM HEPES) to complete the crosslinking process at the end of 5, 15, or 30 minutes.

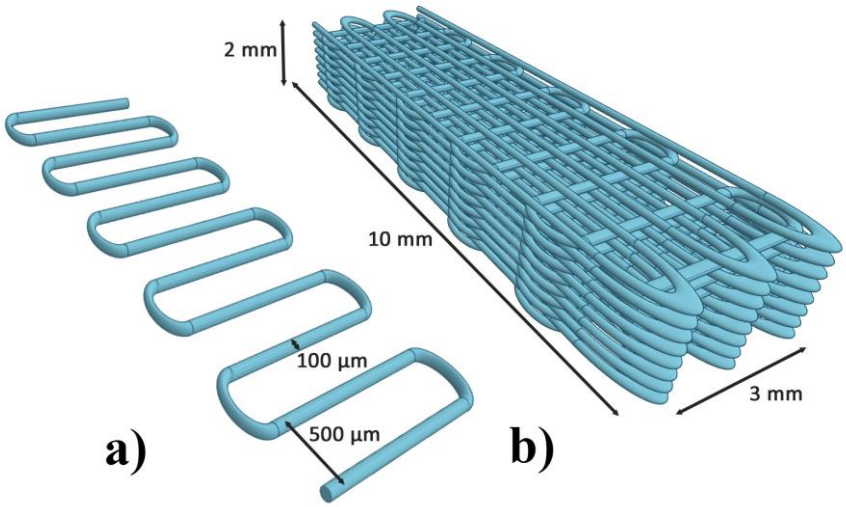

Figure 3.1 a) Single layer of plotted hydrogel pattern. b) Multi-layered (16 layers) 3D hydrogel scaffold with dimensions of 10 x 3 x 2 mm.

3.2.4 Evaluation of print fidelity

The intended strand dimensions and interstrand spacing programmed on the software controlling the 3D-Bioplotter® machine were compared with their actual dimensions as measured post-fabrication. This gives a measure of the 'print fidelity' and depends on the properties of the hydrogel material and the accuracy of the dispensing technique (Chung *et al.*, 2013). A single-layer pattern (Fig. 3.1a) was bioplotted either into the crosslinking solution or in air and then imaged. The strand width and inter-strand distance of the patterns were measured on the images. The dispensing pressure was fixed, while the horizontal speed of needle was varied. The intended strand width was 100 µm (the needle internal diameter) and the interstrand spacing was set at 500 µm, measured between the mid-points of adjacent strands.

3.2.5 Evaluation of cell survival after dispensing

We used a calcein-AM/propidium iodide microscopic assay (Anaspec, CA, USA) to study the effects of the scaffold fabrication technique on cell viability. A suspension of RSC96 cells or primary Schwann cells (5.2×10^5 cells/ml) in 50 µL of DMEM with 10% FBS was mixed with the alginate/HA solution and then plotted either into the crosslinking solution containing 100 mM calcium chloride, 25 mM HEPES, 0.1% w/v PEI (0.05 % to 0.2% w/v), and PVA (0.95 % w/v) or into a similar solution containing glycerol (35% v/v) instead of PVA. The crosslinking solution was removed after 5 minutes and the single-layer scaffolds (strands with a width of

approximately 120 μm printed in a 10 x 10 mm pattern) were washed thrice with a solution of 0.35 M sucrose and 4.2 mM HEPES, then maintained under standard culture conditions. Short term viability of RSC96 cells was assessed on single-layered patterns up to 30 min after crosslinking.; Viability of primary Schwann cells was assessed on days 0 (1 hour after dispensing) 3, 10, and 21.

Cell viability was compared between strands plotted into the crosslinking solution and those plotted over a surface (in air) and nebulized with 100 mM calcium chloride and 25 mM HEPES. The patterns plotted in air were nebulized with 100 mM calcium chloride for 5, 15, or 30 minutes and then immersed into the crosslinking solution for 5 minutes to complete the crosslinking process. The patterns plotted directly into the crosslinking solution were held in the solution for a comparable 5, 15, or 30 minutes before carrying out the viability assay.

A solution of DMEM containing calcein-AM (8 μl/ml) and propidium iodide (15 μl/ml) was added to each sample and incubated for one hour at 37°C. Calcein-AM is converted into a fluorescent calcein dye by intracellular esterase activity to label live cells, while the staining of cells with propidium iodide (cell membrane impermeant) is specific to dead cells. The viability of cells was assessed by counting the live (green fluorescent) and dead (red fluorescent) cells (Fernandez *et al.*, 2000) on images captured using a fluorescent microscope (Carl Zeiss Axiovert 100). Images were randomly taken from each of three single-layered patterns in all test conditions (n = 10) and analyzed using ImageJ (National Institutes of Health, Bethesda, Maryland, USA). The viability was calculated as the percentage of live cells among the total number of live and dead cells detected.

3.3 Data analysis

The mean and standard error of the mean (SEM) of the data were calculated for each experimental test. Statistical significance was assessed by a one-way or two-way analysis of variance (ANOVA) followed by the Tukey's 'honestly significant difference' (HSD) test using Graphpad Prism 5.0a (GraphPad Software, San Diego, CA, USA). Statistical significance was accepted at the level of $p<0.05$, estimated for comparisons between groups.

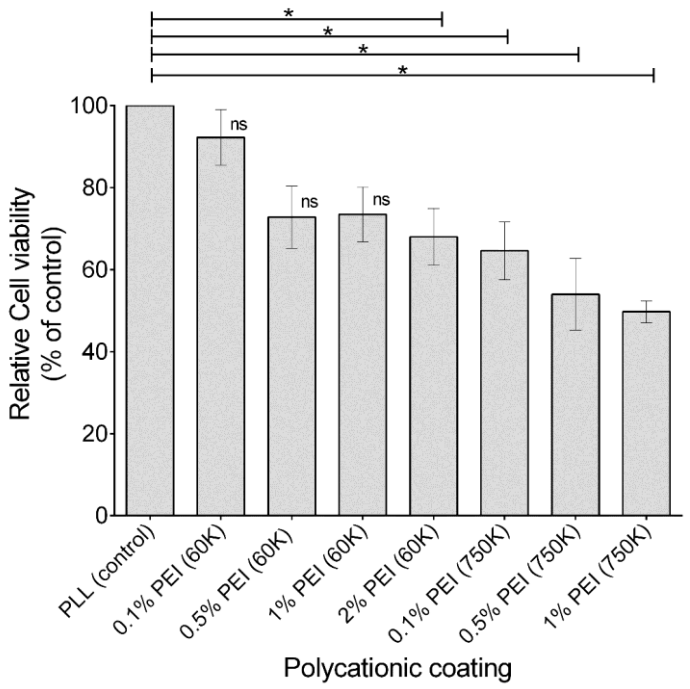

Figure 3.2 MTT assay comparing viability of RSC96 cells at the end of 12 hours when grown on surfaces coated with different concentrations of PEI [n = 8; * $p<0.05$; ns = not significant when compared with PLL].

3.4 Results

Dispensed strands of alginate/HA were well adhered to the surfaces coated with both the high and low molecular weight formulations of PEI. Firm attachment of alginate/HA onto the surface was ascertained as the plotted gel strands had a regular and reproducible shape and did not detach after fabrication or washing with phosphate buffered saline.

The MTT assay was used to assess the viability of cells grown 12 hours on PEI-coated surfaces (Fig. 3.2). Culture plates coated with 0.1% PEI (MW 60,000) supported cell viability of greater than 90%, as compared to PLL control cultures. Coating the plates with higher concentrations of PEI (MW 60,000) appears to further reduce cell viability; and this effect becomes statistically significant when 2% PEI (MW 60,000) is used as compared to the control. Coating the plates with the high molecular weight form of PEI (MW 750,000) significantly reduce cell viability even at modest concentrations, 0.1 – 1%.

Plotting alginate/HA into a simple calcium chloride/HEPES solution did not result in good scaffold architecture as the alginate/HA strands lifted up on the edges due to mismatched buoyancy between the hydrogel and calcium chloride solution. After preliminary trials in which

scaffolds were plotted into crosslinking medium containing varying concentrations of PVA (0.7% to 1.10% w/v) or glycerol (25% to 40% v/v), the concentrations of these components which most effectively eliminated the buoyancy effect were found to be 0.95% w/v and 35% v/v, respectively (data not shown). Inclusion of PEI in the crosslinking medium appeared to enhance gelation and intra-strand adherence of alginate/HA. A comparison of 3D scaffolds fabricated in the presence and absence of PVA and PEI is shown in Fig. 3.3. Having obtained good adhesion and structure with single-layer scaffolds, we fabricated 3D alginate/HA scaffolds with dimensions of 10 x 3 x 2 mm. With the presence of PEI and PVA in the calcium chloride crosslinking solution, a good 3D scaffold structure containing vertically interconnected pores was achieved (Fig. 3.4).

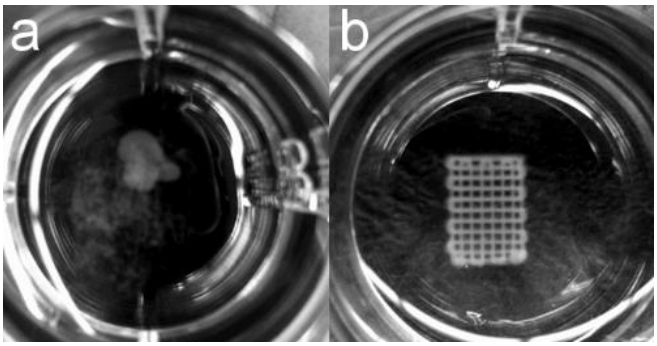

Figure 3.3 10 x 6 x 2 mm alginate/HA scaffold fabricated a) without PVA and PEI in the crosslinking solution b) with 0.95% PVA and 0.1% PEI in the crosslinking solution.

Greater control of the geometry of dispensed biomaterial strands was obtained when plotting alginate/HA into a liquid crosslinking medium, as compared to plotting into air and crosslinking with a nebulized solution (Fig 3.5). When a single-layered pattern of alginate/HA was plotted in air at a dispensing speed of 4 mm/s, the resultant strand width was measured at 462±5 μm (about 4.5 times of the needle internal diameter , 100 μm). Increasing the dispensing speed to 8 mm/s resulted in strand width of 353±7 μm. The significant difference between the strand width obtained and the diameter of the dispensing needle diameter is mainly caused by the initial spread of the alginate/HA solution when plotted over the platform surface. When using the same dispensing needle to plot strands into liquid crosslinking medium, we obtained strand widths of 108±2 μm and 53±4 μm at plotting speeds of 4 mm/s and 8 mm/s, respectively (Fig. 3.6). These findings suggest that when plotting strands into liquid crosslinking medium, the

spread of the stands can be significantly reduced due to buoyancy and rapid gelation in liquid, and that the strand width is linearly dependent on the horizontal speed of the dispensing needled. Decreased strand width resulted in increased interstrand spacing (Fig. 3.6b) which ultimately leads to the creation of scaffolds with higher porosity.

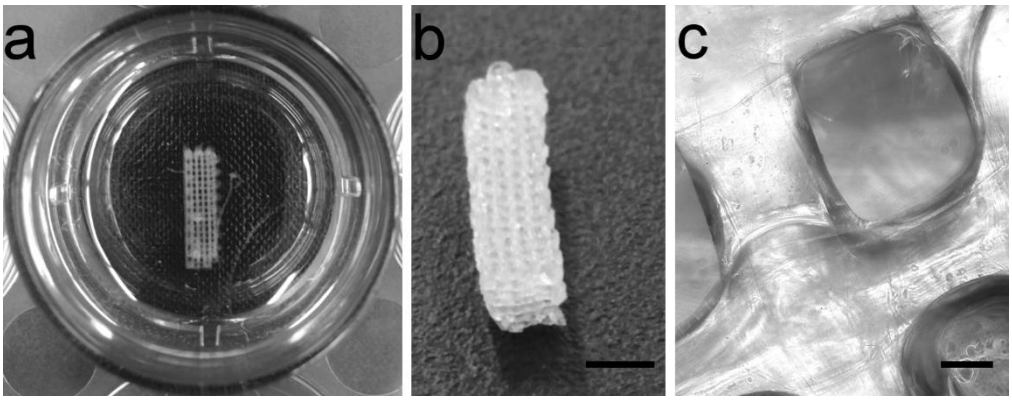

Figure 3.4 a) Alginate/HA scaffold in crosslinking solution immediately after being plotted. b) Scaffold imaged after being removed from the crosslinking medium (scale bar = 3 mm). c) Microscopic image of scaffold showing its porous structure (scale bar = 100 μm).

The calcein-AM/propidium iodide assay was used study the biocompatibility of crosslinking medium additives. RSC96 cell viability within alginate/HA 5 min after dispensing into a simple calcium chloride/HEPES crosslinking medium was 64% (Fig.3.7). No significant change was seen with the inclusion of 0.1% PEI in the solution. However, with the addition of 0.95% PVA, the RSC96 cell viability increased significantly to 83%. Conversely, although scaffolds with good structural integrity were successfully plotted when using 35% v/v glycerol in the crosslinking medium (Maher, Keatch, Donnelly, and Paxton, 2009), the viability of RSC96 cells was reduced drastically if glycerol was substituted for PVA (Fig. 3.7a). Because PEI is known to be toxic to cells, we studied whether soluble PEI in the crosslinking medium could be tolerated as well as surface-adsorbed PEI. We found no significant effect of PEI in the crosslinking solution at lower concentrations (0.05 - 0.1% w/v) but a nearly 25% reduction (68.8 ± 1.2) in cell viability when PEI was included at a concentration of 0.2% (Fig. 3.8). Thus we were able to show that a 0.1% concentration of PEI in the crosslinking solution that was effective in improving crosslinking of alginate/HA during fabrication of the scaffolds was safe for cell viability.

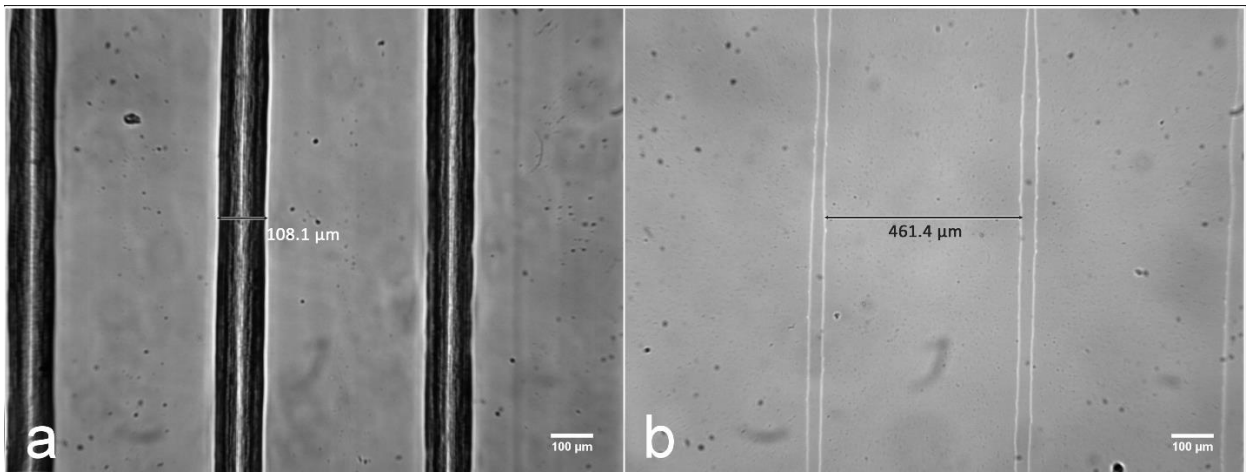

Figure 3.5 a) Alginate/HA strands plotted into crosslinking medium. b) Strands plotted in air. Measurements denote strand width. Intended dimensions: strand width of 100 µm and interstrand spacing of 500 µm, center to center.

We studied the feasibility of plotting scaffolds in air by dispensing alginate/HA containing RSC96 cells onto a dry platform, nebulizing the strands for 5, 15 or 30 min with calcium chloride/HEPES solution, then flooding them with crosslinking solution for 5 minutes. The viability of RSC96 cells dispensed in air was measured at 61%, 5%, and 0% after being nebulized with calcium chloride solution for 5, 15 and 30 minutes, respectively (Fig. 3.9). By comparison, when plotting the strands directly into the crosslinking solution, RSC96 cell viability was 91%, 77%, and 68% after 5, 15 and 30 minutes, respectively.

The long-term cell viability of primary rat Schwann cells was studied after using a dispensing process optimized for best results (Fig. 3.10). Primary Schwann cells were suspended in alginate/HA, then dispensed into complete crosslinking medium containing optimal concentrations of PVA and PEI. Exposure to this (non-physiological) solution was limited to 5 minutes before the completed scaffolds were transferred to standard tissue culture conditions. We found that, similar to the RSC96 cells, primary Schwann cell viability is at a value of 92.3% immediately after plotting, then increases to 94.3% on Day 3, and is maintained at 83.2% at the end of 3 weeks. It should be noted that our cell measurements at multiday survival intervals were likely influenced not only by the death rate, but also by cell proliferation and disappearance of dead cells.

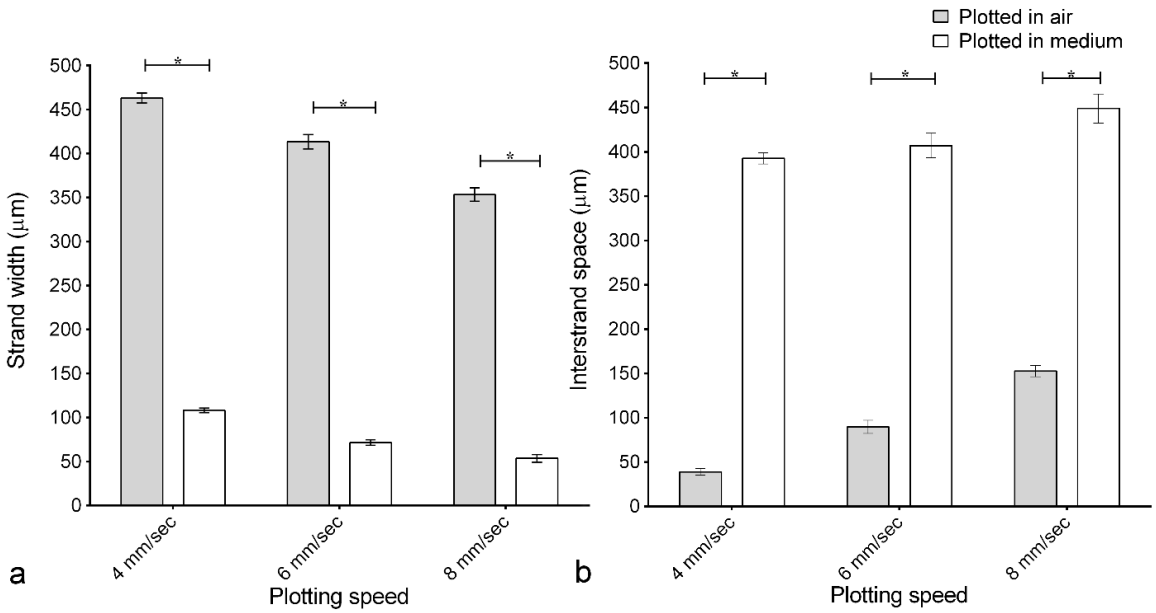

Figure 3.6 a) Strand width compared between patterns plotted in air or plotted into liquid medium at different plotting speeds. b) Interstrand space compared between patterns plotted in air or plotted into liquid medium at different plotting speeds [n = 5; *p < 0.001].

3.5 Discussion

Alginate can be ionically crosslinked in a calcium chloride solution. Although high concentrations of calcium ions could damage cellular membranes, Cao *et al.*, (2012) showed that encapsulating RSC96 cells in alginate resulted in better viability, even at relatively high concentrations of calcium. Best results are obtained when exposure to high calcium is brief.

PEI interacts with alginate to enhance crosslinking (Devi *et al.*, 2007). However, PEI was primarily used in this study to enhance alginate adhesion. The negative charges of alginate interact strongly with positively charged PEI coated surfaces. Chen *et al.*, (2010) used a 0.5% w/v of PEI to coat the interior of microfluidic channels and found this to improve the adhesion of alginate to a glass surface. In the present study, we found that coating with the polycation PEI could stabilize the first layer of alginate-based materials. Also, we noticed that when single layers of alginate/HA containing cells were plotted on PEI-coated surface, the layers did not detach from the surface during the culture process. This also facilitates easier examination of the contained cells during imaging as the strands do not move while being imaged. On the uncoated surface, however, the plotted alginate/HA detached when it was immersed in the culture medium for few days.

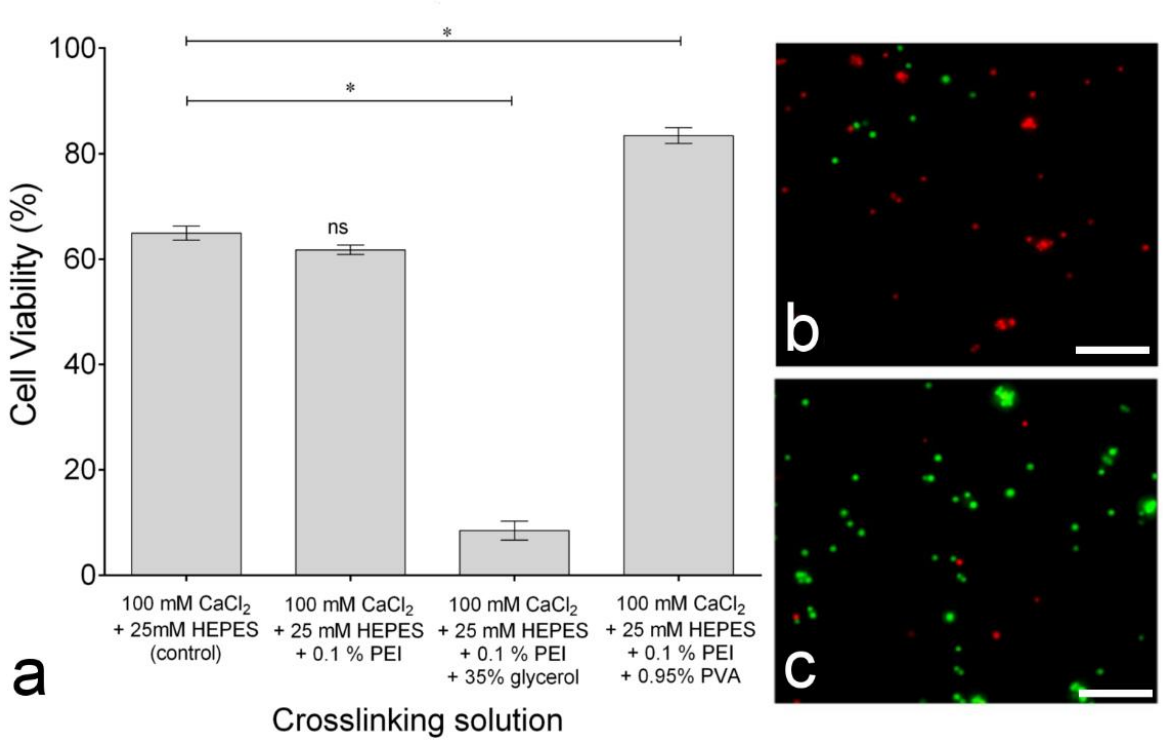

Figure 3.7 a) RSC96 cell viability in alginate/HA strands 5 min after bioplotting into different crosslinking solutions [n = 10, *p < 0.0001; ns = not significant when compared with control]. b) RSC96 cells in alginate/HA strands stained with calcein-AM (green) and propidium iodide (red) after plotting into crosslinking solution containing 35% v/v glycerol. c) RSC96 cells in alginate/HA strands stained with calcein-AM (green) and propidium iodide (red) after plotting into crosslinking solution containing 0.95% w/v PVA (scale bar = 100 µm).

Because exposure to PEI may damage cells, we explored a range of PEI coating conditions and found that coating the surface with a low concentration of 0.5% PEI (M_w 60,000) was effective in promoting adhesion, yet displayed good biocompatibility. The addition of PEI to the crosslinking solution as subsequent scaffold layers are plotted is also helpful for promoting interstrand adhesion and stabilizing the 3D scaffold structure. We found that inclusion of soluble PEI at low concentrations of up to 0.1% in the crosslinking medium enabled good scaffold architecture, meanwhile having no negative effect on cell viability. Although the 3D scaffolds that we produced had good porosity on the Z-axis, the X- and Y-direction lacked the presence of obvious pores. This could be because the lower viscosity of the alginate/HA solution used to fabricate the scaffolds allowed a degree of collapse and compaction of the stacked layers. Therefore any strategy use of our Schwann cell-laden alginate/HA scaffolds for peripheral nerve

repair may need to be supplemented with nerve conduit tubes with high porosity (Cerri *et al.*, 2014).

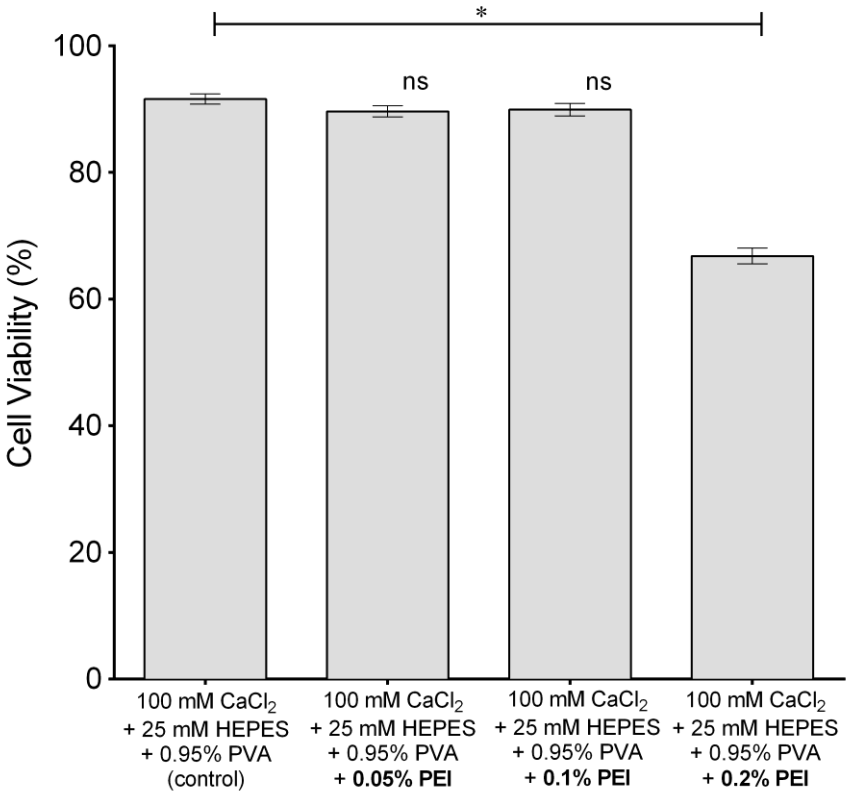

Figure 3.8 RSC96 cell viability in alginate/HA strands after bioplotting into crosslinking solutions with different concentrations of PEI, assessed 5 min after crosslinking [n = 10, *p < 0.0001; ns = not significant when compared with control]

We investigated the inclusion of substances in the crosslinking medium to combat the disruptive effect of strand buoyancy during the fabrication process, and obtained good results with 0.95% PVA. At this concentration of PVA, the extruded strands of alginate/HA did not lift up or float towards the surface of the crosslinking solution. Although glycerol can also be used for the same purpose, PVA is a biomaterial that has previously been used with alginate in composite scaffolds to improve cell biocompatibility (Cho *et al.*, 2005). We find that, compared to glycerol, which markedly reduces cell viability, the inclusion of 0.95% PVA in the crosslinking medium has a protective effect on the RSC96 cells. Future fabrication of larger scaffolds may be more time-consuming, and use of crosslinking solutions containing PVA could help maintain cell viability until completion of scaffold fabrication.

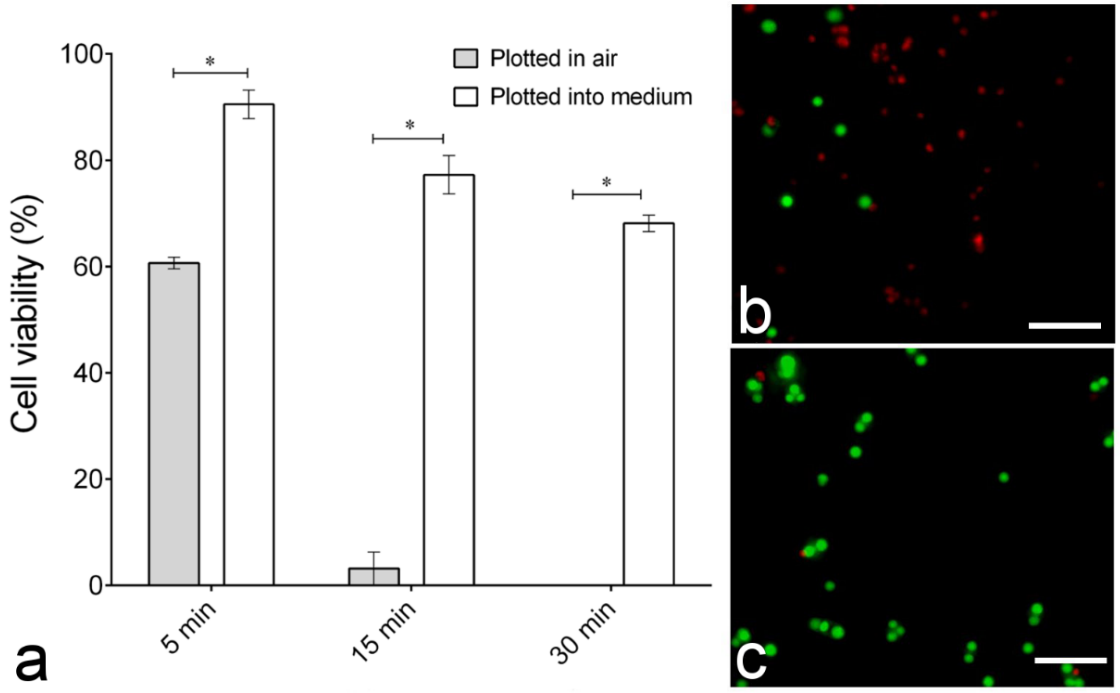

Figure 3.9 a) RSC96 cell viability in alginate/HA strands compared at various times after plotting in air with calcium chloride nebulization (then immersed in crosslinking solution) or directly into the crosslinking solution (100 mM $CaCl_2$ and 0.95% PVA in 25 mM HEPES) [n = 5; *p < 0.001]. RSC96 cells in strands plotted in (b) air (5 min, as above) and (c) into crosslinking solution and stained with calcein-AM (green) or propidium iodide (red) (scale bars=100 µm).

Over time in culture, it is seen that the viability of the primary rat Schwann cells reduces to 83.3% from an initial 92.5%. In our preparations, a few cells also escaped from the hydrogel patterns after a few days and attached to the bottom of the culture plate. This leads to decreased cells within the hydrogel pattern and affects assessment of viability over time. Further development of this technology may improve long-term cell survival. For example, alginate can be modified with cell adhesion peptides or other extracellular matrix proteins to enable better cell proliferation (Rowley *et al.*, 1999). Schwann cells in standard cultures have a bipolar or trigonal morphology and assemble into sheets. However, when they are cultured in a simple alginate hydrogel they have a circular morphology and form clusters (Novikova *et al.*, 2006), apparently due to the lack of adhesion to their surroundings. Biological cell adhesion, mediated for example by integrin receptors, can influence cell survival.

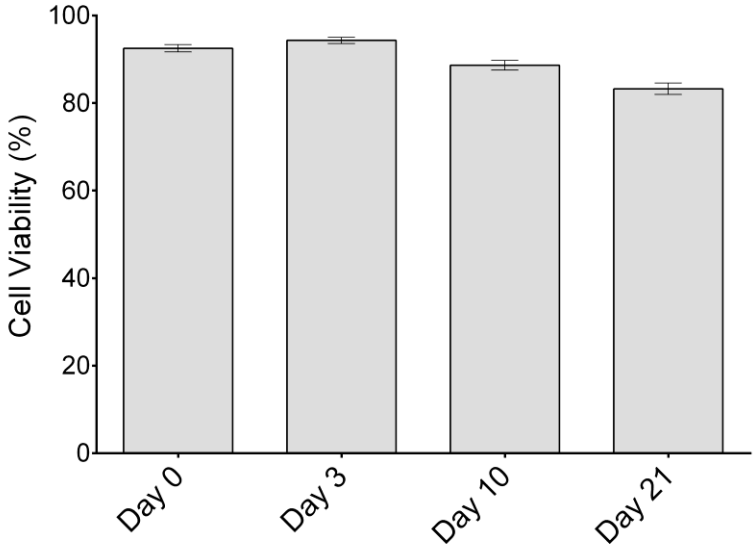

Figure 3.10 Primary rat Schwann cell viability in single-layered alginate/HA strands maintained post-fabrication for the indicated times in culture [n=10].

On comparing the plotting of scaffold patterns into the crosslinking medium with that in air, we found that the strand width and inter-strand space in patterns plotted into liquid medium conform much more closely to the programmed dimensions set on the dispensing machine. Apparently, strands with lower viscosity plotted in air spread and collapse before they can be stabilized with nebulized calcium chloride solution. Furthermore, the thin profile of strands (10 x 10 mm pattern with strand-width of approximately 120 µm) printed on a dry surface caused them to dry over time, despite nebulization with calcium spray, leading to rapid cell death. In contrast low viscosity alginate/HA material plotted into the liquid crosslinking solution maintains hydration, and the buoyant forces exerted by the crosslinking solution prevent the hydrogel from spreading over the surface, allowing them to retain a cylindrical structure while ionic crosslinking takes place. Luo *et al.*, (2013) have successfully printed scaffolds using high concentrations of alginate (16.7% w/v) in air and characterized the scaffolds, showing them to have a uniform and continuous porous structure. Plotting alginate or alginate-based hydrogels in air is feasible if the viscosity of the alginate solution is high. However highly viscous hydrogels require higher dispensing pressures and this can induce damage to cells suspended in the hydrogel solution (Kong *et al.*, 2003). Khalil and Sun, (2009) printed scaffolds using low viscosity of alginate (1.5% w/v) with suspended cells into a crosslinking solution and obtained

high cell viability. Our study also demonstrates that much higher cellular viability can be achieved by plotting low viscosity biomaterial strands directly into a crosslinking solution.

It has been well established that the use of low dispensing pressure and extrusion needle-tips with large internal diameter lead to increased cell viability during the plotting process (Chang *et al.*, 2008). Li *et al.*, (2010), have established a model to help estimate resulting cell damage based on shear and process-induced forces experienced by cells during the dispensing process. Mixing of the hydrogel and cell suspension until homogeneity is achieved helps in preserving the mechanical integrity of the scaffold and also increases the viability of the cells within them (Cohen *et al.*, 2011). Thus, while our study examines chemical and geometric techniques to maintain cell viability immediately after plotting, control of other parameters such as speed and pressure while plotting the material also helps in improving cell viability.

In early strategies of tissue engineering scaffold construction, living cells were randomly seeded over porous, biodegradable scaffolds. More recent and sophisticated strategies involve the creation of cell sheets, or the positioning of cell-laden 'bio-ink" onto pre-formed artificial structures (Owens *et al.*, 2013). These strategies may create scaffolds that more closely imitate the native biological architecture of tissues and organs (Mironov *et al.*, 2009). In a more sophisticated example, cellular aggregates can be deposited over easily degradable hydrogels to eventually fuse and form a biomimetic construct (Marga, *et al.*, 2012). The techniques described in the present study constitute yet another approach, whereby bioplotting might be used to position cells precisely and in defined geometry, for example to mimic oriented chains of Schwann cells (bands of Büngner) that appear to play an important guidance role in the regeneration of severed axons in injured peripheral nerve. The eventual goal of using 3D freeform fabrication techniques is to form precise and fully functional organs. Given their complexity and high cellular density, fabricating scalable organs could take several hours (Ozbolat and Yu, 2013). Therefore plotting cellular aggregates and scaffold material into biocompatible liquid solutions would enable better viability during an extended fabrication procedure.

3.6 Conclusion

Manufacturing scaffolds from biomaterials using advanced biofabrication techniques can be automated to lower material consumption and fabrication time. Though such advances have

been made in biofabrication techniques for tissue engineering purposes, the inclusion of cells in intricate scaffold designs is challenging, as many parameters need to be scrutinized. In this study, we have shown that bioplotting can be used for the dispensing of cell-laden alginate/HA hydrogel material with high cell viability. The use of PEI and PVA in the crosslinking medium helps stabilize scaffold structure and improve cell survival during the bioplotting process. Plotting scaffolds directly into the crosslinking solution resulted in better cell viability than plotting in air, and adjusting parameters such as speed and pressure helped in achieving the intended strand width and interstrand spacing. Evaluation of these above parameters is suggested in the plotting of any hydrogel material to enable a porous scaffold structure with good cell viability.

CHAPTER 4

USE OF THE POLYCATION POLYETHYLENEIMINE TO IMPROVE THE PHYSICAL PROPERTIES OF ALGINATE–HYALURONIC ACID HYDROGEL DURING FABRICATION OF TISSUE REPAIR SCAFFOLDS*

*This chapter has been published as Rajaram A, Schreyer DJ, Chen XB. (2015) Use of the polycation polyethyleneimine to improve the physical properties of alginate–hyaluronic acid hydrogel during fabrication of tissue repair scaffolds. *Journal of Biomaterials Science, Polymer Edition*. 9: 1-23". According to the Copyright Agreement, "the authors retain the right to include the journal article, in full or in part, in a thesis or dissertation".

4.1 Introduction

Alginate is a naturally occurring polysaccharide that has been used extensively as a biomaterial. Alginate solutions rapidly gel through ionic crosslinking upon exposure to divalent cations, allowing creation of complex structures by controlled dispensing into calcium chloride solutions (Stevens *et al.*, 2004). Alginate gels have been used in drug delivery (Izawa *et al.*, 2013), delivery of growth factors (Freeman and Cohen, 2009), regeneration of cartilage (Wang, Yang, *et al.*, 2012), cardiac remodelling (Landa *et al.*, 2008), hepatic repair (Shteyer *et al.*, 2014), peripheral nerve regeneration (Sufan *et al.*, 2001), and wound healing (Lee *et al.*, 2009). However the low mechanical strength and rapid degradation characteristics of ionically crosslinked alginate gels are problematic when using this material to fabricate three-dimensional scaffolds for use in tissue repair.

Hyaluronic acid (HA) is a glycosaminoglycan with repeating disaccharide units of glucuronic acid and N-acetylglucosamine residues (Fraser *et al.*, 1997b). It has various applications in tissue engineering (Collins and Birkinshaw, 2013). HA has a positive influence on cell proliferation, attachment, and migration (Toole, 2004; Collins, 2014; Rizzo *et al.*, 2014). HA prevents perineural scarring and results in enhanced peripheral nerve regeneration (Ozgenel, 2003). Covalent crosslinking of hyaluronic acid improves its elastic moduli (Sahiner *et al.*, 2008). However, even in the absence of covalent crosslinking, nearly 50% of HA is retained in ionically crosslinked alginate at the end of 4 weeks (Lindenhayn *et al.*, 1999). Composite alginate-HA hydrogels have improved mechanical properties upon ionic crosslinking with

calcium chloride, and the interaction of HA with water significantly decreases the rate of weight loss of alginate-HA gels (Oerther *et al.*, 1999).

The mechanical properties of alginate are correlated with the content of polyguluronate blocks in their chains (Smidsrød and Skjak-Braek, 1990). While covalent crosslinking has been performed to increase the mechanical properties of alginate with high guluronate content (Rowley *et al.*, 1999), another plausible strategy is the formation of polyelectrolyte complexes. Polyelectrolyte complexes are formed due to electrostatic interactions between macromolecules of opposite charges (Manning, 1972). The hydrophilic nature, better mechanical properties, and low toxicity of polyelectrolyte complexes (Kotz, 1996), could make them suitable materials for tissue engineering. Alginate, being a polyanionic polysaccharide forms complexes with polycations like chitosan (Tapia *et al.*, 2004) and PEI (Batyrbekov *et al.*, 2011).

Polyethyleneimine (PEI) is a synthetic aliphatic amine with a linear or branched primary structure. Although branched PEI is cytotoxic and has low hemocompatibility (Neu *et al.*, 2005), linear PEI is less toxic and has been used as a vector in gene transfer (Fischer *et al.*, 2002) and in plasmid DNA-based vaccines (Toke *et al.*, 2010). As it is well established that the cytotoxicity of PEI is also molecular weight-dependent, PEI of low molecular weight is more favorable (Morimoto *et al.*, 2003). Rat neuronal cell lines proliferate well on PEI-coated surfaces (Lakard *et al.*, 2004) and PEI has also been electrospun into biocompatible scaffolds for potential use in tissue engineering and regenerative medicine (Khanam *et al.*, 2007).

On addition of PEI to alginate, strong ionic interactions result in a stable polymer with the linear alginate chains neutralizing the positive charges of PEI (Joung *et al.*, 1987). Alginate beads coated with PEI tend to release entrapped drugs more slowly than uncoated beads (Halder *et al.*, 2005). The extended release profile is dependent on the successful formation of a polyelectrolyte complex and the time of exposure to PEI (Setty *et al.*, 2005). Coating alginate-based scaffolds with polycations could particularly be useful when incorporating growth factors and extracellular matrix proteins.

Formation of these complexes can delay the degradation of ionically crosslinked alginate even in the presence of calcium chelators (Smidsrød, 1973). The mechanical properties of alginate are also affected by PEI. For example, the Young's (compressive) modulus of alginate was found to increase with addition of PEI (Mohamed and Salleh, 1982). While alginate-based polyelectrolyte complex microspheres have been extensively studied, tissue engineered scaffolds

have not been well characterized. In the present study, we compare the effects of PEI on the physical properties of alginate-HA gel scaffolds.

4.2 Materials and methods

Alginate (sodium salt from brown algae), calcium chloride dihydrate, hyaluronic acid (HA) (sodium salt from *S. equi*), polyvinyl alcohol (PVA) (M_W 85,000-124,000), 4-(2-hydroxyethyl)-1-piperazineethanesulfonic acid (HEPES), bovine serum albumin (BSA), Bradford's reagent, and Hoechst 33342 were purchased from Sigma Aldrich, Canada. PEI (linear with M_W 60,000, 50% w/v in H_2O) was purchased from Alfa Aesar, MA, USA. Propidium iodide was purchased from Anaspec, CA, USA.

4.2.1 Preparation of the hydrogel and fabrication of the scaffolds

Alginate (2.5% w/v) was mixed with hyaluronic acid (0.25% w/v) in 0.3 M sucrose with 25 mM HEPES to prepare the hydrogel solution. The osmolality of the alginate solution was made physiological by using sucrose as a solvent. Solutions containing phosphate and monovalent ions were avoided as they affect the crosslinking of alginate (Drury *et al.*, 2004a). Cuboid scaffolds with dimensions of 10 x 3 x 2 mm were fabricated from alginate-HA hydrogel using a 3D-Bioplotter (envisionTEC, Gladbeck, Germany). The composite hydrogel solution was plotted into the crosslinking solution using a steel-tip dispensing needle (EFD Nordson, Westlake, OH, USA) with an internal diameter of 100 µm. The crosslinking solution contained 100 mM $CaCl_2$, 0.95% PVA, and PEI (0.1%, 0.2% or 0.5% w/v). The addition of PVA increases the viscosity of the crosslinking solution and helps control buoyancy during the fabrication process. This prevents the printed hydrogel strands from floating in the crosslinking solution. PEI was added to the crosslinking solution as it augments ionic interactions during the crosslinking of alginate (Devi *et al.*, 2007). PEI also binds ionically with HA forming a complex between its imino group and the carboxylic group (in HA) (Collins and Birkinshaw, 2008). Fabrication parameters such as speed, extrusion pressure, scaffold dimension and properties were similar to those used in our previous study and the time taken to fabricate the scaffold was 5 minutes (Rajaram *et al.*, 2014). As shown in our previous study, fabrication of multi-layered alginate-HA scaffolds was not feasible without addition of PEI to the crosslinking solution (100

mM calcium chloride and 0.95% w/v polyvinyl alcohol). Therefore assessment of the mechanical properties, swelling, and degradation rate of alginate-HA scaffolds, in the absence of PEI was not achieved.

4.2.2 Mechanical properties

The Young's modulus of the alginate-HA scaffolds fabricated using crosslinking solutions containing either 0.1% or 0.5% PEI was assessed by compression testing, performed using a texture analyzer machine (Texture Technologies, MA, USA). The scaffolds underwent crosslinking for 30 minutes and their dimensions were measured using a digital caliper. They were subjected to compression until fracture, at a speed of 0.01 mm/second. The Young's modulus of the scaffolds was determined from the slope of stress vs. strain plots, limited to the linear first 10% strain of the plot (Semmling *et al.*, 2013). The average Young's modulus was determined for both scaffold groups.

4.2.3 Swelling index

The swelling behavior of the alginate-HA scaffolds was studied in HEPES buffered saline (HBS), a physiological buffer. After fabrication of the scaffolds (crosslinked for 5 minutes), they were immersed in 1.5 ml of the buffer and incubated at 37° C. Swelling was assessed at day 3, 7, 14, and 21. At the scheduled times, the scaffolds were blotted to remove excess buffer using Kimwipe® sheets and then weighed (W_t). The initial wet weight (W_0) was obtained immediately after plotting the scaffolds in crosslinking solutions containing calcium chloride, HEPES, and either 0.1% or 0.5% PEI. The results are reported in a ratio, calculated using the formula,

$$Swelling\ index = [(W_t - W_0)/W_0] * 100 \quad (4.1)$$

where W_0 is the initial wet weight of the scaffolds and the W_t is the wet weight of the scaffold (at time t). Three scaffolds were used for each group and the mean ± SEM is reported.

4.2.4 Degradation

The degradation of scaffolds fabricated into crosslinking solutions containing either 0.1% or 0.5% PEI was studied in HBS. The scaffolds were kept in HBS at 37° C soon after fabrication (crosslinked for 5 minutes) and degradation was assessed at day 3, 7, 14, 21, and 28. To estimate degradative loss of the scaffolds, the dry weight (polymer content) was determined by weighing the scaffold at the mentioned time-points after complete drying (37°C for 48 h). The initial dry weight of was obtained by drying scaffolds immediately after fabrication. The percentage weight loss is determined by the formula,

$$Percentage\ weight\ loss = [(W_0 - W_t)/W_0] * 100 \quad (4.2)$$

where W_0 is the initial weight of dry gel before degradation and W_t is the weight of dry gel at each time-point. Three samples were tested for each group and the mean ± SEM is reported.

4.2.5 BSA release

Bovine serum albumin (BSA) was mixed with the alginate-HA solution at a concentration of 1.66 mg/ml of hydrogel. Twenty µl of the resulting hydrogel was extruded into square-shaped patterns and crosslinked for 5 minutes. PEI at a concentration of 0.1% or 0.5% PEI at pH 7.4 was added to the crosslinking solution or omitted. BSA in the crosslinking solutions was estimated at the end of 5 minutes to ascertain the encapsulation efficiency of alginate-HA and further *in vitro* release was then performed in either 1 ml of 25 mM HEPES buffer (pH 7.4) or HEPES buffered saline (HBS). Sampling of the buffer solutions for released BSA was done at the end of 30 minutes, 1, 3, 6, 12, 24, 72, 96, and 120 hours. Five µl of each sample (n=5) was mixed with 250 µl of Bradford reagent (Sigma Aldrich, Canada) and light absorbance was measured at 595 nm using an ultraviolet-visual spectrophotometer (Spectra Max Plus 384, Molecular Devices, CA, USA). Fresh buffer of equal volume was added to replace the buffer removed for analysis each time to maintain a sink condition. The BSA released in the samples was estimated using a standard curve and the value is reported as the percentage of initially incorporated BSA released.

4.2.6 Cell viability

Primary Schwann cells were isolated from rat sciatic nerves according to the method by Kaewkhaw *et al.* (2012). ATDC-5 cells were purchased from Sigma Aldrich (ON, Canada). ATDC5 cells, a chondrogenic cell line is derived from mouse teratocarcinoma and is promising to study chondrogenesis *in vitro* (Yao and Wang, 2013). To study the effect of the PEI on cell viability, a suspension of rat Schwann cells (1.6×10^6 cells/ml) was mixed with the alginate-HA solution and then plotted as strands into the crosslinking solution containing 100 mM $CaCl_2$ with 25 mM HEPES with or in the absence of PEI (0.1%, 0.2%, or 0.5% w/v). The same was done with the ATDC-5 cells. High concentrations of PEI, particularly high molecular weight PEI, are known to be toxic to mammalian cells (Florea *et al.*, 2002). Lower molecular weight PEI was used in this study as the toxicity profile is reduced (Patnaik *et al.*, 2006). The crosslinking solutions were removed after five minutes and the single-layer strands were washed thrice with Dulbecco's modified Eagle's medium. The viability of cells was assessed on day 1, 3, and 7 by counting the total and dead cells after staining the cell-laden hydrogel strands with Hoechst 33342 (2.5 μg/ml) and propidium iodide (25 μg/ml) (Fernandez *et al.*, 2000). All the cells in the printed strands were counted on the single layered hydrogel patterns (n=3) from images taken using a fluorescent microscope (Carl Zeiss Axiovert 100). The images were analyzed using ImageJ (National Institutes of Health, Bethesda, Maryland, USA) and viability was calculated as the percentage of live cells among the total number cells counted. To enable easier and automated counting of nuclei, the z-project plugin on ImageJ was used to merge cells focused on multiple planes to a single projection (Cai *et al.*, 2011).

4.3 Data analysis

The mean and standard error of the mean (SEM) of the data are reported for each experimental test. Statistical significance for the analysis of grouped data was assessed by two-way analysis of variance (ANOVA) followed by Bonferroni's correction for multiple comparisons. However for the compressive modulus measurements, Student's t-test was used. GraphPad Prism 5.0a (GraphPad Software, San Diego, CA, USA) was used for data analysis.

4.4 Results

The fabrication of 3-D scaffolds with good architecture was feasible in the presence of PEI (0.1% or greater) and PVA in the crosslinking solution. PEI increases the ionic crosslinking of alginate (Devi *et al.*, 2007) in the presence of divalent calcium ions and PVA was included in the crosslinking solution to prevent the strands from floating while being plotted. The printed 3d alginate-HA scaffolds are shown in Fig. 4.1 and it is seen that the porosity along the vertical axis is maintained.

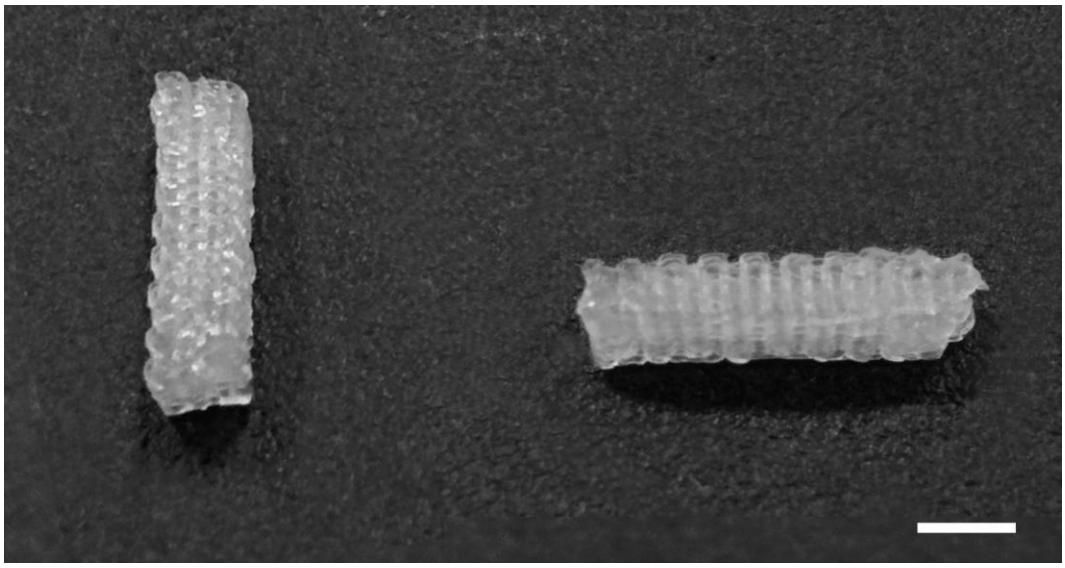

Figure 4.1 Alginate-HA scaffold (scale bar = 3 mm).

To examine the effect of PEI on the mechanical properties of the scaffolds, the Young's (compressive) modulus was estimated. The stress-strain curve of the scaffolds is shown in Fig. 4.2a. The mean Young's modulus of the scaffolds crosslinked with solution containing 0.1% PEI was 0.0014 MPa, while that of scaffolds crosslinked with solution containing 0.5% PEI was 0.0016 MPa. Although the Young's modulus trended higher with the use of 0.5% PEI, there was no statistically significant difference between the two groups (Fig. 4.2b).

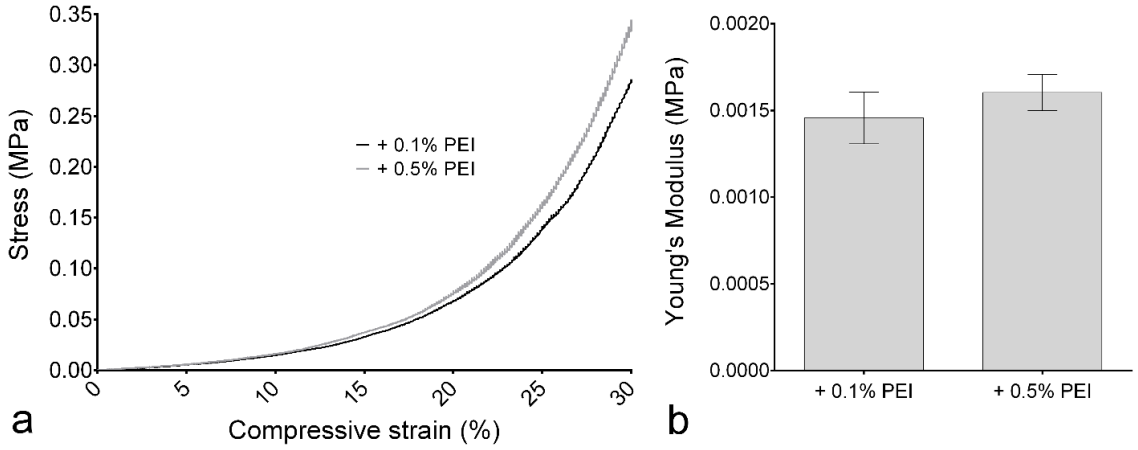

Figure 4.2 a) Stress-strain curve of alginate-HA scaffolds crosslinked in the presence of 0.1% and 0.5% PEI b) Young's moduli of the scaffolds [n=3].

The swelling index of the scaffolds fabricated in 0.1% PEI was 37.9 ± 8.6% on day 3, while that of scaffolds fabricated in 0.5% PEI was 85 ± 2.8% (Fig. 4.3a). By the end of day 21, these decreased to 16.3 ± 8% and 65.3 ± 1.4% respectively. Higher concentrations of PEI, (0.5%) led to an increase in scaffold swelling by 55.3% when compared to using 0.1% PEI. At the end of 3 weeks, the percentage dry weight loss of scaffolds fabricated in the presence of 0.5% PEI was 12.1 ± 6.6%, while that for the 0.1% PEI was only 40.6 ± 3.1%. This increased to 45.4 ± 5.2% and 65.6 ± 3.1%, at the end of a month (Fig. 4.3b). Therefore at the end of one month, scaffolds fabricated in 0.5% PEI retained 44.37% more mass than those fabricated in 0.1% PEI.

The percentage of BSA initially entrapped in the alginate-HA strands differed with the varying presence of PEI in the crosslinking solution (Fig. 4.4). It was 57 ± 0.8% in the absence of PEI. However in the presence of 0.1% or 0.5% PEI, it increased to 91 ± 0.6% and 92 ± 0.9% respectively. The release of BSA from the alginate-HA strands was estimated in HBS or 25 mM HEPES buffer (both at pH of 7.4) at various intervals. The presence of monovalent sodium ions in HBS leads to faster degradation of alginate, presumably through competition with calcium ions, eventually leading to greater BSA release. Although the presence of PEI during alginate-HA crosslinking resulted in greater BSA content in the strands, the release of BSA in HBS was similar in all the groups by the end of 96 hours (Fig. 4.5a). In HEPES buffer, the release of BSA was not complete (Fig. 4.5b) and relatively more BSA (nearly 30%) was contained in strands that lacked PEI even the end of 96 hours.

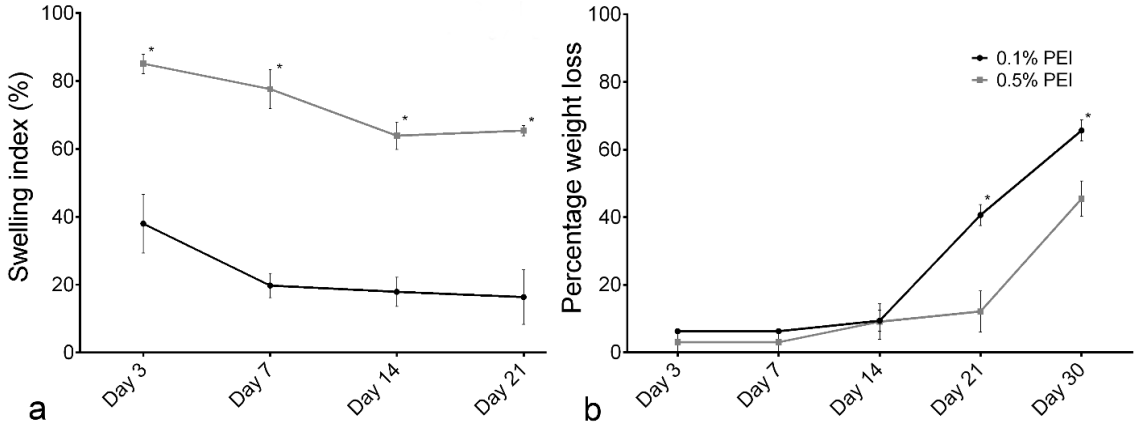

Figure 4.3 (a) Swelling index in HEPES buffered saline (b) Percentage weight loss of scaffold in HEPES buffered saline at 37° C; [n=3, *p<0.005].

In the cell survival studies, viability of primary Schwann cells included in the alginate-HA strands crosslinked in solutions with no PEI, 0.1%, 0.2%, and 0.5% PEI at day 1 was 78.3 ± 1.2%, 78.9 ± 0.6%, 75.6 ± 1.7% and 66.7 ± 1.9% respectively. Similarly the viability for ATDC-5 cells was 82.4 ± 0.7%, 78.2 ± 1.3%, 75.8 ± 3.9% and 72.4 ± 1.3% respectively. It was higher for the ATDC-5 cells as they are a cell line. At the end of 1 week, the viability of rat Schwann cells crosslinked in solutions with no PEI, 0.1%, 0.2%, and 0.5% PEI, reduced to 85.4 ± 1.7%, 77.1 ± 1.5%, 60.5 ± 2.5%, and 68.8 ± 1.4% respectively. Similarly the viability of ATDC-5 cells at the end of 1 week was 74.1 ± 2.3%, 66.5 ± 1.2%, 58.7 ± 0.5%, and 58.1 ± 4.2% when alginate-HA strands were crosslinking in the absence of PEI, in 0.1%, 0.2, and 0.5% PEI respectively (Fig. 4.6). While the addition of 0.1% PEI had no significant effect on cell viability (both primary Schwann cells and ATDC-5 cells) at day 1 or at the end of 1 week, significant cell loss occurred with 0.2% PEI, and 0.5% PEI.

4.5 Discussion

For effective tissue regeneration using tissue repair scaffolds, porosity and the presence of interconnected spaces is of great importance (Malda *et al.*, 2013). Porous alginate hydrogels provide a more favorable environment for cell proliferation due to enhanced mass transfer of nutrients and oxygen (Hwang *et al.*, 2010). The process of dispensing alginate-HA strands in this study into a crosslinking solution containing calcium, PVA, and PEI resulted in scaffolds with interconnected pores. While the influence of PEI and PVA on the fabrication of the scaffold was

described in our previous article, here we show the addition advantages of PEI on the physical properties of the scaffold.

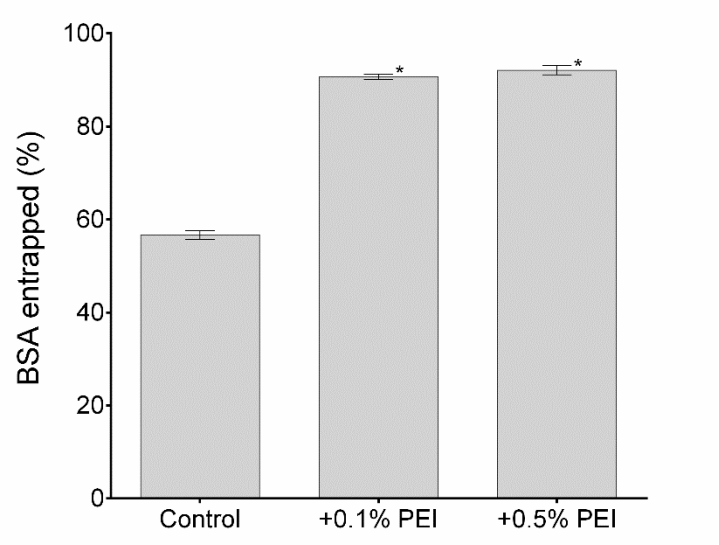

Figure 4.4 Loading efficiency of BSA after crosslinking of alginate-HA strands for 5 min in 100 mM $CaCl_2$ with 25 mM HEPES (control), with added 0.1% or 0.5% PEI [n=5; *p<0.0001].

Increasing the concentration of PEI in the crosslinking solution decreases the percentage weight loss or degradation of plotted alginate-HA scaffolds. High molecular weight PEI more effectively delays the degradation of alginate gels when compared to PEI of lower molecular weight (Kong and Mooney, 2003). Therefore besides the absolute concentration of PEI, the molecular weight of PEI also affects gel degradation. PEI of higher molecular weight affects cells viability, similar to increasing concentrations of PEI. On comparing the viability of RSC96 (rat Schwann cell line) cells cultured on surfaces coated with 0.1% PEI of molecular weight 60,000 and 750,000, it was observed that viability declined with the use of PEI having larger molecular weight (Rajaram *et al.*, 2014).

Higher concentrations of PEI however, tend to induce greater swelling of alginate. This is a known feature of polyelectrolyte complexes and they can contain more that 85% of the solvent they are exposed to (Philipp *et al.*, 1989). The interaction between alginate and PEI increases the mechanical strength of the scaffolds and the elastic modulus increases with higher concentrations of PEI (Kong and Mooney, 2003). Altering the mechanical properties of scaffolds can positively affect human chondrocyte behavior (Klein *et al.*, 2010) and differentiate neural progenitor cells (Seidlits *et al.*, 2010). Addition of PEI to other hydrogel scaffolds composed of chitosan and

polyethylene oxide improves the attachment, proliferation, and activity of chondrocytes (Kuo and Ku, 2009). In our study however there was no significant increase in the mechanical properties, even when the PEI concentration was increased by five-fold. Alginate-HA is commonly used as an injectable scaffold for tissue regeneration (Dahlmann *et al.*, 2013; Coates *et al.*, 2013). Therefore the addition of PEI having varying molecular weights and/or concentration could be used to control the degradation and mechanical properties of alginate and alginate-HA scaffolds.

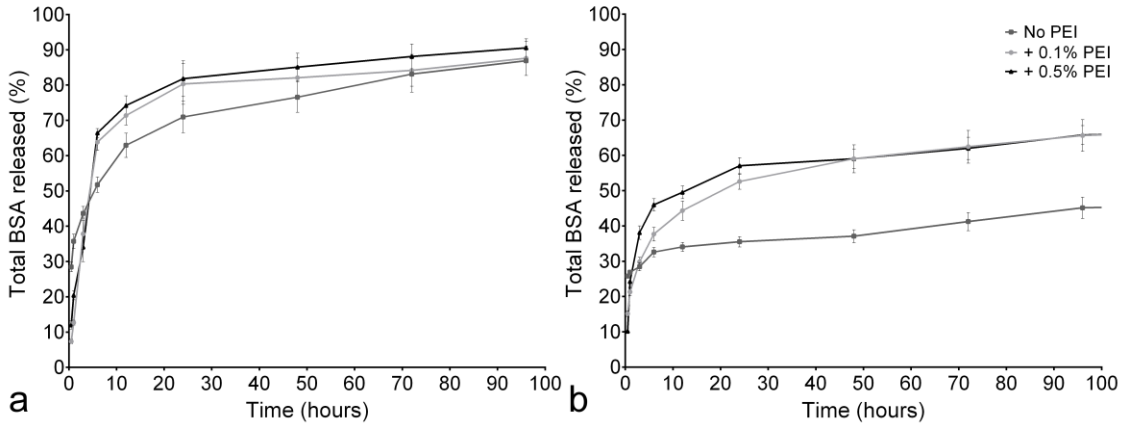

Figure 4.5 Percentage of entrapped BSA release over time in a) HEPES buffered saline or b) 25 mM HEPES.

Incorporating crosslinked HA in gelatin constructs led to an increase in its compressive modulus (Levett *et al.*, 2014). Using varying concentrations and composition of alginate and HA enabled good control over the mechanophysical properties of injectable scaffolds (Dahlmann *et al.*, 2013). In this study, HA was not crosslinked to alginate. However besides its biological benefits, addition of HA to alginate, also increased the viscosity of the composite hydrogel and helped attain good strands during 3D plotting. Combining HA with alginate facilitates easier fabrication of 3D scaffolds using extrusion-based techniques (Wang *et al.*, 2013).

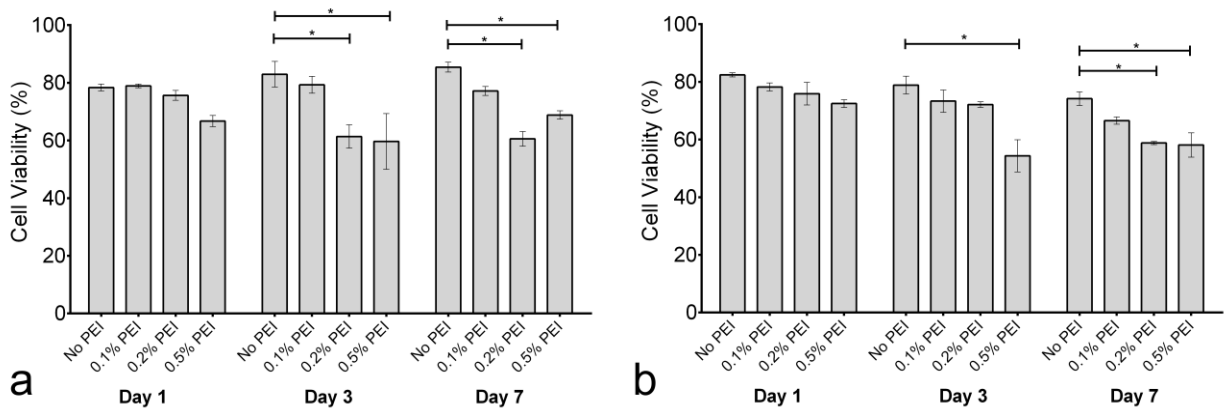

Figure 4.6 Effects of PEI and time on a) primary rat Schwann cell and b) ATDC-5 cell viability within scaffolds [n=3]. Significant difference between each time point within a group ($p<0.01$) is indicated by *.

Although alginate is usually biologically inert, a few proteins, such as transforming growth factor beta, can be inactivated by alginate (Mumper *et al.*, 1994). However BSA maintains its structure when incorporated in alginate (Zhao *et al.*, 2009). BSA is initially contained within the alginate gel by entrapment as the gel forms. In our study we find that the inclusion of PEI during the crosslinking of alginate-HA strands increases the entrapment efficiency of BSA. Proteins encapsulated in alginate may be released either by diffusion or upon its degradation. The calcium-induced ionic crosslinking of alginate is sufficiently stable in aqueous media. The exchange of between Na^+ and Ca^{2+} ions leads to subsequent degradation of alginate (Bajpai and Sharma, 2004). The high concentration of sodium ions in saline-based buffers displaces calcium ions in crosslinked alginate, leading to destabilization of the gels and release of BSA. Thus the release of BSA in alginate is greater in HEPES buffered saline compared with HEPES buffer alone. The addition of PEI appeared to slow the sustained release of BSA in our study as it improves the integrity of the gel and slows its degradation. In our study the larger surface area of the porous alginate-HA scaffolds, and/or the presence of HA may have accelerated the release of BSA. We also did not account for the loss of BSA to adsorption on to the surface of the tissue culture plate, in which the study was performed. The loss of BSA activity was also not assessed. However sustained release of proteins from alginate microbeads, even in the presence of PEI has been observed in various studies. Proteins like fibrinogen, interleukins, insulin, nerve growth factor, fibroblast growth factor, etc., have been incorporated into alginate matrices (Gombotz and Wee, 1998). Therefore the addition of low concentrations of

low molecular weight PEI during fabrication of the alginate scaffolds would likely enable better encapsulation of most of these proteins, providing a better *in vivo* delivery system.

Advanced tissue engineering applications are being developed which allow the entrapment of living cells within the scaffold material during the fabrication process, provided that all steps of scaffold fabrication can be carried out under physiologically mild conditions. Alginate and alginate-HA gels are particularly suitable for the inclusion of cells; as gel formation can be accomplished by ionic crosslinking or polyelectrolyte complex formation. Human stem cells derived from adipose tissue have enhanced cell adhesion and proliferation when cultured in alginate-HA (Son *et al.*, 2013). Schwann cells proliferate more on surfaces coated with PEI (Vleggeert-Lankamp *et al.*, 2004). As guidance of regenerating axons is greatly influenced by Schwann cells, their role in nerve repair scaffolds is pivotal (Nguyen *et al.*, 2002). Coating polymeric surfaces with alginate/PEI also improves the attachment, proliferation, and activity of chondrocytes (Zhu *et al.*, 2004). Though most cell types are compatible with alginate-HA, primary rat Schwann cells and a chondrogenic cell line (ATDC-5) were studied here due to the positive effects of PEI on them. Our findings show that viability of encapsulated Schwann cells and ATDC-5 can be adequately maintained for long periods following the formation of polyelectrolyte complexes using PEI. Indeed, the known toxic effects of PEI may be mitigated precisely because the PEI is bound into a polyelectrolyte complex. Nevertheless, the best cell survival results appear to be dependent on PEI concentration, and any application involving living cells will have to find the optimal balance between the advantageous physical improvements resulting from the use of PEI, and the possible decrease in cell survival that may occur at higher concentrations.

4.6 Conclusion

We have shown that the physical properties of alginate-HA tissue repair scaffolds can be tuned by the addition of PEI during the crosslinking process. Many such scaffolds are also being designed to act as vehicles of growth factor delivery to the site of tissue repair. The addition of PEI to alginate-based scaffolds could result in more efficient entrapment and prolonged delivery of such growth factors. While adjusting the physical parameters of polyanionic biomaterials by the addition of PEI could lead to harsher environments for cells, we have shown that at low concentrations of PEI, the viability of Schwann cells is not severely affected. From this study, it

is inferred that low molecular weight PEI at concentrations of up to 0.1% have no detrimental effect on cells and its use can significantly improve the entrapment of protein within scaffolds. Therefore the strategy of using PEI in alginate-based biomaterials will likely be beneficial in the future design of tissue repair scaffolds, especially those that require encapsulation of growth factors and/or living cells for regenerative applications.

CHAPTER 5

PRELIMINARY STUDY ON THE USE OF 3D-PRINTED ALGINATE-HYALURONIC ACID NERVE CONDUITS FOR THE REGENERATION OF RAT SCIATIC NERVE *IN VIVO*

5.1 Introduction

Clinical use of nerve conduits is currently limited to 30mm defects (Battiston *et al.*, 2009). Most clinically approved nerve conduits have a basic hollow cylindrical design made using biomaterials such as collagen, polycaprolactone, polyglycolate, and polyvinyl alcohol (Pabari *et al.*, 2014). Strategies to improve the design of single-lumen nerve conduits include improving conduit permeability (de Ruiter *et al.*, 2009), filling the conduit with hydrogels (Belkas *et al.*, 2005), inclusion of Schwann cells (Rodríguez *et al.*, 2000), and addition of neurotrophic factors (Midha *et al.*, 2003). Inclusion of Schwann cells have additional advantages like the production of neurotrophic factors and the alignment of axons.

Schwann cells in nerve conduits increase the expression of growth factors, axonal regeneration, and motor function (Jesuraj *et al.*, 2014). Nerve repair using acellular nerve conduits is limited due to the senescence of Schwann cells that migrate into the conduit (Saheb-Al-Zamani *et al.*, 2013). Segmental nerve defects have shown better regeneration by including Schwann cells into repair conduits (Berrocal *et al.*, 2013). Aligned Schwann cells have the ability to direct axonal growth (Thompson and Buettner, 2006). Axons are directed along oriented Schwann cell in monolayer cultures even in the absence of other directional cues (Seggio *et al.*, 2010). Schwann cells can also be aligned within a three dimensional hydrogel matrix (Georgiou *et al.*, 2013).

Advances in fabrication techniques have resulted in better nerve scaffold designs. Three dimensional (3D) bioprinting is compatible with natural biomaterials and can be carried out under physiologically mild conditions (Peltola *et al.*, 2008). It enables cell deposition within biomaterials at very high densities (Marga *et al.*, 2012). This approach can allow specific and directed incorporation of living cells anywhere within the scaffold, which would be difficult to achieve otherwise. Improved porosity and permeability, precise control over scaffold geometry, and cell alignment within the scaffold are feasible using layer-by-layer rapid prototyping techniques. Cells are capable of aligning themselves along the direction of hydrogel strands,

printed using these techniques (Barry *et al.*, 2009). Neurons cultured *in vitro* can align themselves along patterns of 3D-printed collagen (Roth *et al.*, 2004).

Alginate, a naturally derived polysaccharide biomaterial, has been used as a Schwann cell matrix (Mosahebi *et al.*, 2001). Alginate is inert and does not evoke an immune response in the body (Wee *et al.*, 1995). Alginate-based hydrogels have been micropattered to culture cortical neurons in three dimensional (3D) environments (Kunze *et al.*, 2011). Alginate also enables Schwann cell migration and promotes axonal regeneration *in vivo* (Hashimoto *et al.*, 2002). Alginate crosslinks rapidly with calcium chloride and this makes it an appropriate material to fabricate scaffolds while using free-form techniques (Song *et al.*, 2011)

Hyaluronic acid has been used to treat neuromas clinically (Monacelli *et al.*), and its inclusion in nerve scaffolds, alleviates neuroma formation in resected peripheral nerves. Hyaluronic acid also has good hydrating properties and lowers the formation of scars. During peripheral nerve repair, it prevents perineural scar formation and enhances regeneration (Ozgenel, 2003). Alginate-based composite hydrogels with hyaluronic acid (HA), enable easier gel-formation and induce good healing (Oerther *et al.*, 2000). The hydrating properties of HA makes it a good carrier of bioactive proteins. Combining alginate with HA results in the HA being trapped in the gel structure as calcium ions crosslink the alginate. Addition of fibronectin to alginate improves the viability of Schwann cells and also enhances axonal regeneration (Mosahebi *et al.*, 2003a). In this study we propose that 3D printed alginate-HA scaffolds, augmented with fibronectin can be used as effective nerve repair conduits in a rat sciatic nerve model. We also include labelled Schwann cells in the scaffolds for *in vivo* tracking.

5.2 Methods

5.2.1 Isolation and staining of primary rat Schwann cells

Primary rat Schwann cells were isolated from the sciatic nerves of Sprague-Dawley rats according to the method described by Kaewkhaw *et al.* (2012). The sciatic nerve was isolated and the epineurium was stripped. The nerve was then cut into smaller 2 mm fragments and digested with collagenase for 1 hour. The resulting cell suspension was filtered and cultured in Dulbecco's Modified Eagle's Medium (DMEM) containing forskolin, N2 supplement, and bovine pituitary extract. D-valine was used in the DMEM preparation as it suppresses fibroblast growth.

The primary Schwann cells were maintained in culture until 5 passages. They were stained for S100 to ascertain the purity of the culture. They were then labelled with PKH26, a cell membrane-labelling fluorophore, according to the manufacturer's instructions (Sigma Aldrich, ON, Canada). The PKH26-labelled Schwann cells were maintained in culture *in vitro* to assess for the stability of the fluorescent marker. The labelled cells were seeded on a tissue culture plate (cell density of 2.8 x 10^5/ml) and cultured in primary rat Schwann cell culture medium (Kaewkhaw *et al.*, 2012) for a month. Images were acquired using a fluorescent microscope (Carl Zeiss Axio Imager A1) and the mean gray value of random cells (n=25) from three separate cultures was assessed.

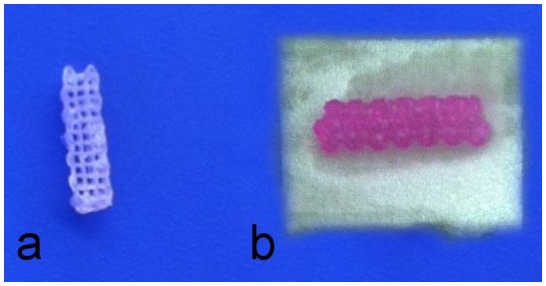

Figure 5.1 a) Alginate-hyaluronic acid scaffold b) Scaffold placed over collagen type-I sheet.

5.2.2 Fabrication of the scaffold conduit

The scaffold used in the study was fabricated using a 3D-Bioplotter (Envisiontec GmbH, Germany). A composite hydrogel solution comprising of alginate (25 mg/ml) and HA (0.25 mg/ml) was extruded into a crosslinking solution of 100 mM $CaCl_2$, 0.1 % polyethyleneimine, and 0.95 % polyvinyl alcohol. The extrusion of alginate-HA was performed layer-by-layer to achieve a cuboid scaffold with dimensions of 10 x 3 x 2 mm (Fig. 5.1a). The diameter of each strand was 80-100 µm and the interspace distance between the strands was 0.75 mm. In some scaffolds, fibronectin (0.1 mg/ml) and/or a suspension of PKH26-labelled primary rat Schwann cells (1.8 x 10^6 cells/ml) was homogenously mixed with the alginate-HA hydrogel solution before the scaffolds were fabricated.

Table 5.2. Groups of rats and procedure performed.

Group	No. of animals	Procedure
1.	5	Sham
2.	4	Primary epineural repair
3.	5	Alginate-HA scaffold
4.	5	Alginate-HA scaffold with fibronectin
5.	5	Alginate-HA scaffold with Schwann cells
6.	5	Alginate-HA scaffold with fibronectin and Schwann cells

5.2.3 Experimental design and *in vivo* implantation of scaffold conduit

Male Sprague-Dawley (SD) rats, weighing 250-300 grams each were randomly divided into 6 groups (n = 4 - 5), as shown in table 1. The *in vivo* studies were performed after approval by the University Committee on Animal Care and Supply (of the University of Saskatchewan). The animals were anesthetized with isoflurane (1.5 – 2% with oxygen; flow rate of 0.8 to 1 L/min) and under aseptic conditions the left sciatic nerve was exposed after a skin incision along the femoral axis and blunt dissection of the underlying muscles. The nerve was either transected (for group 2) or resected (10 mm), 1 cm above its trifurcation. In the transected nerve, the ends were approximated and secured using two 8-0 sutures. In the groups of rats with scaffold implant (groups 3-6), a collagen sheet (Colactive Plus, Covalon) measuring 12 x 6 mm was placed beneath the nerve prior to its resection (Fig. 5.1b). After resection of the nerve, the scaffold was placed over the collagen sheet and approximated to contact both ends of the nerve. The collagen sheet was wrapped around the nerve and 15 µL of fibrin glue was instilled around the collagen and the nerve at both ends. In the sham-operated group, the sciatic nerve was only exposed without being damaged. In all animals, the muscles were reapposed with 6-0 polyglactin sutures and the skin was sutured using 4-0 silk. Post-operative buprenorphine injections (0.05 mg/kg) were provided for all animals every 8 hours, until the end of 24 hours. All the animals were housed separately in a temperature-controlled room with 12 hours light and 12 hours dark cycle. Food and water was available *ad libitum*. Grannick's bitter apple deterrent solution (Greenwich, CT, USA) was sprayed daily on the feet of all animals to prevent them from chewing their toes.

Frequent monitoring of all animals for autotomy was performed. The animals were sacrificed at the end of 8 weeks or when they showed signs of severe autotomy.

5.2.4 Behavioral study

Sciatic Functional Index (SFI) is useful in the evaluation of functional motor recovery of the sciatic nerve (Monte-Raso *et al.*, 2008). The foot pads of the rats were inked and they were allowed to walk over a sheet of paper placed in a box with dimensions of 50 x 8 cm. The clearly demarcated footprints were analyzed for various parameters. The SFI was estimated pre-operatively in all animals and once every week (post-operatively). The Bain formula was used to calculate SFI and is given by:

$$SFI = -38.3*[(EPL-NPL)/NPL]+109.5*[(ETS-NTS)/NTS]+13.3*[(EIT-NIT)/NIT]- 8.8..(5.1)$$

where EPL is the print length in the operated leg, ETS is the total toe spread in the operated leg and EIT is the intermittent toe spread in the operated rat. NPL, NTS and NIT are similar parameters on the normal leg. Print length is the longitudinal distance between the tip of the longest toe and the heel, total toe spreading is the cross-sectional distance between the first and fifth toes and intermediate toes spread is that between the second and the fourth toes (Fig. 5.2).

5.2.5 Immunohistochemistry

The animals were sacrificed at the end of eight weeks from the day of scaffold implantation or nerve transection. They were anesthetized by administering pentobarbital (80 mg/kg) intraperitoneally. Transcardial perfusion and fixation of the rats was performed using cold phosphate buffered saline and 4% paraformaldehyde respectively. The left legs of the animals were dissected to extract the sciatic nerve. The nerve specimen were stored in 4% paraformaldehyde for 12 hours and transferred to sucrose (0.2 g/ml) for 1 day. They were then transferred to cryomolds (Tissue-Tek) filled with optimum cutting temperature embedding solution (OCT) and frozen. Longitudinal sections (10-12 μm thick) of the nerve specimen were obtained using a cryostat and mounted on gelatin subbed glass slides. Immunohistochemistry for S-100 and βIII-tubulin was done using antibodies (1:1000 dilution; Sigma-Aldrich, ON, Canada) against each of the proteins. The immunoreaction was visualized by using a secondary

fluorescent antibody (1:500 dilution; Life technologies, ON, Canada). Small square-shaped images (n=25) of the dimension 150 µm x 150 µm were acquired randomly at regions, both proximal and distal to the initial nerve injury using a fluorescent microscope (Carl Zeiss Axio Imager A1). The immunoreactivity was assessed by measuring mean gray value from these images using the software ImageJ (National Institutes of Health, Bethesda, Maryland, USA) and is presented as a ratio between the distal and proximal site (Berg *et al.*, 2013).

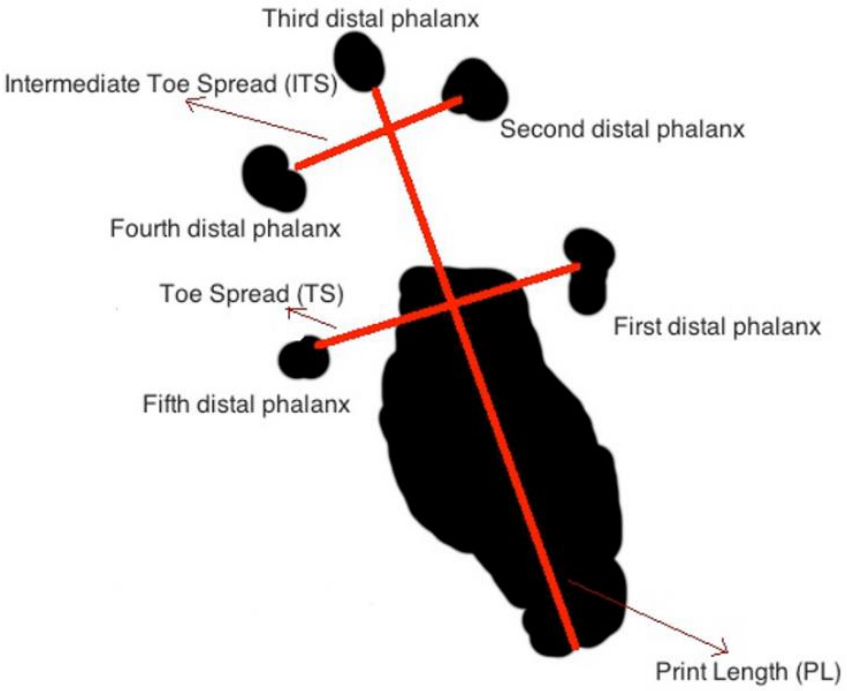

Figure 5.2 Measurements used in the calculation of sciatic function index (SFI).

5.2.6 Statistical analysis

All data is expressed as the mean ± standard error of the mean (SEM). One-way analysis of variance (ANOVA) was used for comparison between groups. $p<0.05$ was considered as statistically significant. Data analysis was performed using Prism (GraphPad Software, San Diego, CA, USA).

5.3 Results and discussion

5.3.1 Purity of Schwann cell culture and PKH26 staining

The primary Schwann cells were maintained in culture and repeatedly passed until there were no fibroblasts in the culture. The purity of the culture was ascertained at the end of 5 passages by performing immunochemistry for S-100 (Fig. 5.3). All the cells stained for S-100, indicating that the culture contained only Schwann cells.

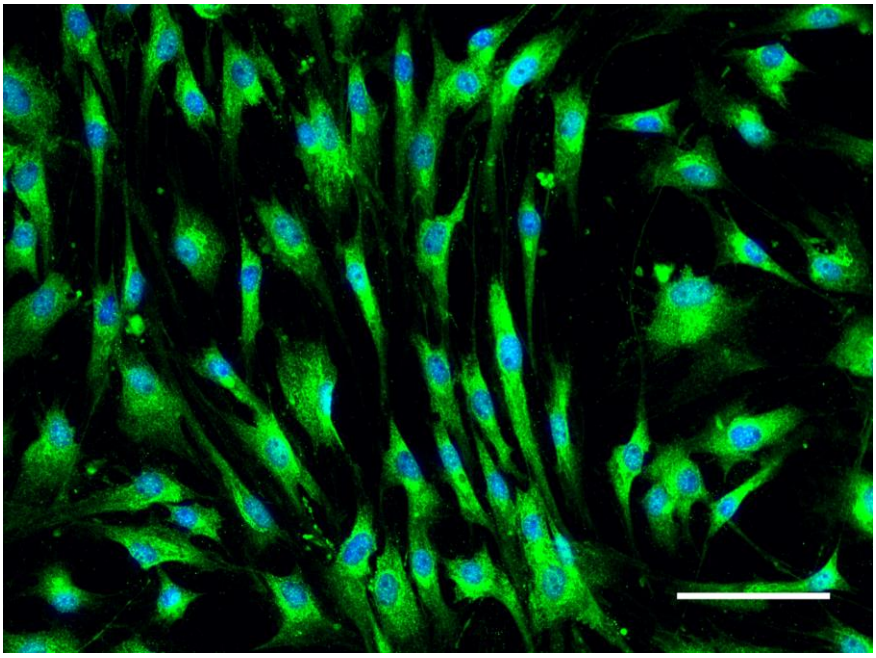

Figure 5.3 S-100 immunohistochemistry (green) on primary Schwann cells with DAPI staining (blue) of nuclei (scale bar = 100 µm).

PKH26-labelled primary Schwann cells (Fig. 5.4a) were maintained *in vitro* culture and it was found that the fluorescence intensity of the dye was stable even at the end of two months. PKH26 is a lipophilic dye that labels the cell membrane and has low cytotoxicity than other cytoplasmic or nuclear dyes (Horan and Slezak, 1989). The mean gray value of the cells on day 3 was 82±4.6 (Fig. 5.4b). This decreased to 47±5.2 by the end of two months. However the labelled cells could still by visualized by increasing the exposure time on the imaging camera. PHK26 has been used for *in vivo* labelling of Schwann cells (Hermanns *et al.*, 1997) and is suitable for long *in vivo* follow-up of labelled cells (Teare *et al.*, 1991). In our study the

fluorescence of PKH26-labelled Schwann cells was still appreciated at the end of 2 months. With promising *in vitro* labelling, the membrane marker was also used for the *in vivo* studies.

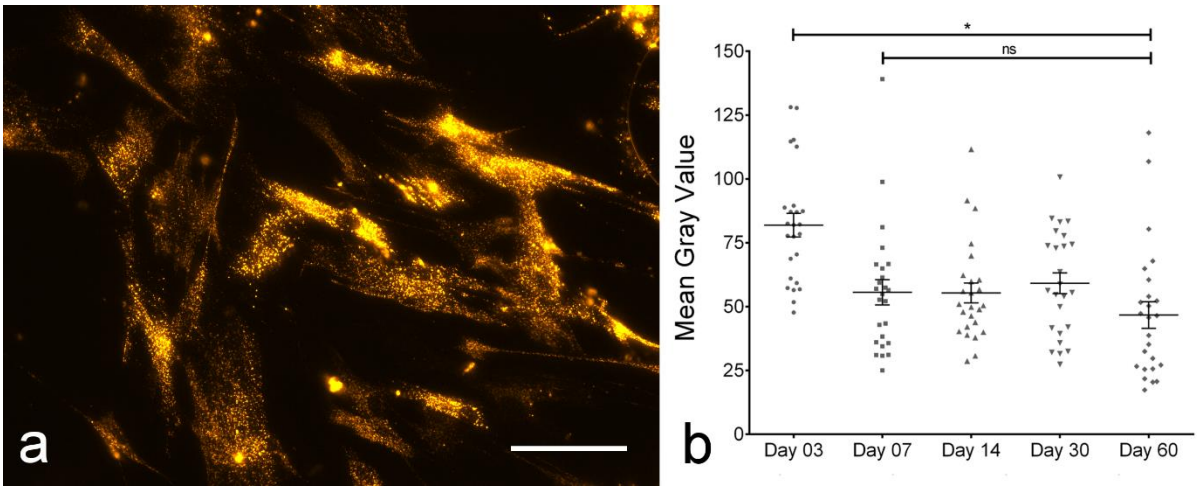

Figure 5.4 a) Primary rat Schwann cells labelled with PKH26 at 2 weeks in culture (scale bar = 100 µm) b) Mean gray values of PKH26-labelled Schwann cells assessed *in vitro* at indicated times in culture. Significant difference between mean gray value at day 03 and that on other days in culture is ($p<0.0001$)] is indicated by *. No significant difference (ns) on comparison between days 7, 14, 30, and 60 (n= 25).

5.3.2 Implantation of the scaffold conduit

The alginate-HA scaffold implanted in the animals resulted in anatomical continuity of the nerve at the end of 8 weeks (Fig. 5.5). Alginate has been suggested to be a suitable nerve conduit material as residual material is not found within the regenerated nerve (Sufan *et al.*, 2001). At the concentration of alginate used in this study, more than 50% of HA can be retained within the scaffold for a prolonged period (Lindenhayn *et al.*, 1999).

PKH26-labelled Schwann cells were visualized in nerve sections obtained from an animal, which was sacrificed at the end of one week (due to autotomy). On Fig. 5.6, the nerve section is stained for S-100 protein (green color), and cell nuclei (blue color) using 4',6-diamidino-2-phenylindole (DAPI). The orange colored cells represent the PKH26-labelled Schwann cells that were initially contained in the alginate-HA scaffold. However labelled Schwann cells were not seen in other animals at the end of 8 weeks. Immunohistochemistry for S100 was positive in all animals; indicating that other native Schwann cells did migrate into the nerve injury site.

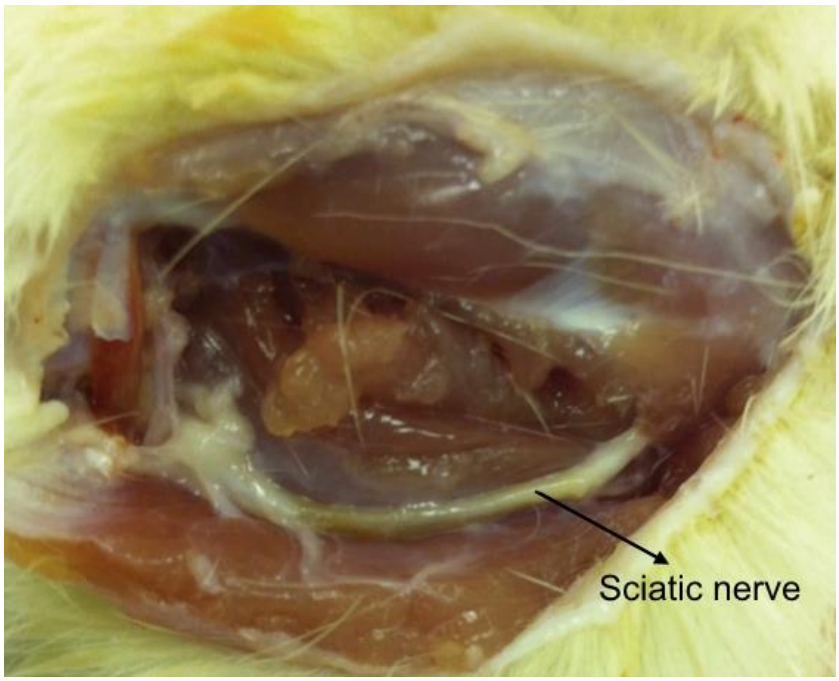

Figure 5.5 Anatomical appearance of sciatic nerve repaired with alginate-HA scaffold at the end of 8 weeks.

Although PKH26 labels the cell membrane, diffusion of the dye can cause cytoplasmic labelling. Therefore this leads to low intensity of the dye in the replicated cells (Parish, 1999). Mosahebi et al. (2000), used Schwann cells labelled with PKH26 and found the dye to be stable *in vivo* for 4 weeks. Other gene transfer-free cell labelling dyes include a more stable cytoplasmic dye, carboxyfluorescein diacetate (Wang *et al.*, 2005). Carboxyfluorescein has been used *in vivo*, to track oligodendrocyte precursor cells for more than a month (Kang *et al.*, 2006). Similarly, Schwann cells have also been tracked *in vivo* (Li *et al.*, 2003). Although gene transfer-free labelling are promising, long-term studies would be more practical by inducing the expression of green fluorescent protein (GFP) in the cells. Schwann cells isolated from transgenic SD rats expressing GFP have been stable for as long as 2 months *in vivo* (Woodhoo *et al.*, 2007).

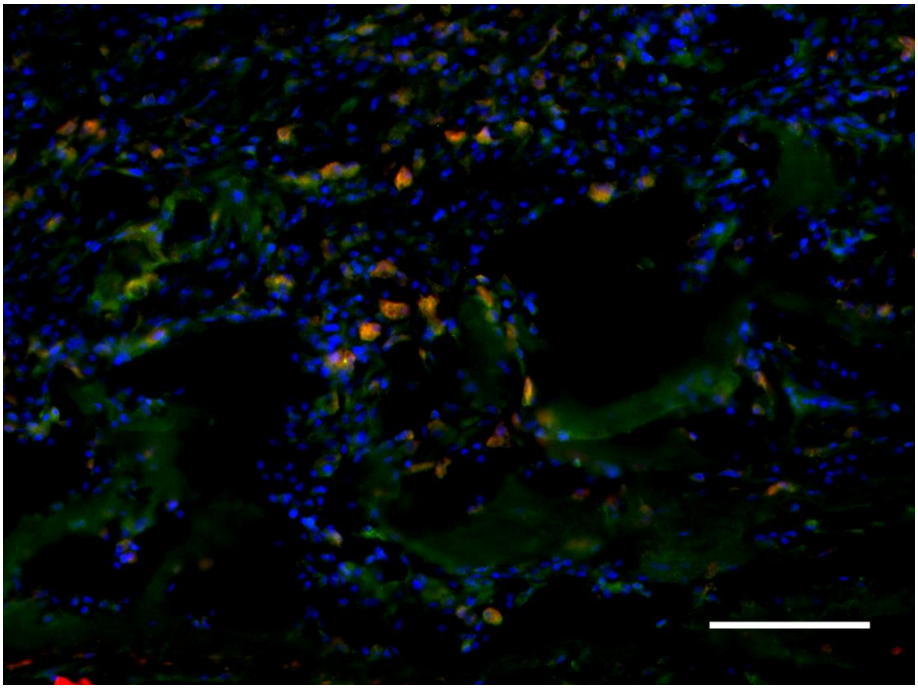

Figure 5.6 PKH26-labelled Schwann cells in section of alginate-HA scaffold recovered after 1 week. Immunohistochemistry for S-100 (green) is also done and nuclei are stained with DAPI (blue). The PKH26 labelled Schwann cells (red) appear orange, as they are merged with the staining for S-100 (scale bar = 100 µm).

5.3.3 Sciatic function index

In general, a SFI value of approximately -10 to 0 indicates normal nerve function and that of approximately -100 or less indicates total dysfunction. As muscle contraction or muscle action potential measurements do not measure actual functional recovery, assessing SFI is crucial to assess functional efficacy of the nerve repair strategy (de Ruiter *et al.*, 2014). After resection or transection of the sciatic nerve, the footprints showed an increase in print length (PL) and a decrease in the TS and ITS (Fig. 5.7). Unfortunately, assessing SFI in our study was not effective, as a result of low sample size because most animals showed autotomy of their toes. Besides one animal each from the alginate-HA and alginate-HA with fibronectin group, and all the sham animals, all other animals succumbed to the loss of one or more toes before the end of the study. The loss of digits in most animals, occurred within the end of 4 weeks, similar to another study that used SD rats (Weber *et al.*, 1993). SFI therefore does have its limitations due to the development of muscular contractures (Dellon and Mackinnon, 1989) and/or autotomy in rats that have complete transection or resection of the sciatic nerve. Although certain strains of

rats have lower incidence of autotomy, preventing contractures of the hind paws after sciatic nerve injury is challenging. Therefore studies have suggested the measurement of the ankle angle, instead of footprint analysis (Varejão *et al.*, 2003). Due to the increased incidence of autotomy in our study, we maintained a timeline of autotomy.

Figure 5.7 Foot prints of a) rat from sham group and b) rat with left sciatic nerve resection and repair using alginate-HA scaffold at week 2 after surgery.

5.3.4 Autotomy timeline

In contrast to other studies that record autotomy scores (Inbal *et al.*, 1980; Wall *et al.*, 1979), we maintained a timeline of when injury (bite wounds with inflammation) and loss of digits occurred in each animal (Fig. 5.8). By the end of 8 weeks, it was noted that only 1 animal in each group (except those with scaffolds including Schwann cells) with damage to the nerve had not lost any digit. The sham animals showed no signs of autotomy at any point in the study. As in previous studies, autotomy in our animals, began with biting of the toes and proceeded to loss of the entire toe(s). However in one animal, autotomy was atypical, beginning at the heel and proceeding to the leg. Due to extensive damage, this animal was sacrificed at the end of one week after the surgery.

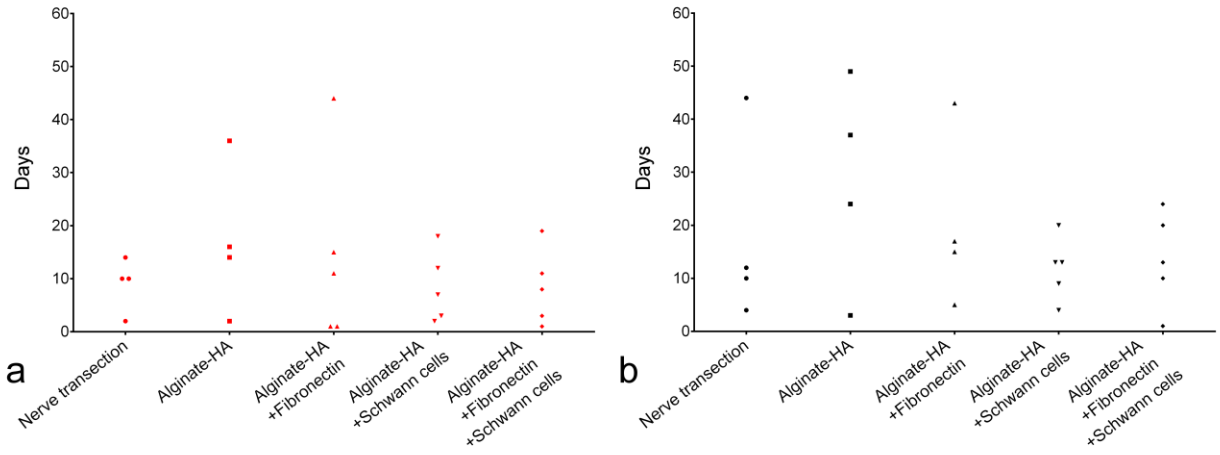

Figure 5.8 a) Occurrence of damage to toe(s) b) Occurrence of complete loss of toe(s). Each dot represents the occurrence of the event in an animal.

Autotomy is frequently seen in animals with limb denervation and is considered to be an equivalent of neuropathic pain (Mogil, 2009). Various approaches have been used to prevent this. We tried using a bitter deterrent solution to prevent autotomy as described in few other studies (Hadlock et al. 2004; Milligan *et al.*, 1999; Hadlock et al. 2005). However the failure of this intervention is clearly evident from the extent of autotomy in our study. Other approaches on preventing autotomy include the use of tricyclic antidepressants (Seltzer et al. 1989), corticosteroids (Kingery et al. 1999), magnesium sulphate (Feria *et al.*, 1993), and tryptophan (Abbott and Young, 1991). The occurrence of autotomy is also regulated by the technique of neurectomy (Zeltser *et al.*, 2000), genetic factors (Inbal *et al.*, 1980), and the strain of rats used (Carr *et al.*, 1992). Lewis rats have a decreased tendency towards autotomy behavior following the implantation of nerve conduits in resected sciatic nerve repair (Harley *et al.*, 2004; Berrocal *et al.*, 2013). In a preliminary study, we performed the similar surgical procedure on Lewis rats and found no autotomy on short-term survival (2 weeks). The use of Lewis rats would therefore be more practical for long-term functional studies.

5.3.5 Immunohistochemistry

The expression of genes and protein synthesis vary at the proximal and distal ends of the injured nerve (Jiang *et al.*, 2014; Li *et al.*, 2014). βIII-tubulin, a neuron-specific microtubular

protein (Karki *et al.*, 2013), is localized in the axons of peripheral nerves. After axotomy, the expression of βIII-tubulin is upregulated at the proximal end of the nerve and it eventually increases at the distal end of the nerve (Hoffman *et al.*, 1992). As regeneration occurs, there is increased βIII-tubulin immunoreactivity at the distal end. The intensity of immunoreactivity to specific proteins, expressed as mean gray value levels has been used to quantify protein expression in peripheral nerve sections (Orita *et al.*, 2013; Nadeau *et al.*, 2014). Immunoreactivity to specific proteins at the distal nerve end is compared to that expressed in the proximal end (Berg *et al.*, 2013) and their ratio is used to quantify regeneration. In this study, βIII-tubulin was quantified in both the proximal and distal ends of the nerve (Fig. 5.9). The ratio of the distal to proximal mean gray values of βIII-tubulin, was 0.94 ± 0.02 in the sham group and 0.95 ± 0.02 in the group with primary epineural suture repair. Similar immunoreactivity on either nerve ends in the primary epineural suture repair group suggest the occurrence of axonal regeneration from the proximal to the distal end. However in all the other groups with nerve resection and alginate-HA scaffold implant, the ratio was lower (0.63 ± 0.02 for the alginate-HA group). This reduction in the ratio was statistically significant when compared with either the sham or the primary epineural suture repair group. The addition of fibronectin or Schwann cells resulted in higher mean values of immunoreactivity (0.66 ± 0.02 and 0.64 ± 0.01 respectively). However there was no significant difference in the βIII-tubulin immunoreactivity when compared with the alginate-HA group. In the group with fibronectin and primary Schwann cells incorporated to the alginate-HA scaffolds, the ratio was lower (0.41 ± 0.02). Therefore there was no synergistic effect on incorporating fibronectin and Schwann cells.

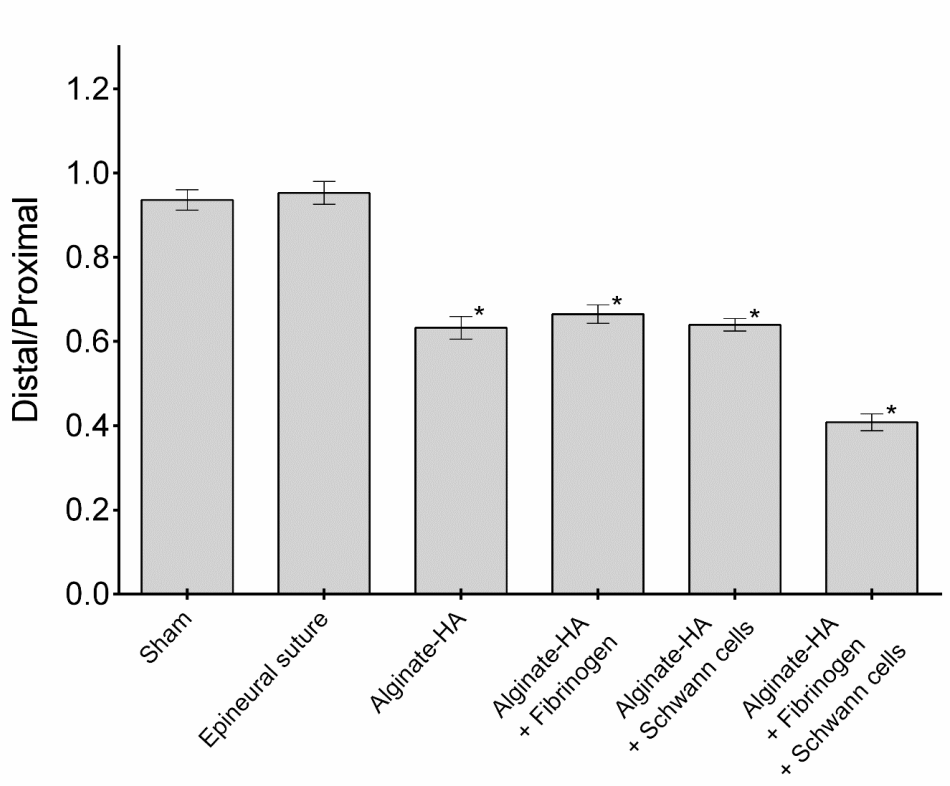

Figure 5.9 Ratio between the mean gray values of β-III tubulin immunoreactivity in the distal nerve end to that of the proximal end in each treatment group. Significant difference between epineural suture repair group and other animal groups ($p<0.0001$)] is indicated by * (n= 25 from each animal in all groups).

Although the dissected sciatic nerves from the animals, showed anatomical continuity without neuroma formation at the end of 8 weeks, βIII-tubulin immunoreactivity in the distal nerve end was low (Fig. 5.10). Therefore the scaffolds used in the study do not seem to be favorable towards axonal guidance. Covalently crosslinked alginate scaffolds have been used successfully in nerve regeneration (Sufan *et al.*, 2001; Wu *et al.*, 2002). The use of ionic crosslinking in this study may have resulted in early degradation of alginate. Although ionically crosslinked alginate have been used earlier, poly(L-lactide-co-D,L-lactide) or polyurethane tubes were used as conduits (Szarek, 2012). Collagen is a preferred nerve conduit due to its permeability. The collagen type-I sheet used in this study lacked adequate mechanical strength when compared with other synthetic polymers. Crosslinking of the collagen in this study would have retained permeability as well as mechanical strength.

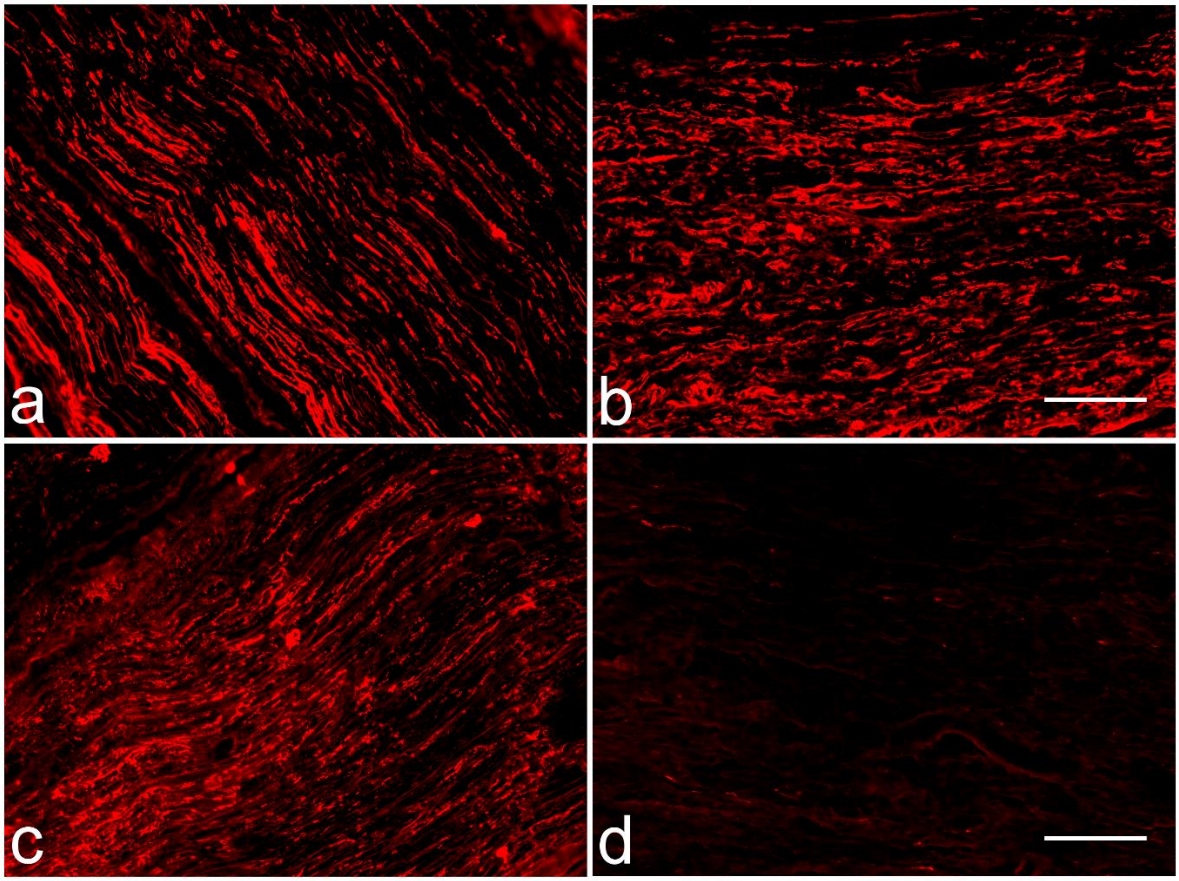

Figure 5.10 βIII-tubulin immunoreactivity in longitudinal sections of sciatic nerve from a rat treated with primary epineural suture; a) at the proximal end of the transected nerve b) at the distal end of nerve. βIII-tubulin immunoreactivity in rat treated with alginate-HA scaffold implant; c) at the proximal end of initially resected nerve d) at the distal end of nerve (scale bar = 100 μm).

The Schwann cells within the alginate-HA scaffolds had spherical morphology, rather than their usual bipolar morphology. Axonal guidance is more effective when Schwann cells retain their bipolar morphology. Also Schwann cell infiltration into the scaffold is higher in porous alginate scaffolds when compared with hydrogels (Loebsack *et al.*, 2001). Fibronectin improves the outcome of Schwann cell proliferation in alginate (Mosahebi, Wiberg, and Terenghi, 2003); however in the absence of covalent binding with the alginate-HA, diffusion of fibronectin from the scaffold is a concern. These drawbacks of using a polysaccharide-based scaffold material, such as alginate can be eliminated by the use of collagen or fibrin-based scaffolds.

5.4 Conclusions

Recent progress in 3D printing has enabled the fabrication of intricate and porous hydrogel scaffolds containing living cells. In this study we used 3D printed alginate-hyaluronic acid scaffolds with or without Schwann cells and/or fibronectin, enclosed within a collagen sheet as nerve repair conduits. At the end of 2 months, despite the anatomical continuity of the resected nerve, it was found that only few axons regenerated across the injury through the scaffolds. The addition of Schwann cells and/or fibronectin did not influence the regeneration of axons across the resected nerve. As polysaccharide hydrogels are less very favorable for Schwann cells, protein-based hydrogels like collagen and fibrin would be better suited materials for fabricating nerve repair scaffolds. Autotomy has always been a concern in rats with complete nerve transection or resection. As SD rats have a high incidence of autotomy, Lewis rats are more practical for long-term nerve regeneration studies, involving functional assessment.

CHAPTER 6

AN *IN VITRO* COMPARISON OF THE 3D BIOPRINTING OF ALGINATE, COLLAGEN, AND FIBRIN HYDROGELS FOR USE IN NERVE TISSUE ENGINEERING*

*This chapter has been submitted as "Rajaram A, England S, Schreyer D, Chen XB. An *in vitro* comparison of the 3D bioprinting of alginate, collagen, and fibrin hydrogels for use in nerve tissue engineering" to the *Journal of Tissue Engineering and Regenerative Medicine* on February 19, 2015.

6.1 Introduction

Schwann cells are the resident glial cells of the peripheral nervous system that normally myelinate or ensheath axons to improve conduction velocity and provide metabolic support (Salzer, 2012). When a peripheral nerve is injured, Schwann cells help scavenge myelin debris and proliferate to form highly aligned arrays in the distal nerve segment called the bands of Büngner (Chaudhry *et al.*, 1992) within spaces confined by retained basal lamina tubes (Bunge, 1994). Guidance of regenerating axons is greatly influenced by extracellular matrix proteins in the basal lamina of Schwann cells (Nguyen *et al.*, 2002). Schwann cells also produce neurotrophic factors that promote axon regeneration. During peripheral nerve regeneration, Schwann cells migrate ahead of the extending axonal growth cones to guide axons (Torigoe *et al.*, 1996). Regenerating axons that grow in proximity to the bands of Büngner and the basal lamina have greater success at reaching their end organ (Campbell, 2008). On the contrary, axons that 'miss' the bands of Büngner often end up being misaligned and may form a neuroma (Ide, 1996). In the event of a breech in the continuity of the existing basal lamina at the distal end of the injured nerve, Schwann cells must accompany the regenerating axons to facilitate repair (Sketelj *et al.*, 1989). Schwann cell morphology and migration are crucial for axonal regeneration and remyelination (Lobsiger *et al.*, 2002). In tissue culture, Schwann cells may have unipolar, bipolar, or multipolar morphology, with the bipolar morphology being most common (Wang, *et al.*, 2012). These polarized morphologies are correlated with substrate adhesion and high motility and Schwann cells can transform from one morphology to another depending on the substrates or materials in their vicinity (Vu *et al.*, 2014).

Various biomaterials, like alginate, collagen, gelatin, fibrin, chitosan, and other synthetic polymers, have been used as luminal fillers in tissue repair scaffolds for nerve tissue engineering applications (Jiang *et al.*, 2010). The interaction of Schwann cells with these materials affects cell proliferation, migration, and differentiation. Collagen and fibrin, in particular, are commonly used luminal fillers, as they are naturally occurring components of the extracellular matrix.

Although alginate is not a component of the nerve matrix, its biocompatibility makes the incorporation of Schwann cells feasible. It can be rapidly crosslinked by calcium ions and its physical properties can be tuned. Freeze-dried alginate permits axonal regeneration across long gaps and has been used to repair 5 cm defects in cat sciatic nerves (Suzuki *et al.*, 1999). Crosslinked alginate sponges without tubular conduits or nerve guidance channels have also been used to repair peripheral nerve injuries (Sufan *et al.*, 2001). It has also been shown that chick embryo dorsal root ganglia (DRG) extend longer axons when they are co-cultured with Schwann cells in alginate (Mosahebi *et al.*, 2001). Alginate with incorporated cells can be 3D-printed as scaffolds for tissue repair (Rajaram *et al.*, 2014).

Collagen promotes neurite outgrowth *in vitro* and when used *in vivo* as a luminal filler in nerve conduit channels, it leads to improved sensory function (Jin *et al.*, 2013). Axon extension in collagen is augmented in the presence of Schwann cells. Rolled sheets of collagen gel with incorporated Schwann cells have been proposed as potential nerve repair conduits (Goto *et al.*, 2010). Three-dimensional (3D) collagen scaffolds have been printed using a cryogenic direct-plotting system, where the extruded collagen is immediately frozen to retain its structure (Kim *et al.*, 2009).

Fibrinogen from blood plasma is converted by thrombin to fibrin and is incorporated as a temporary extracellular matrix protein of the nerve (Akassoglou *et al.*, 2000). Fibrin gel has been used as a vehicle to deliver nerve growth factor (Sakiyama-Elbert and Hubbell, 2000) and fibrin containing Schwann cells has been used as a luminal filler to promote axonal regeneration (Galla *et al.*, 2004). The addition of neurotrophins along with Schwann cells into fibrin has also been used for the regeneration of rat sciatic nerves (Ma *et al.*, 2013). Inkjet 3D printing has enabled layers of neural cells and fibrin to be stacked over each other to form a 3D nerve repair scaffold (Xu *et al.*, 2006).

Recently, 3D biofabrication techniques have been drawing much attention for the fabrication of hydrogel-based nerve repair scaffolds. One key strategy in these scaffolds is the formation of structures resembling the bands of Büngner (Ribeiro-Resende *et al.*, 2009). Micropatterning cells with high resolution cannot be achieved using current bioprinting techniques (Derby, 2012). While this is feasible with laser-based microfabrication techniques, photon-induced cellular damage and transfer of metallic particles along with the deposited hydrogel or cells are a few drawbacks (Smausz *et al.*, 2006). Therefore, 3D bioprinting of appropriate hydrogels that enable Schwann cell alignment is a practical strategy. Because Schwann cell morphology influences the outcome of nerve repair, inducing favorable cell morphology in 3D culture is crucial. Alignment is another important parameter to be considered. Cell alignment can be induced by forming grooves on culture surfaces (Kim *et al.*, 2007), fabricating microchannels (Sarig-Nadir *et al.*, 2009), micropatterning (Nikkhah *et al.*, 2012), or by using extracellular matrix proteins as haptotatic cues (Zhu *et al.*, 2010). Schwann cells aligned using micropatterning techniques can direct neurite outgrowth (Thompson and Buettner, 2004; Schmalenberg and Uhrich, 2005).

In this study, we examined the suitability of various hydrogels that are potentially useful in nerve tissue engineering, including alginate, collagen type-I, fibrin, and composite hydrogels composed of alginate with collagen type-I or fibrin with hyaluronic acid. The fidelity of printing each of these hydrogels using a commercial 3D printer is examined. The viability, morphology, and alignment of Schwann cells within these hydrogels are also studied. Our findings provide guidance for future strategies to engineer the creation of 3D bands of Büngner for *in vivo* nerve repair.

6.2 Methods

6.2.1 Preparation of the hydrogels

Alginate

Alginate (from brown seaweed) (Sigma, Oakville, ON, Canada) was dissolved in 0.3 M sucrose and 4.2 mM HEPES buffer (pH 7.4) and was used at a concentration of 20 mg/ml. The osmolality of the alginate solution was made physiological by using sucrose. Solutions containing phosphate ions were avoided as they affect the crosslinking of alginate (Drury *et al.*,

2004b). The alginate was crosslinked for 5 minutes in a solution containing 20 mM calcium chloride, 110 mM sodium chloride, and 20 mM HEPES.

Collagen type-I

Collagen type-I solution from rat tail (4 mg/ml from Advanced Biomatrix, CA, USA) was mixed in equal volume with a neutralizing solution containing 10% Dulbecco's modified Eagle's medium (DMEM), 10% fetal bovine serum (FBS), 10% 0.1 N sodium hydroxide, and 20% of concentrated (3.5x) DMEM. Both the solutions were kept in ice, until being mixed together. The final concentration of collagen was 2 mg/ml.

Fibrin

Fibrinogen from bovine plasma (Sigma, Oakville, ON, Canada) was dissolved at 20 mg/ml with 0.5 mg/ml of aprotinin, a serine protease inhibitor because Schwann cells secrete the fibrinolytic, plasminogen activator (Krystosek, 1984), which can result in degradation of fibrin. Human thrombin (from Tisseel kit, Baxter, Canada) at a final concentration of 4.2 U/ml in a solution containing 20 mM calcium chloride, 110 mM sodium chloride, and 20 mM HEPES, was used to gel the fibrinogen for 5 minutes to form fibrin.

Alginate/collagen type-I

Alginate (40 mg/ml) was mixed with neutralized collagen (2 mg/ml) at a ratio of 1:1. The resulting hydrogel, containing 20 mg/ml alginate and 1 mg/ml collagen type-I was left in room temperature for 2 minutes and then crosslinked for 5 minutes with a solution containing 20 mM calcium chloride, 110 mM sodium chloride, and 20 mM HEPES.

Alginate/fibrin

Alginate (40 mg/ml) was mixed with a solution of fibrinogen (40 mg/ml) and aprotinin (1 mg/ml), at a ratio of 1:1. Thrombin (final concentration of 4.2 U/ml) was instilled into the hydrogel to initiate gelling of the fibrinogen. After 2 minutes, the crosslinking was completed by using a solution containing 20 mM calcium chloride, 110 mM sodium chloride, and 20 mM HEPES.

Fibrin/hyaluronic acid

Fibrinogen (20 mg/ml) containing 0.5 mg/ml of aprotinin was mixed with 4 mg/ml of hyaluronic acid sodium salt (Sigma, Oakville, ON, Canada) at a ratio of 1:5. Human thrombin (final concentration of 4.2 U/ml) in a solution of 20 mM calcium chloride, 110 mM sodium chloride, and 20 mM HEPES, was used to gel the fibrinogen/hyaluronic acid mixture for 5 minutes.

Table 6.3. Extrusion pressure and printing speed used for bioprinting hydrogels.

Hydrogel	Extrusion pressure (Barr)	Printing speed (mm/s)
Alginate	0.3	12
Collagen type-I	0.1	12
Fibrin	0.1	16
Alginate + collagen type-I	0.3	12
Alginate + fibrin	0.3	12
Fibrin + hyaluronic acid	0.1	12

6.2.2 Printing of hydrogel strands

A 3D-Bioplotter (envisionTEC, Gladbeck, Germany) was used to print single-layered patterns using each of the hydrogels. The hydrogel solutions were extruded into respective crosslinking or gelling solutions (except collagen type-I) through steel-tip dispensing needles (EFD Nordson, Westlake, OH, USA) with an internal diameter of 100 µm. When using extrusion-based biofabrication, parameters such as the speed of dispensing head, extrusion pressure, and flow rate of the material must be optimized in order to obtain continuous scaffold strands (Li, *et al.*, 2009). The speed of printing was 12 mm/s for all of the gels (except for fibrin, which was 16 mm/s). The extrusion pressure was adjusted depending on the viscosity. Hydrogels of low viscosity were printed with 0.1 bar, while alginate and alginate-based gels were printed with 0.3 bar. Fibrin is less viscous and therefore a lower printing speed and pressure was used. The extrusion pressure and speed of printing for each hydrogel is given in Table 6.1.

Alginate and alginate/collagen type-I were printed into a solution containing 20 mM calcium chloride, 110 mM sodium chloride, and 20 mM HEPES. Fibrin and alginate/fibrin were printed into the same solution with added thrombin (25 U/mL). Collagen type-I was printed onto a dry slide and then incubated at 37°C to gel for 5 minutes. A schematic of the printing method used is shown in Fig. 6.1.

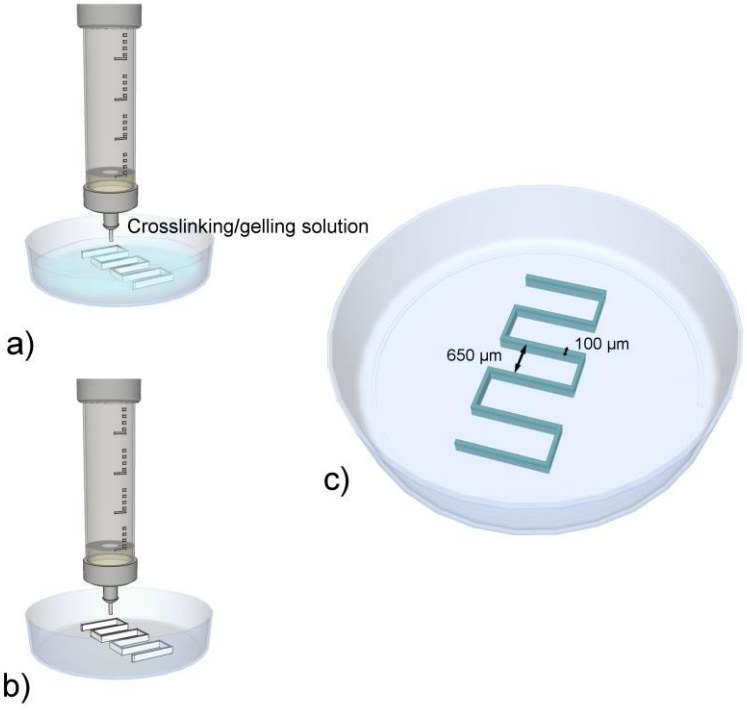

Figure 6.1 a) Bioprinting into a crosslinking/gelling solution for alginate, alginate/fibrin, alginate/collagen, fibrin, and fibrin/hyaluronic acid. b) Bioprinting in air for collagen type-I. c) Schematic of a printed single layered strand.

6.2.3 Print fidelity

Strand print fidelity depends on the physical properties of the extruded hydrogel and the accuracy of the machine (Chung *et al.*, 2013). To assess the final morphology of printed strands, we measured the areas occupied by the materials after extrusion to the intended area, as reported previously (Rajaram *et al.*, 2014). Briefly, the 3D-Bioplotter® was used to extrude each of the hydrogel in a pattern as shown in Fig. 6.1c. The intended strand dimension was 100 µm (similar to the internal diameter of the dispensing needle) and the interstrand spacing was programmed to be 650 µm on the software controlling the machine. Final adherence to these parameters was

assessed from measurement of images of the printed strands and compared with the intended dimensions.

6.2.4 Isolation of rat primary Schwann cells

Enriched primary rat Schwann cells were isolated from the sciatic nerves of Sprague-Dawley rats using a D-valine selection method (Kaewkhaw et al. 2012). Briefly, the sciatic nerve was isolated, the epineurium was removed and the nerve was cut into 2 mm fragments. The fragments were digested with collagenase for 1 hour. The resulting cell suspension was filtered and cultured in Dulbecco's Modified Eagle's Medium (DMEM) containing D-valine (instead of L-valine), 10% fetal bovine serum (FBS) and mitogens (forskolin, N2 supplement, and bovine pituitary extract). The presence of only D-valine successfully suppresses fibroblast overgrowth.

6.2.5 Schwann cell viability and proliferation

Primary Schwann cells were added to the hydrogels at a density of 5×10^5 cells/ml. The cells were suspended in 10 µl of DMEM, added directly to the alginate, fibrinogen, or neutralized collagen type-I and mixed by repeated pipetting. For the alginate-based composite hydrogels, the cell suspension was added into the alginate solution, prior to mixing with either fibrinogen or collagen type-I. 5 µL droplets of each hydrogel containing primary Schwann cells was pipetted into the wells of a 96-well tissue culture plate. To prevent the hydrogels droplets from dislodging, the plate was coated previously with a solution of 0.5% polyethyleneimine and thoroughly washed with sterile distilled water. Each hydrogel was gelled or crosslinked as mentioned before and maintained in DMEM with 10% fetal bovine serum in a 37°C humidified incubator containing 5% CO_2.

Viability of Schwann cells was assessed on day 3 in culture. The culture medium was replaced with DMEM containing calcein-AM (1 µg/ml, AnaSpec, CA, USA) and propidium iodide (10 µg/ml, AnaSpec, CA, USA) and the hydrogel samples were incubated for 1 hour at 37°C. Images of the stained cells in the hydrogels were captured using a fluorescence microscope (Axiovert 100, Zeiss). The images (n=5) were analyzed using ImageJ (National Institutes of Health, MD, USA). Cell viability was ascertained from the ratio of live cells (green fluorescent) to total cells (green + red fluorescent) in the images captured.

Because Schwann cell viability was found to vary little between culture conditions, total cell number was used to estimate cell proliferation over time. Proliferation of Schwann cells within hydrogels (Galateanu *et al.*, 2012) was assessed on days 3 and 7, using 3-(4,5-dimethylthiazol-2-yl)-2,5-diphenyltetrazolium bromide (MTT) assay. MTT solution (5 mg/ml) was added to the culture medium of each well and the gels were incubated for 5 hours at 37°C. The medium was aspirated and 1 ml of dimethyl sulfoxide (DMSO) was added to each well. The hydrogel droplets were mechanically disrupted to thoroughly solubilize the formazan contained within them. The resulting solution was centrifuged to remove hydrogel fragments and 200 µl of the supernatant was plated into another 96-well plate. The absorbance of the supernatant (n=5) was measured at 560 nm using a micro-plate reader (Molecular Devices SpectraMax 340, California, USA). The blank absorbance value of each hydrogel (from hydrogels containing cells but not treated with MTT) was subtracted.

6.2.6 Schwann cell morphology

To assess morphology of Schwann cells cultured in the hydrogels, similar droplet cultures as done for viability assessment were prepared. Schwann cells were stained using calcein-AM (1 µg/ml) on days 1, 3, and 10, and fluorescent images were captured. Morphology was analyzed by calculating circularity using the software ImageJ. Circularity is a measure of the roundedness of a cell, related to its area and perimeter, and can theoretically range between 0 and 1, with 1 indicating a perfect circle (Wittmer *et al.*, 2007).

6.2.7 Schwann cell alignment in printed strands

To assess alignment of cells in printed strands, primary Schwann cells were mixed into each hydrogel at a density of 4 x 10^5 cells/ml and single strands of 10 mm length were printed into the respective gelling or crosslinking solutions (except collagen type-I) using the same printing parameters as mentioned earlier. Each hydrogel was crosslinked or gelled for 5 minutes, after which it was maintained in culture in DMEM with 10% FBS in an incubator at 37°C. The cells in the hydrogel strands were stained with calcein-AM on day 3, as described above, and fluorescent images were collected for analysis.

6.2.8 Statistical analysis

All data is expressed as the mean ± standard error of the mean (SEM). One-way analysis of variance (ANOVA) with Bonferroni post-test correction was used for comparison between groups. $p<0.05$ was considered as statistically significant. Data analysis was performed using Graphpad Prism (GraphPad Software, San Diego, CA, USA).

6.3 Results

Single-layered hydrogel strands were printed by extruding material through a dispensing needle with an internal diameter of 100 μm. Alginate crosslinks instantly on interaction with calcium ions, and fibrinogen gels quickly in the presence of thrombin and calcium ions. Printed strands of alginate and alginate/fibrin were linear and uniform in dimension (Fig. 6.2a, 6.2c, 6.2f). However, the final strand width of fibrin gels is greater than alginate as the gelation of fibrinogen is not as quick as the crosslinking of alginate (Fig. 6.2e). The addition of hyaluronic acid made the fibrinogen solution more viscous and the strand width was significantly decreased (Fig. 6.2f). Unlike fibrin and alginate, collagen type-I did not gel quickly. On printing, collagen type-I spread out on the printing surface. By the time complete gelation after incubation at 37°C occurred, individual strands had coalesced such that interstrand spaces were eliminated (Fig. 6.2d). Even when mixed with alginate, the collagen type-I spread out and the strand width was significantly higher than alginate alone and alginate/fibrin (Fig. 6.2b, 6.2c).

The strand width and interstrand spacing of each hydrogel is shown in Fig. 6.3. It is seen that alginate represents the intended dimensions more closely than the other hydrogels (strand width of 120 ± 5.3 μm and interstrand space of 629 ± 6.9 μm). Fibrinogen was printed into a solution containing thrombin; however, its dimensions were larger than those intended. The addition of hyaluronic acid decreased the strand width from 787 ± 23 μm to 183 ± 3.7 μm and the interstrand space was increased from 42 ± 11 μm to 555 ± 8.9 μm. Collagen type-I could not be printed into strands.

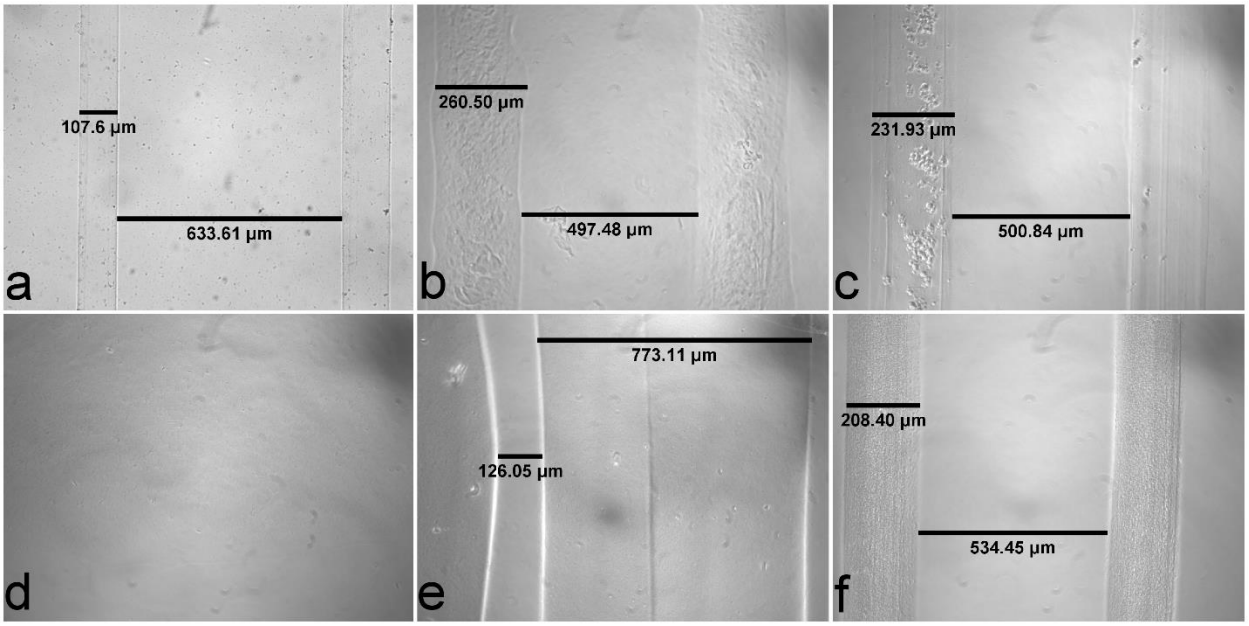

Figure 6.2 3D printed strands of a) alginate b) alginate/collagen type-I c) alginate/fibrin d) collagen type-I e) fibrin f) fibrin/hyaluronic acid.

A live/dead assay, using calcein-AM and propidium iodide staining, was done to compare the biocompatibility of the different hydrogels. Primary Schwann cells were cultured in hydrogel droplets. Cell viability, measured by calculating the percent of all cells that were still alive on day 3 in culture, was very similar in all the hydrogels. Although viability trended highest in fibrin (89.2 ± 2.9), no significant statistical difference was found between different hydrogel formulations (Fig. 6.4a).

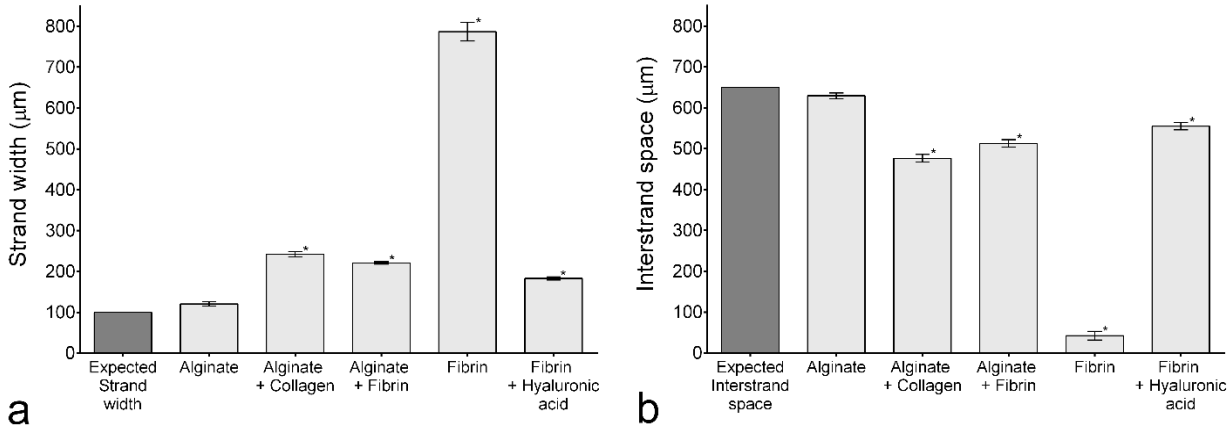

Figure 6.3 a) Strand width of printed hydrogels b) interstrand spacing between adjacent hydrogel strands [n = 5; *p<0.001 on comparing the strand width or interstrand space in each hydrogel with the respected intended dimension].

An MTT assay was used to assess proliferation of primary rat Schwann cells in each hydrogel (Fig. 6.4b). MTT assays have been used to study proliferation of cells cultured within hydrogels (Galateanu *et al.*, 2012). On both day 3 and day 7, greater cell proliferation was observed in fibrin (absorbance of 0.248 ± 0.002 at day 3 and 0.696 ± 0.016 at day 7). Measured absorbance related to cell number in collagen type-I was low and that of alginate was the least (0.099 ± 0.004 at day 7). The addition of fibrin to alginate led to increased proliferation of Schwann cells. Besides fibrin, no other hydrogel showed a significant increase in the absorbance when maintained in culture over time.

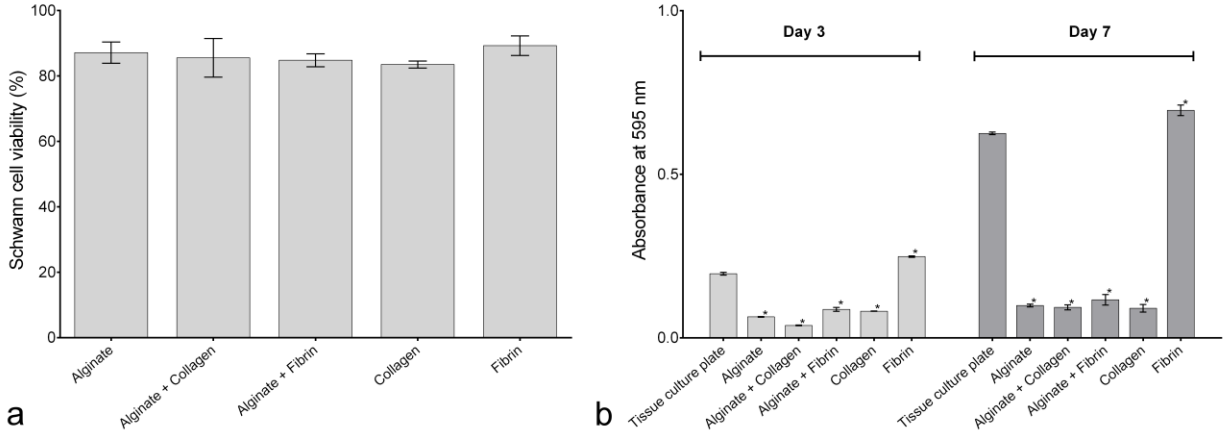

Figure 6.4 a) Schwann cell viability in different hydrogels at the end of day 3 b) MTT assay on day 3 and 7 [n=5; *p<0.0001 when compared with the control (tissue culture plate)].

Hydrogel droplets were also used to examine the morphology of incorporated cells. Schwann cells, normally multipolar in two dimensional culture, extended multiple processes when cultured within collagen type-I or fibrin. When cultured in alginate, they remained nearly spherical throughout the study. While the cells cultured in alginate/fibrin and alginate/collagen type-I attached and spread better than those in alginate, most cells remained spherical, unlike those in collagen or fibrin. On day 1, cell circularity was lowest in fibrin and collagen type-I (0.56 ± 0.02) (Fig. 6.5). On day 5, cells in alginate/fibrin had further slightly decreased their circularity. The results on day 10 were similar to those obtained on day 5.

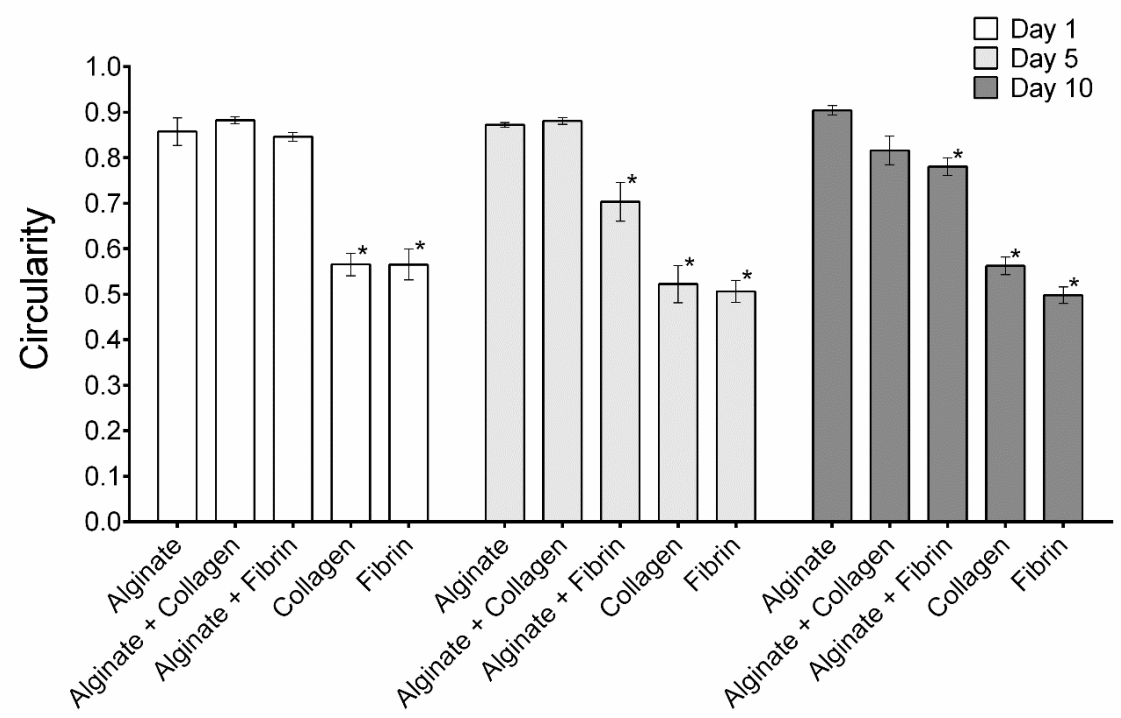

Figure 6.5 Circularity of primary Schwann cells cultured in various hydrogels [n = 5; *p<0.05 on comparing circularity of cells cultured in indicated hydrogels with those cultured in alginate].

Qualitative assessment of Schwann cells in printed hydrogel strands suggests that cell proliferation was highest in fibrin (Fig. 6.6j) confirming the results of proliferation assays (MTT) on droplet hydrogel cultures. Neutralized collagen-type I (Fig. 6.6i) could not be printed into strands and has many cells due to larger volume of the gel dispensed. Similarly as Schwann cell proliferation was found to be low in the presence of alginate, we observed fewer cells in printed strands containing alginate (Fig. 6.6f, 6.6g, and 6.6h). Schwann cells were also more spherical in printed alginate strands (Fig. 6.6f). Schwann cells were observed to be arranged along the edges of printed fibrin strands (Fig. 6.6e, 6.6j). Although Schwann cells incorporated into a fibrin droplet had a random pattern of process extension, those in the 3D printed strands are aligned along the longitudinal axis of the fibrin strand (Fig. 6.7). The addition of hyaluronic acid to fibrinogen also promoted the alignment of Schwann cells in printed strands (Fig. 6.8).

6.4. Discussion

Extrusion-based bioprinting techniques depend on the physical properties and gelation of the hydrogel material (Chung *et al.*, 2013). Alginate and alginate/fibrin did not spread out much because they were quickly crosslinked by calcium in the crosslinking solution. Fibrinogen was successfully printed into strands; however, the dimensions of fibrin strands were much larger due to its lower viscosity. Fibrinogen can be made more viscous by the addition of hyaluronic acid and can be gelled more quickly using a higher concentration of thrombin in the gelation solution. Collagen type-I could not be printed with the intended strand dimensions because of its low viscosity, as well as its slow and difficult to control gelation.

Collagen scaffolds are generally fabricated by casting into a pre-formed mold and then crosslinked or frozen (Sachlos, 2003). Although these casting techniques result in good collagen scaffolds (Liu *et al.*, 2008), the addition of cells into the collagen is not feasible because of the necessary crosslinking chemistry, or freezing step. Alginate/collagen type-I was successfully printed into strands, as the alginate was easily crosslinked. However, the presence of alginate affected Schwann cell morphology. To include incorporated cells in our study, collagen was neutralized prior to printing. Following neutralization, the viscosity of the gel changes with time and printing parameters such as speed and extrusion pressure must be adjusted accordingly. Printing collagen type-I led to either the extrusion of a large amount of material (due to lower viscosity) or clogging of the needle (as it had gelled in the needle before extrusion). Our findings suggest that achieving good print fidelity with collagen and progressing to complete scaffold fabrication would be very challenging.

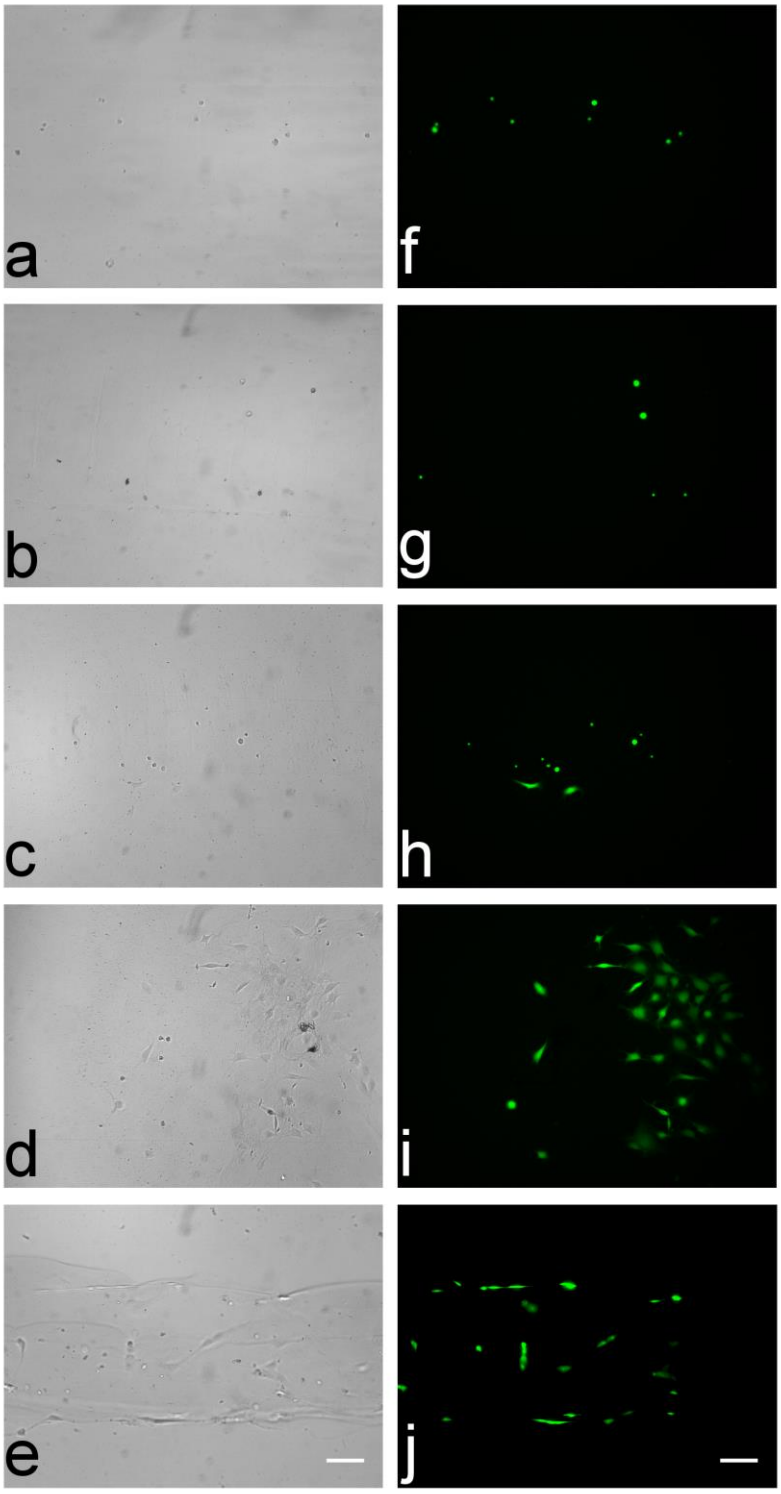

Figure 6.6 Phase-contrast images of printed strands taken at day 3 in culture; a) alginate b) alginate/collagen type-I c) alginate/fibrin d) collagen type-I and e) fibrin. The corresponding fluorescent images showing Schwann cells stained with calcein-AM contained within the strands are also shown (f-j) [Scale bar = 100 μm].

To improve the print fidelity of fibrinogen, we increased its viscosity by including hyaluronic acid, a natural glycosaminoglycan polymer (Fraser *et al.*, 1997b). While a few studies state that fibrin could induce scarring of nerves, hyaluronic acid has been shown to prevent excessive surgical scarring during nerve repair (Ozgenel, 2003). When hyaluronic acid was added, printing of fibrinogen was easier and strand width and interstrand space were closer to the intended dimensions (Fig. 6.3a, 6.3b). Schwann cells continued to align along the edge of the strands in the presence of hyaluronic acid (Fig. 6.8). Thus, bioprinting fibrin enabled Schwann cell alignment and the incorporation of hyaluronic acid improved the fidelity of printing.

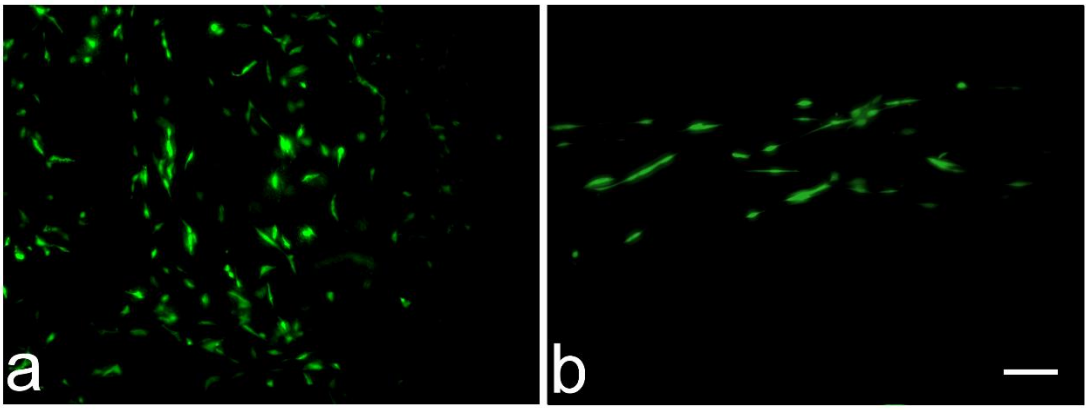

Figure 6.7 a) Schwann cells (stained with calcein-AM) cultured in a droplet of fibrin b) 3D printed strands of fibrin containing Schwann cells [Scale bar = 100 µm].

The viability of Schwann cells cultured in hydrogels was high, as was expected because alginate, collagen type-I, and fibrin are natural biomaterials. Previous studies (Mosahebi *et al.*, 2001) involving long-term cultures of Schwann cells seeded over the same hydrogels resulted in good viability. Our study shows good viability of hydrogel incorporated Schwann cells for each of the compared formulations. Providing a suitable substrate to enable proliferation and long-term survival of Schwann cells is vital. Although collagen-type I is a component of the nerve matrix, it has been observed that the proliferation of Schwann cells is low when they are seeded over collagen-type I coated surfaces (Vleggeert-Lankamp *et al.*, 2004). Collagen type-I preparations from several different sources have been shown to impede the rate of DNA synthesis in glial cells (Eccleston *et al.*, 1989). It is also know that this is not seen with collagen-types III, IV, and V. In our study, though Schwann cell viability in collagen-type I was high, cell

proliferation was not inspiring. It has previously been shown that alginate can reduce viability and proliferation of Schwann cells *in vivo* (Pannunzio *et al.*, 2005) likely because of its lack of cell binding domains (Dhoot *et al.*, 2004). Cellular proliferation in alginate is also negatively influenced by its mechanical properties (Banerjee *et al.*, 2009) and the mitotic activity of the cells is reversed when they are released from the hydrogel (Hunt *et al.*, 2009). In this study, Schwann cell proliferation was lowest in alginate and the addition of collagen-type I or fibrin did not 'rescue' the cells.

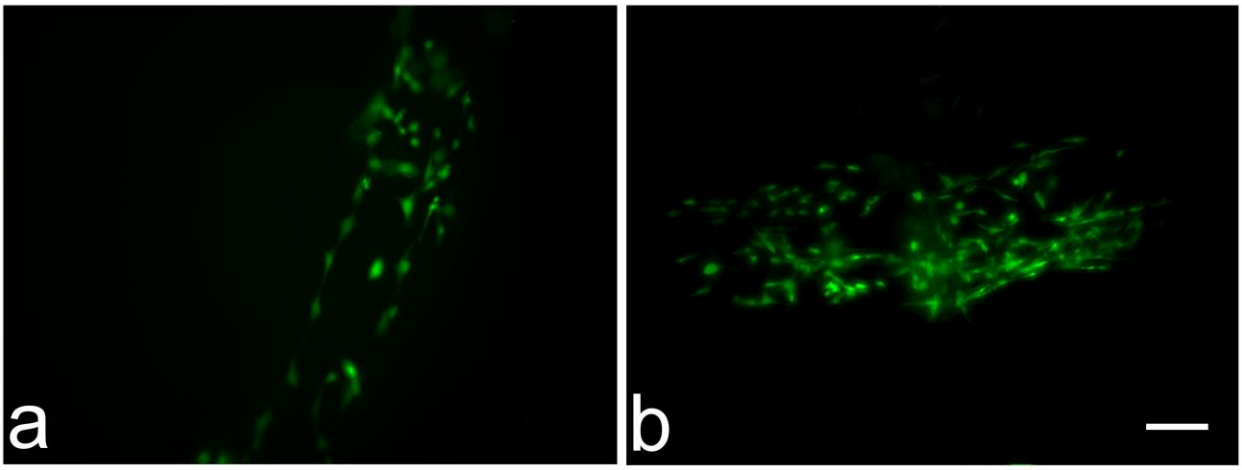

Figure 6.8 a) 3D printed fibrin strand containing Schwann cells (stained with calcein-AM) b) 3D printed fibrin/hyaluronic acid strand containing Schwann cells (stained with calcein-AM) [scale bar = 100 µm].

In order to recreate bands of Büngner in a nerve repair scaffold, we would hope to see elongation of Schwann cells indicative of cell adhesion and capacity for migration. Calcein-AM stains the cytoplasm of Schwann cells uniformly and has been used in the assessment of cell morphology (DeCoster *et al.*, 2010). Alginate, though favorable for encapsulating pancreatic islet cells (Calafiore, 2003) and chondrocytes (Chia *et al.*, 2004), is not ideal for the culture of Schwann cells due to their resulting spherical morphology. Better morphology is obtained by the addition of fibronectin (Mosahebi *et al.*, 2003b) or other cell adhesion peptides (Liu *et al.*, 2009). The morphology of Schwann cells in fibrin and collagen-type I remained bipolar with low circularity for up to 10 days in culture. Therefore, fibrin and collagen type-I would be more beneficial than unmodified alginate or alginate/fibrin and alginate/collagen type-I for the culture of Schwann cells. Kalbermatten *et al.* (2008), have shown that in the presence of fibrin, Schwann

cell adhered better to polyhydroxybutyrate nerve conduits. Schwann cell cultures in collagen type-I have good viability and morphology, but have a low proliferation rate. On the other hand, cultures in fibrin showed good viability, morphology, and proliferation.

While Schwann cells in alginate-containing strands remained spherical, Schwann cells tended to align within printed fibrin strands. During printing the extruded material undergoes various shear stresses at the dispensing nozzle (Aguado *et al.*, 2012). Fibrin filaments align themselves along the direction of induced stress (Hudson *et al.*, 2010), so printing of fibrinogen by extruding it through a fine nozzle may induce fiber alignment. Because Schwann cells tend to align along fibrin filaments, the result is that the long axes of Schwann cells and the fibrin strands are parallel.

Autologous platelet-rich fibrin matrices have been used successfully for nerve repair (Choi *et al.*, 2005), but the mere filling of nerve conduit tubes with fibrin-rich plasma could prevent the longitudinal alignment of fibrin filaments (Williams, 1987). Pre-aligning the fibrin filaments and with them the incorporated Schwann cells is a good strategy. Magnetic fields (Dubey, 2001) or the continuous application of lateral strain (Matsumoto *et al.*, 2007) can align fibrin fibrils. We show that 3D bioprinting of fibrinogen into a solution containing thrombin results in alignment of incorporated Schwann cells, probably due to the alignment of fibrin fibrils. As Schwann cells cultured in fibrin have good viability, the desired bipolar morphology, and also align when bioprinted, better strategies to improve bioprinting of fibrin need to be considered.

Fibrinogen forms an insoluble gel on interaction with thrombin, but the resulting fibrin fibrils become crosslinked only with the addition of activated factor XIII, also known as plasma transglutaminase (Kanaide and Shainoff, 1975). Incorporation of activated factor XIII during the 3D printing of strands is expected to cause crosslinking of fibrin. Factor XIII also improves alignment of the fibrin filaments (Lorand, 2006) and the extensibility of individual filaments (Collet *et al.*, 2005). It can also covalently bind extracellular proteins such as fibronectin to fibrin (Kanaide and Shainoff, 1975), possibly advantageous because Schwann cell proliferation is augmented by fibronectin (Baron-Van Evercooren *et al.*, 1982). In our future studies, we intend to add factor XIII and fibronectin to fibrinogen/hyaluronic acid. Bioprinting into thrombin would activate factor XIII, and result in a more robust scaffold. As the cells align along the long axis of the printed strands, 3D bioprinting multiple layers of crosslinked fibrin strands could be used to

fabricate a nerve conduit mimicking the bands of Büngner. While synthetic polymers have been used to model the bands of Büngner in nerve conduits (Lietz *et al.*, 2006), the use of natural biomaterials like fibrin may have additional advantages. A similar strategy could also be used to 3D print autologous platelet rich fibrin matrix, to achieve better efficacy in nerve repair.

6.5. Conclusions

Advanced biofabrication techniques have enabled the inclusion of cells within tissue scaffolds. As morphological characteristics of Schwann cells determine the outcome of nerve repair, we compared the morphology and viability of Schwann cells cultured in naturally occurring hydrogels. Because they are proteins, fibrin and collagen type-I enabled better adhesion of Schwann cells and led to its more favorable bipolar morphology. With printing of collagen being complicated by its time-dependent gelation and varying viscosity, fibrin was found to be the more appropriate material for 3D printing. The bipolar Schwann cells aligned parallel to the long axis of the printed fibrin strands. The addition of hyaluronic acid to fibrinogen improved the accuracy of printing. This study suggests that strategic stacking of fibrin strands can be accomplished to create 3D scaffolds with a pattern of longitudinally arranged Schwann cells.

CHAPTER 7
CONCLUSIONS AND FURTHER RESEARCH

7.1 Conclusions

Many techniques to improve nerve regeneration such as the incorporation of neurotrophins, and/or extracellular proteins have been explored earlier. Modification of nerve conduit materials has been achieved to make scaffolds more adhesive, thereby promoting nerve repair. Schwann cells are the principal cells of the peripheral nervous system and as such, incorporating them in nerve conduits is rational for nerve repair. This PhD research is aimed at fabricating scaffolds incorporating Schwann cells for nerve repair, with the conclusions surmised as follows.

1) To enable the inclusion of Schwann cells in intricate nerve scaffold design, a unique technique of bioplotting was optimized, wherein the use of polyethyleneimine and polyvinyl alcohol in the crosslinking medium stabilized the structure of alginate-hyaluronic acids scaffolds.
2) The survival of Schwann cells during the bioplotting process was increased by plotting the hydrogel directly into the crosslinking solution, rather than plotting in air.
3) Extruding hydrogels into crosslinking solutions with similar density and viscosity resulted in strands having their intended width and interstrand spacing, enabling a more porous scaffold structure.
4) The addition of polyethyleneimine to alginate-based scaffolds result in more efficient entrapment and prolonged delivery of proteins. PEI also improves the mechanical properties and decreases the degradation of alginate-HA scaffolds.
5) Alginate-based hydrogels are less favorable for Schwann cells culture and the guidance of axons than collagen and fibrin.
6) Fibrin and collagen type-I enable better adhesion of Schwann cells in culture, leading to its more favorable bipolar morphology.
7) Bipolar Schwann cells have a tendency to align parallel to the long axis of 3D printed fibrin strands.

8) Addition of hyaluronic acid, improves the 3D printing accuracy while printing most hydrogels, as it increases the viscosity of the composite hydrogel.
9) Autotomy, a concern in rat sciatic nerve injury model, is also strain-dependent. Sprague-Dawley rats have a high incidence of autotomy than Lewis rats. The use of Lewis rats would be more practical for long-term nerve regeneration studies, involving functional assessment.

Extrusion-based bioprinting techniques depend on the physical properties and gelation of the hydrogel material. This research has shown that the properties of alginate can be modified by the addition of polyethyleneimine and hyaluronic acid. While alginate may not be appropriate for nerve regeneration, it is useful for the culture of chondrocytes and islet cells. The incorporation of PEI to alginate during these cultures will also be beneficial.

Fibrin filaments align themselves along the direction of induced stress. While various techniques are used to align Schwann cells in hydrogels, this research has showed that the same can be achieved using 3D printing. During bioplotting the extruded hydrogel undergoes shear stresses at the dispensing nozzle. Therefore Schwann cells in fibrin, were shown to align along the long axis of the printed strands. 3D bioprinting multiple layers of crosslinked fibrin strands could be used to fabricate a nerve conduit with aligned Schwann cells.

While other synthetic polymers have been used to model the bands of Büngner in nerve conduits, this research shows that natural biomaterials like fibrin may also be used. This similar strategy could also be extended to autologous platelet-rich fibrin matrices, which have been used successfully for nerve repair. As mere filling of nerve conduit tubes with fibrin-rich plasma prevents longitudinal alignment of fibrin filaments, 3D printing plate-rich fibrin using the techniques described in this research can be promising.

7.2 Recommendations for future research

Understanding cellular mechanisms of nerve repair can be used to further improve the engineering of biofabricated nerve scaffolds. Axonal misdirection is one of the primary reasons of nerve conduit failure. Dr. Sydney Sunderland, an anatomist, stated that "*the core of the*

problem is not promoting axon regeneration, but in getting them back to where they belong" (Sunderland, 1978).

Guiding axons to their end targets is the key to success for any nerve repair technique. During surgical anastomosis of transected nerves, fascicular groups on the proximal end of the nerve are anastomosed to their corresponding distal ends. Neglecting fascicular mapping while using nerve conduits could lead to axonal misdirection. Precise 3D printing techniques can be used to fabricate customized multichannel nerve conduits, which enable fascicular continuity. The bioplotting technique discussed in this dissertation can be helpful to achieve the fabrication of a complex nerve conduit.

It has been shown that Schwann cells align along the strands when fibrin is 3D printed, thus resembling the bands of Büngner. Similar alignment can also be achieved using autologous platelet rich fibrin (PRF). As PRF is autologous and enriched with various growth factors, including neurotrophins, it would be a great filler material in nerve conduits.

REFERENCES

1. Abbott FV, Young SN. 1991, The effect of tryptophan supplementation on autotomy induced by nerve lesions in rats, *Pharmacol Biochem Behav*, **40**: 301–304.
2. Abidian MR, Corey JM, Kipke DR, Martin DC. 2010, Conducting-polymer nanotubes improve electrical properties, mechanical adhesion, neural attachment, and neurite outgrowth of neural electrodes, *Small*, **6**: 421–429.
3. Agius E, Cochard P. 1998, Comparison of neurite outgrowth induced by intact and injured sciatic nerves: a confocal and functional analysis, *J Neurosci*, **18**: 328–338.
4. Aguado BA, Mulyasasmita W, Su J, Lampe KJ, Heilshorn SC. 2012, Improving viability of stem cells during syringe needle flow through the design of hydrogel cell carriers, *Tissue Eng Part A*, **18**: 806–15.
5. Ahn S, Lee H, Puetzer J, Bonassar LJ, Kim G. 2012, Fabrication of cell-laden three-dimensional alginate-scaffolds with an aerosol cross-linking process, *J Mater Chem*, **22**: 18735–18740.
6. Aigner L, Caroni P. 1993, Depletion of 43-kD growth-associated protein in primary sensory neurons leads to diminished formation and spreading of growth cones, *J Cell Biol*, **123**: 417–429.
7. Aizawa Y, Wylie R, Shoichet M. 2010, Endothelial cell guidance in 3D patterned scaffolds, *Adv Mater*, **22**: 4831–5.
8. Akassoglou K, Kombrinck KW, Degen JL, Strickland S. 2000, Tissue plasminogen activator-mediated fibrinolysis protects against axonal degeneration and demyelination after sciatic nerve injury, *J Cell Biol*, **149**: 1157–1166.
9. Albala DM, Lawson JH. 2006, Recent clinical and investigational applications of fibrin sealant in selected surgical specialties, *J Am Coll Surg*, **202**: 685–697.
10. Al-Majed AA, Neumann CM, Brushart TM, Gordon T. 2000, Brief electrical stimulation promotes the speed and accuracy of motor axonal regeneration, *J Neurosci*, **20**: 2602–2608.
11. Augst AD, Kong HJ, Mooney DJ. 2006, Alginate hydrogels as biomaterials., *Macromol Biosci*, **6**: 623–633.
12. Bajpai SK, Sharma S. 2004, Investigation of swelling/degradation behaviour of alginate beads crosslinked with Ca2+ and Ba2+ ions, *React Funct Polym*, **59**: 129–140.
13. Banerjee A, Arha M, Choudhary S, Ashton RS, Bhatia SR, Schaffer D V, *et al.* 2009, The influence of hydrogel modulus on the proliferation and differentiation of encapsulated neural stem cells, *Biomaterials*, **30**: 4695–4699.
14. Baron-Van Evercooren A, Kleinman HK, Seppä HE, Rentier B, Dubois-Dalcq M. 1982, Fibronectin promotes rat Schwann cell growth and motility, *J Cell Biol*, **93**: 211–216.
15. Barrington MJ, Watts SA, Gledhill SR, Thomas RD, Said SA, Snyder GL, *et al.* 2009, Preliminary Results of the Australasian Regional Anaesthesia Collaboration, *Reg Anesth Pain Med*, **34**: 534–541.
16. Barron JA, Wu P, Ladouceur HD, Ringeisen BR. 2004, Biological Laser Printing: A Novel Technique for Creating Heterogeneous 3-dimensional Cell Patterns, *Biomed Microdevices*, **6**: 139–147.
17. Barron JA, Young HD, Dlott DD, Darfler MM, Krizman DB, Ringeisen BR. 2005, Printing of protein microarrays via a capillary-free fluid jetting mechanism, *Proteomics*, **5**: 4138–4144.

18. Barry RA, Shepherd RF, Hanson JN, Nuzzo RG, Wiltzius P, Lewis JA. 2009, Direct-Write Assembly of 3D Hydrogel Scaffolds for Guided Cell Growth, *Adv Mater*, **21**: 2407–2410.
19. Battiston B, Raimondo S, Tos P, Gaidano V, Audisio C, Scevola A, *et al.* 2009, Chapter 11: Tissue engineering of peripheral nerves, *Int Rev Neurobiol*, **87**: 227–49.
20. Batyrbekov EE, Akylbekova TN, Iskakov RM. 2011, Modified Microparticles of Calcium Alginate Gel for Controlled Release of Anesthetics, *MRS Proc*, **1060**: 1060–LL03–07.
21. Beirowski B, Adalbert R, Wagner D, Grumme DS, Addicks K, Ribchester RR, *et al.* 2005, The progressive nature of Wallerian degeneration in wild-type and slow Wallerian degeneration (WldS) nerves, *BMC Neurosci*, **6**: 6.
22. Belfield KD, Ren X, Van Stryland EW, Hagan DJ, Dubikovsky V, Miesak EJ. 2000, Near-IR two-photon photoinitiated polymerization using a fluorone/amine initiating system, *J Am Chem Soc*, **122**: 1217–1218.
23. Belkas JS, Munro CA, Shoichet MS, Midha R. 2005, Peripheral nerve regeneration through a synthetic hydrogel nerve tube, *Restor Neurol Neurosci*, **23**: 19–29.
24. Berg A, Zelano J, Pekna M, Wilhelmsson U, Pekny M, Cullheim S. 2013, Axonal regeneration after sciatic nerve lesion is delayed but complete in GFAP- and vimentin-deficient mice, *PLoS One*, **8**: e79395.
25. Berrocal YA, Almeida VW, Gupta R, Levi AD. 2013, Transplantation of Schwann cells in a collagen tube for the repair of large, segmental peripheral nerve defects in rats, *J Neurosurg*, **119**: 720–732.
26. Berry M, Barrett L, Seymour L, Baird A, Logan A. 2001, Gene therapy for central nervous system repair, *Curr Opin Mol Ther*, **3**: 338–349.
27. Le Bihan D, Mangin JF, Poupon C, Clark C, Pappata S, Molko N, *et al.* 2001, Diffusion tensor imaging: concepts and applications, *J Magn Reson Imaging*, **13**: 534–546.
28. Blessberger H, Binder T. 2010, Non-invasive imaging: Two dimensional speckle tracking echocardiography: basic principles, *Heart*, **96**: 716–722.
29. Borgens RB. 1999, Electrically mediated regeneration and guidance of adult mammalian spinal axons into polymeric channels, *Neuroscience*, **91**: 251–264.
30. Bork P, Downing AK, Kieffer B, Campbell ID. 1996, Structure and distribution of modules in extracellular proteins, *Q Rev Biophys*, **29**: 119–167.
31. Bourde O, Kiefer R, Toyka K V, Hartung HP. 1996, Quantification of interleukin-6 mRNA in wallerian degeneration by competitive reverse transcription polymerase chain reaction, *J Neuroimmunol*, **69**: 135–140.
32. Branski LK, Mittermayr R, Herndon DN, Jeschke MG, Hofmann M, Masters OE, *et al.* 2011, Fibrin sealant improves graft adherence in a porcine full-thickness burn wound model, *Burns*, **37**: 1360–1366.
33. Brooks DN, Weber R V, Chao JD, Rinker BD, Zoldos J, Robichaux MR, *et al.* 2012, Processed nerve allografts for peripheral nerve reconstruction: a multicenter study of utilization and outcomes in sensory, mixed, and motor nerve reconstructions, *Microsurgery*, **32**: 1–14.
34. Brown MC, Perry VH, Lunn ER, Heumanns R. 1991, Macrophage Dependence of Peripheral Sensory Nerve Regeneration: Possible Involvement of Nerve Growth Factor, **6**: 359–370.
35. Brushart TM, Jari R, Verge V, Rohde C, Gordon T. 2005, Electrical stimulation restores the specificity of sensory axon regeneration, *Exp Neurol*, **194**: 221–229.

36. Brushart TM, Tarlov EC, Mesulam MM. 1983, Specificity of muscle reinnervation after epineurial and individual fascicular suture of the rat sciatic nerve, *J Hand Surg Am*, **8**: 248–253.
37. Buchthal F, Kuhl V. 1979, Nerve conduction, tactile sensibility, and the electromyogram after suture or compression of peripheral nerve: a longitudinal study in man, *J Neurol Neurosurg Psychiatry*, **42**: 436–451.
38. Bunge RP. 1994, The role of the Schwann cell in trophic support and regeneration, *J Neurol*, **242**: S19–21.
39. Cai Z, Chattopadhyay N, Liu WJ, Chan C, Pignol J-P, Reilly RM. 2011, Optimized digital counting colonies of clonogenic assays using ImageJ software and customized macros: comparison with manual counting, *Int J Radiat Biol*, **87**: 1135–1146.
40. Calafiore R. 2003, Alginate microcapsules for pancreatic islet cell graft immunoprotection: struggle and progress towards the final cure for type 1 diabetes mellitus, *Expert Opin Biol Ther*, **3**: 201–205.
41. Cameron MGP, Stewart OJ. 1975, Ulnar nerve injury associated with anaesthesia, *Can Anaesth Soc J*, **22**: 253–264.
42. Campbell WW 2008, Evaluation and management of peripheral nerve injury, *Clin Neurophysiol*, **119**: 1951–65.
43. Canonico S, Benevento R, Perna G, Guerniero R, Sciaudone G, Pellino G, *et al.* 2013, Sutureless fixation with fibrin glue of lightweight mesh in open inguinal hernia repair: effect on postoperative pain: a double-blind, randomized trial versus standard heavyweight mesh, *Surgery*, **153**: 126–130.
44. Cao N, Chen XB, Schreyer DJ. 2012, Influence of Calcium Ions on Cell Survival and Proliferation in the Context of an Alginate Hydrogel, *ISRN Chem Eng*, **2012**: 1–9.
45. Cao X, Shoichet M. 2001, Defining the concentration gradient of nerve growth factor for guided neurite outgrowth, *Neuroscience*, **103**: 831–840.
46. Cao X, Shoichet M. 2003, Investigating the synergistic effect of combined neurotrophic factor concentration gradients to guide axonal growth, *Neuroscience*, **122**: 381–389.
47. Carr MM, Best TJ, Mackinnon SE, Evans PJ. 1992, Strain differences in autotomy in rats undergoing sciatic nerve transection or repair, *Ann Plast Surg*, **28**: 538–544.
48. Cerri F, Salvatore L, Memon D, Martinelli Boneschi F, Madaghiele M, Brambilla P, *et al.* 2014, Peripheral nerve morphogenesis induced by scaffold micropatterning, *Biomaterials*, **35**: 4035–4045.
49. Chalazonitis A, Kessler JA, Twardzik DR, Morrison RS. 1992, Transforming growth factor alpha, but not epidermal growth factor, promotes the survival of sensory neurons in vitro, *J Neurosci*, **12**: 583–594.
50. Chalfoun CT, Wirth GA, Evans GRD. 2006, Tissue engineered nerve constructs: where do we stand?, *J Cell Mol Med*, **10**: 309–317.
51. Chang R, Nam J, Sun W. 2008, Effects of dispensing pressure and nozzle diameter on cell survival from solid freeform fabrication-based direct cell writing, *Tissue Eng Part A*, **14**: 41–48.
52. Chaudhry V, Glass JD, Griffin JW. 1992, Wallerian degeneration in peripheral nerve disease, *Neurol Clin*, **10**: 613–627.
53. Chen CY, Barron J, Ringeisen BR. 2006, Cell patterning without chemical surface modification: Cell–cell interactions between printed bovine aortic endothelial cells (BAEC) on a homogeneous cell-adherent hydrogel, *Appl Surf Sci*, **252**: 8641–8645.

54. Chen S, Bisby MA. 1993, Impaired motor axon regeneration in the C57BL/Ola mouse, *J Comp Neurol*, **333**: 449–454.
55. Chen MCW, Gupta M, Cheung KC. 2010, Alginate-based microfluidic system for tumor spheroid formation and anticancer agent screening, *Biomed Microdevices*, **12**: 647–654.
56. Chernousov MA, Carey DJ. 2003, alphaVbeta8 integrin is a Schwann cell receptor for fibrin, *Exp Cell Res*, **291**: 514–524.
57. Chia SH, Schumacher BL, Klein TJ, Thonar EJ-MA, Masuda K, Sah RL, *et al.* 2004, Tissue-engineered human nasal septal cartilage using the alginate-recovered-chondrocyte method, *Laryngoscope*, **114**: 38–45.
58. Chien KB, Makridakis E, Shah RN. 2013, Three-dimensional printing of soy protein scaffolds for tissue regeneration, *Tissue Eng Part C Methods*, **19**: 417–426.
59. Chierzi S, Ratto GM, Verma P, Fawcett JW. 2005, The ability of axons to regenerate their growth cones depends on axonal type and age, and is regulated by calcium, cAMP and ERK., *Eur J Neurosci*, **21**: 2051–2062.
60. Cho SH, Oh SH, Lee JH. 2005, Fabrication and characterization of porous alginate/polyvinyl alcohol hybrid scaffolds for 3D cell culture, *J Biomater Sci Polym Ed*, **16**: 933–947.
61. Choi B-H, Han S-G, Kim S-H, Zhu S-J, Huh J-Y, Jung J-H, *et al.* 2005, Autologous fibrin glue in peripheral nerve regeneration in vivo, *Microsurgery*, **25**: 495–499.
62. Christensena BE. 2011, Alginates as biomaterials in tissue engineering, *Carbohydr Chem Chem Biol Approaches*, **37**: 227–258.
63. Chung JHY, Naficy S, Yue Z, Kapsa R, Quigley A, Moulton SE, *et al.* 2013, Bio-ink properties and printability for extrusion printing living cells, *Biomater Sci*, **1**: 763.
64. Claeyssens F, Hasan EA, Gaidukeviciute A, Achilleos DS, Ranella A, Reinhardt C, *et al.* 2009, Three-dimensional biodegradable structures fabricated by two-photon polymerization, *Langmuir*, **25**: 3219–3223.
65. Coates EE, Riggin CN, Fisher JP. 2013, Photocrosslinked alginate with hyaluronic acid hydrogels as vehicles for mesenchymal stem cell encapsulation and chondrogenesis, *J Biomed Mater Res A*, **101**: 1962–70.
66. Cohen DL, Lo W, Tsavaris A, Peng D, Lipson H, Bonassar LJ. 2011, Increased mixing improves hydrogel homogeneity and quality of three-dimensional printed constructs, *Tissue Eng Part C Methods*, **17**: 239–248.
67. Collet JP, Shuman H, Ledger RE, Lee S, Weisel JW. 2005, The elasticity of an individual fibrin fiber in a clot, *Proc Natl Acad Sci U S A*, **102**: 9133–9137.
68. Collins MN. 2014, *Hyaluronic acid for biomedical and pharmaceutical applications* (MN Collins, Ed.). Smithers Rapra: Shawbury.
69. Collins MN, Birkinshaw C. 2008, Investigation of the swelling behavior of crosslinked hyaluronic acid films and hydrogels produced using homogeneous reactions, *J Appl Polym Sci*, **109**: 923–931.
70. Collins MN, Birkinshaw C. 2013, Hyaluronic acid based scaffolds for tissue engineering - A review, *Carbohydr Polym*, **92**: 1262–1279.
71. Czaja K, Burns GA, Ritter RC. 2008, Capsaicin-induced neuronal death and proliferation of the primary sensory neurons located in the nodose ganglia of adult rats, *Neuroscience*, **154**: 621–630.

72. Dahlmann J, Krause A, Möller L, Kensah G, Möwes M, Diekmann A, *et al.* 2013, Fully defined in situ cross-linkable alginate and hyaluronic acid hydrogels for myocardial tissue engineering, *Biomaterials*, **34**: 940–951.
73. DeCoster MA, Maddi S, Dutta V, McNamara J. 2010, Microscopy and image analysis of individual and group cell shape changes during apoptosis, *Microsc Sci Technol Appl Educ*, 836–843.
74. Dellon AL, Mackinnon SE. 1989, Sciatic nerve regeneration in the rat. Validity of walking track assessment in the presence of chronic contractures, *Microsurgery*, **10**: 220–225.
75. Derby B. 2012, Printing and prototyping of tissues and scaffolds, *Science*, **338**: 921–926.
76. Deumens R, Bozkurt A, Meek MF, Marcus MAE, Joosten EAJ, Weis J, *et al.* 2010, Repairing injured peripheral nerves: Bridging the gap, *Prog Neurobiol*, **92**: 245–276.
77. Devi DA, Smitha B, Sridhar S, Jawalkar SS, Aminabhavi TM. 2007, Novel sodium alginate/polyethyleneimine polyion complex membranes for pervaporation dehydration at the azeotropic composition of various alcohols, *J Chem Technol Biotechnol*, **82**: 993–1003.
78. Devon R, Doucette R. 1992, Olfactory ensheathing cells myelinate dorsal root ganglion neurites, *Brain Res*, **589**: 175–179.
79. Dewitt DD, Kaszuba SN, Thompson DM, Stegemann JP. 2009, Collagen I-matrigel scaffolds for enhanced Schwann cell survival and control of three-dimensional cell morphology, *Tissue Eng Part A*, **15**: 2785–2793.
80. Dhoot NO, Tobias C, Fischer I, Wheatley M. 2004, Peptide-modified alginate surfaces as a growth permissive substrate for neurite outgrowth, *J Biomed Mater Res A*, **71**: 191–200.
81. Dinca V, Palla-Papavlu A, Paraico I, Lippert T, Wokaun A, Dinescu M. 2011, 2D spatially controlled polymer micro patterning for cellular behavior studies, *Appl Surf Sci*, **257**: 5250–5254.
82. Dodla MC, Bellamkonda RV. 2008, Differences between the effect of anisotropic and isotropic laminin and nerve growth factor presenting scaffolds on nerve regeneration across long peripheral nerve gaps, *Biomaterials*, **29**: 33–46.
83. Draget KI, Skjak-Braek G, Smidsrod O 1997, Alginate based new materials., *Int J Biol Macromol*, **21**: 47–55.
84. Drury JL, Dennis RG, Mooney DJ. 2004, The tensile properties of alginate hydrogels, *Biomaterials*, **25**: 3187–3199.
85. Dubey N. 2001, Neuronal contact guidance in magnetically aligned fibrin gels: effect of variation in gel mechano-structural properties, *Biomaterials*, **22**: 1065–1075.
86. Ducatman BS, Scheithauer BW, Piepgras DG, Reiman HM, Ilstrup DM. 1986, Malignant peripheral nerve sheath tumors. A clinicopathologic study of 120 cases, *Cancer*, **57**: 2006–2021.
87. Dvali L, Mackinnon S. 2003, Nerve repair, grafting, and nerve transfers, *Clin Plast Surg*, **30**: 203–221.
88. Eccleston PA, Mirsky R, Jessen KR. 1989, Type I collagen preparations inhibit DNA synthesis in glial cells of the peripheral nervous system, *Exp Cell Res*, **182**: 173–185.
89. El-Barrany WG, Marei AG, Vallée B. 1999, Anatomic basis of vascularised nerve grafts: the blood supply of peripheral nerves, *Surg Radiol Anat*, **21**: 95–102.
90. Eser F, Aktekin LA, Bodur H, Atan C. 2009, Etiological factors of traumatic peripheral nerve injuries, *Neurol India*, **57**: 434–437.

91. Eto M, Yoshikawa H, Fujimura H, Naba I, Sumi-Akamaru H, Takayasu S, *et al.* 2003, The role of CD36 in peripheral nerve remyelination after crush injury, *Eur J Neurosci*, **17**: 2659–2666.
92. Evans GRD, Brandt K, Katz S, Chauvin P, Otto L, Bogle M, *et al.* 2002, Bioactive poly (l - lactic acid) conduits seeded with Schwann cells for peripheral nerve regeneration, **23**: 841–848.
93. Fawcett JW, Keynes RJ. 1990, Peripheral nerve regeneration, *Annu Rev Neurosci*, **13**: 43–60.
94. Fedorovich NE, De Wijn JR, Verbout AJ, Alblas J, Dhert WJA. 2008, Three-dimensional fiber deposition of cell-laden, viable, patterned constructs for bone tissue printing, *Tissue Eng Part A*, **14**: 127–133.
95. Feria M, Abad F, Sánchez A, Abreu P. 1993, Magnesium sulphate injected subcutaneously suppresses autotomy in peripherally deafferented rats, *Pain*, **53**: 287–293.
96. Fernandez PA, Tang DG, Cheng L, Prochiantz A, Mudge AW, Raff MC. 2000, Evidence that axon-derived neuregulin promotes oligodendrocyte survival in the developing rat optic nerve, *Neuron*, **28**: 81–90.
97. Fernandez-Valle C, Bunge RP, Bunge MB. 1995, Schwann cells degrade myelin and proliferate in the absence of macrophages: evidence from in vitro studies of Wallerian degeneration, *J Neurocytol*, **24**: 667–679.
98. Fernyhough P, Smith DR, Schapansky J, Van Der Ploeg R, Gardiner NJ, Tweed CW, *et al.* 2005, Activation of nuclear factor-kappaB via endogenous tumor necrosis factor alpha regulates survival of axotomized adult sensory neurons, *J Neurosci*, **25**: 1682–1690.
99. Fernyhough P, Willars GB, Lindsay RM, Tomlinson DR. 1993, Insulin and insulin-like growth factor I enhance regeneration in cultured adult rat sensory neurones, *Brain Res*, **607**: 117–124.
100. Ferrara N. 1999, Role of vascular endothelial growth factor in the regulation of angiogenesis, *Kidney Int*, **56**: 794–814.
101. Fischer D, von Harpe A, Kunath K, Petersen H, Li Y, Kissel T. 2002, Copolymers of ethylene imine and N-(2-hydroxyethyl)-ethylene imine as tools to study effects of polymer structure on physicochemical and biological properties of DNA complexes, *Bioconjug Chem*, **13**: 1124–1133.
102. Florea BI, Meaney C, Junginger HE, Borchard G. 2002, Transfection efficiency and toxicity of polyethylenimine in differentiated Calu-3 and nondifferentiated COS-1 cell cultures, *AAPS PharmSci*, **4**: E12.
103. Fornaro M, Lee JM, Raimondo S, Nicolino S, Geuna S, Giacobini-Robecchi M 2008, Neuronal intermediate filament expression in rat dorsal root ganglia sensory neurons: an *in vivo* and *in vitro* study, *Neuroscience*, **153**: 1153–1163.
104. Fraser JR, Laurent TC, Laurent UB 1997, Hyaluronan: its nature, distribution, functions and turnover., *J Intern Med*, **242**: 27–33.
105. Freeman I, Cohen S. 2009, The influence of the sequential delivery of angiogenic factors from affinity-binding alginate scaffolds on vascularization, *Biomaterials*, **30**: 2122–31.
106. Freitas Jr RA. 1999, *Nanomedicine, Volume I: Basic Capabilities*. Landes Bioscience: Georgetown, TX.
107. Fu SY, Gordon T. 1997, The cellular and molecular basis of peripheral nerve regeneration, *Mol Neurobiol*, **14**: 67–116.

108. Fugleholm K, Schmalbruch H, Krarup C. 1994, Early peripheral nerve regeneration after crushing, sectioning, and freeze studied by implanted electrodes in the cat, *J Neurosci*, **14**: 2659–2673.
109. Funakoshi H, Frisén J, Barbany G, Timmusk T, Zachrisson O, Verge VM, *et al.* 1993, Differential expression of mRNAs for neurotrophins and their receptors after axotomy of the sciatic nerve, *J Cell Biol*, **123**: 455–465.
110. Gaebel R, Ma N, Liu J, Guan J, Koch L, Klopsch C, *et al.* 2011, Patterning human stem cells and endothelial cells with laser printing for cardiac regeneration, *Biomaterials*, **32**: 9218–9230.
111. Galateanu B, Dimonie D, Vasile E, Nae S, Cimpean A, Costache M. 2012, Layer-shaped alginate hydrogels enhance the biological performance of human adipose-derived stem cells, *BMC Biotechnol*, **12**: 35.
112. Galla TJ, Vedecnik SV, Halbgewachs J, Steinmann S, Friedrich C, Stark GB 2004, Fibrin/Schwann cell matrix in poly-epsilon-caprolactone conduits enhances guided nerve regeneration, *Int J Artif Organs*, **27**: 127–136.
113. Georgiou M, Bunting SCJ, Davies HA, Loughlin AJ, Golding JP, Phillips JB. 2013, Engineered neural tissue for peripheral nerve repair, *Biomaterials*, **34**: 7335–7343.
114. Geremia NM, Gordon T, Brushart TM, Al-Majed A, Verge VMK. 2007, Electrical stimulation promotes sensory neuron regeneration and growth-associated gene expression, *Exp Neurol*, **205**: 347–359.
115. Glicklis R, Shapiro L, Agbaria R, Merchuk JC, Cohen S. 2000, Hepatocyte behavior within three-dimensional porous alginate scaffolds, *Biotechnol Bioeng*, **67**: 344–353.
116. Goligorsky MS, Budzikowski AS, Tsukahara H, Noiri E. 1999, Co-operation between endothelin and nitric oxide in promoting endothelial cell migration and angiogenesis, *Clin Exp Pharmacol Physiol*, **26**: 269–271.
117. Golub JS, Kim Y, Duvall CL, Bellamkonda RV, Gupta D, Lin AS, *et al.* 2010, Sustained VEGF delivery via PLGA nanoparticles promotes vascular growth, *Am J Physiol Heart Circ Physiol*, **298**: H1959–1965.
118. Gombotz WR, Wee S. 1998, Protein release from alginate matrices, *Adv Drug Deliv Rev*, **31**: 267–285.
119. González-Hernández T, Rustioni A. 1999, Expression of three forms of nitric oxide synthase in peripheral nerve regeneration, *J Neurosci Res*, **55**: 198–207.
120. Goodrum JF, Earnhardt T, Goines N, Bouldin TW. 1994, Fate of myelin lipids during degeneration and regeneration of peripheral nerve: an autoradiographic study, *J Neurosci*, **14**: 357–367.
121. Goto E, Mukozawa M, Mori H, Hara M. 2010, A rolled sheet of collagen gel with cultured Schwann cells: model of nerve conduit to enhance neurite growth, *J Biosci Bioeng*, **109**: 512–518.
122. Graf J, Iwamoto Y, Sasaki M, Martin GR, Kleinman HK, Robey FA, *et al.* 1987, Identification of an amino acid sequence in laminin mediating cell attachment, chemotaxis, and receptor binding, *Cell*, **48**: 989–996.
123. Greenlund LJ, Deckwerth TL, Johnson EM. 1995, Superoxide dismutase delays neuronal apoptosis: a role for reactive oxygen species in programmed neuronal death, *Neuron*, **14**: 303–315.
124. Griffin JW, George R, Ho T. 1993, Macrophage systems in peripheral nerves. A review, *J Neuropathol Exp Neurol*, **52**: 553–560.

125. Grothe C, Nikkhah G. 2001, The role of basic fibroblast growth factor in peripheral nerve regeneration, *Anat Embryol*, **204**: 171–177.
126. Guillemot F, Chanseau C, Lesage S, Dulpuch M, Rémy M, Bordenave L, *et al.* 2008, REDV peptide patterning onto PET using laser induced forward transfer. In: *2008 E-MRS Fall Meeting*, Poland.
127. Gundersen RW, Barrett JN. 1979, Neuronal chemotaxis: chick dorsal-root axons turn toward high concentrations of nerve growth factor, *Science*, **206**: 1079–1080.
128. Guo B-F, Dong MM. 2009, Application of neural stem cells in tissue-engineered artificial nerve, *Otolaryngol Head Neck Surg*, **140**: 159–164.
129. Hadlock TA, Heaton J, Cheney M, Mackinnon SE. 2005, Functional recovery after facial and sciatic nerve crush injury in the rat, *Arch Facial Plast Surg*, **7**: 17–20.
130. Hadlock T, Sundback C, Hunter D, Cheney M, Vacanti JP. 2004, A Polymer Foam Conduit Seeded with Schwann Cells Promotes Guided Peripheral Nerve Regeneration, *Tissue Eng*, **6**: 119–127.
131. Halder A, Maiti S, Sa B. 2005, Entrapment efficiency and release characteristics of polyethyleneimine-treated or -untreated calcium alginate beads loaded with propranolol-resin complex, *Int J Pharm*, **302**: 84–94.
132. Hall SM. 1986, Regeneration in cellular and acellular autografts in the peripheral nervous system, *Neuropathol Appl Neurobiol*, **12**: 27–46.
133. Hall S. 2005, The response to injury in the peripheral nervous system, *J Bone Joint Surg Br*, **87**: 1309–1319.
134. Harley BA, Spilker MH, Wu JW, Asano K, Hsu H-P, Spector M, *et al.* 2004, Optimal degradation rate for collagen chambers used for regeneration of peripheral nerves over long gaps, *Cells Tissues Organs*, **176**: 153–65.
135. Harris ML, Doraiswamy A, Narayan RJ, Patz TM, Chrisey DB. 2008, Recent progress in CAD/CAM laser direct-writing of biomaterials, *Mater Sci Eng C*, **28**: 359–365.
136. Hashimoto T, Suzuki Y, Kitada M, Kataoka K, Wu S, Suzuki K, *et al.* 2002, Peripheral nerve regeneration through alginate gel: analysis of early outgrowth and late increase in diameter of regenerating axons, *Exp brain Res*, **146**: 356–68.
137. Hermanns S, Wunderlich G, Rosenbaum C, Hanemann CO, Müller HW, Stichel CC. 1997, Lack of immune responses to immediate or delayed implanted allogeneic and xenogeneic Schwann cell suspensions, *Glia*, **21**: 299–314.
138. Hobson MI, Green CJ, Terenghi G. 2000, VEGF enhances intraneural angiogenesis and improves nerve regeneration after axotomy, *J Anat*, **197 Pt 4**: 591–605.
139. Hoffman PN, Lasek RJ. 1980, Axonal transport of the cytoskeleton in regenerating motor neurons: constancy and change, *Brain Res*, **202**: 317–333.
140. Hoffman PN, Lopata MA, Watson DF, Luduena RF. 1992, Axonal transport of class II and III beta-tubulin: evidence that the slow component wave represents the movement of only a small fraction of the tubulin in mature motor axons, *J Cell Biol*, **119**: 595–604.
141. Höke A 2006, Mechanisms of Disease: what factors limit the success of peripheral nerve regeneration in humans?, *Nat Clin Pract Neurol*, **2**: 448–454.
142. Hopp B, Smausz T, Nógrádi A. 2010, Absorbing-Film Assisted Laser Induced Forward Transfer of Sensitive Biological Subjects. In: Ringeisen BR, Spargo BJ, Wu PK (eds) *Cell and Organ Printing*, Springer Netherlands, pp 115–134.
143. Horan PK, Slezak SE. 1989, Stable cell membrane labelling, *Nature*, **340**: 167–168.

144. Huang EJ, Reichardt LF. 2001, Neurotrophins: roles in neuronal development and function, *Annu Rev Neurosci*, **24**: 677–736.
145. Hubert T, Grimal S, Carroll P, Fichard-Carroll A. 2009, Collagens in the developing and diseased nervous system, *Cell Mol Life Sci*, **66**: 1223–1238.
146. Hudson NE, Houser JR, O'Brien ET, Taylor RM, Superfine R, Lord ST, *et al.* 2010, Stiffening of individual fibrin fibers equitably distributes strain and strengthens networks, *Biophys J*, **98**: 1632–40.
147. Hudson TW, Liu SY, Schmidt CE. 2004, Engineering an improved acellular nerve graft via optimized chemical processing, *Tissue Eng*, **10**: 1346–1358.
148. Hudson BG, Reeders ST, Tryggvason K. 1993, Type IV collagen: structure, gene organization, and role in human diseases. Molecular basis of Goodpasture and Alport syndromes and diffuse leiomyomatosis, *J Biol Chem*, **268**: 26033–26036.
149. Hudson TW, Zawko S, Deister C, Lundy S, Hu CY, Lee K, *et al.* 2004, Optimized acellular nerve graft is immunologically tolerated and supports regeneration, *Tissue Eng*, **10**: 1641–1651.
150. Hunt NC, Shelton RM, Grover LM. 2009, Reversible mitotic and metabolic inhibition following the encapsulation of fibroblasts in alginate hydrogels, *Biomaterials*, **30**: 6435–6443.
151. Hutmacher DW. 2001, Scaffold design and fabrication technologies for engineering tissues--state of the art and future perspectives, *J Biomater Sci Polym Ed*, **12**: 107–124.
152. Hwang CM, Sant S, Masaeli M, Kachouie NN, Zamanian B, Lee S-H, *et al.* 2010, Fabrication of three-dimensional porous cell-laden hydrogel for tissue engineering, *Biofabrication*, **2**: 035003.
153. Ide C. 1996, Peripheral nerve regeneration, *Neurosci Res*, **25**: 101–21.
154. Ilkhanizadeh S, Teixeira AI, Hermanson O. 2007, Inkjet printing of macromolecules on hydrogels to steer neural stem cell differentiation, *Biomaterials*, **28**: 3936–3943.
155. Imaizumi T, Lankford KL, Kocsis JD. 2000, Transplantation of olfactory ensheathing cells or Schwann cells restores rapid and secure conduction across the transected spinal cord, *Brain Res*, **854**: 70–78.
156. Inbal R, Devor M, Tuchendler O, Lieblich I. 1980, Autotomy following nerve injury: Genetic factors in the development of chronic pain, *Pain*, **9**: 327–337.
157. Itoh S, Takakuda K, Samejima H, Ohta T, Shinomiya K, Ichinose S. 1999, Synthetic collagen fibers coated with a synthetic peptide containing the YIGSR sequence of laminin to promote peripheral nerve regeneration in vivo, *J Mater Sci Mater Med*, **10**: 129–134.
158. Iwanaga S, Gokudan S, Mizuguchi J. 2008, Molecular Evolution of Blood Clotting Factors with Special Reference to Fibrinogen and von Willebrand Factor. In: Tanaka K, Davie E, Ikeda Y, Iwanaga S, Saito H, Sueishi K (eds) *Recent Advances in Thrombosis and Hemostasis 2008*, Springer Japan: Tokyo, pp 439–461.
159. Izawa H, Kawakami K, Sumita M, Tateyama Y, Hill JP, Ariga K. 2013, β-Cyclodextrin-crosslinked alginate gel for patient-controlled drug delivery systems: regulation of host–guest interactions with mechanical stimuli, *J Mater Chem B*, **1**: 2155.
160. Jeng CL, Torrillo TM, Rosenblatt M. 2010, Complications of peripheral nerve blocks, *Br J Anaesth*, **105 Suppl** : i97–107.
161. Jesuraj NJ, Santosa KB, Macewan MR, Moore AM, Kasukurthi R, Ray WZ, *et al.* 2014, Schwann cells seeded in acellular nerve grafts improve functional recovery, *Muscle Nerve*, **49**: 267–276.

162. Jiang N, Li H, Sun Y, Yin D, Zhao Q, Cui S, *et al.* 2014, Differential gene expression in proximal and distal nerve segments of rats with sciatic nerve injury during Wallerian degeneration, *Neural Regen Res*, **9**: 1186–1194.
163. Jiang X, Lim SH, Mao H-Q, Chew SY. 2010, Current applications and future perspectives of artificial nerve conduits, *Exp Neurol*, **223**: 86–101.
164. Jiankang H, Dichen L, Bingheng L, Zhen W, Tao Z. 2006, Custom fabrication of composite tibial hemi-knee joint combining CAD/CAE/CAM techniques, *Proc Inst Mech Eng Part H J Eng Med*, **220**: 823–830.
165. Jin J, Limburg S, Joshi SK, Landman R, Park M, Zhang Q, *et al.* 2013, Peripheral nerve repair in rats using composite hydrogel-filled aligned nanofiber conduits with incorporated nerve growth factor, *Tissue Eng Part A*, **19**: 2138–2146.
166. Johann RM, Renaud P. 2007, Microfluidic patterning of alginate hydrogels, *Biointerphases*, **2**: 73–79.
167. Johnson FA, Craig DQ, Mercer AD. 1997, Characterization of the block structure and molecular weight of sodium alginate, *J Pharm Pharmacol*, **49**: 639–643.
168. Joung JJ, Akin C, Royer GP. 1987, Immobilization of growing cells by polyethyleneimine-modified alginate, *Appl Biochem Biotechnol*, **14**: 259–275.
169. Kaewkhaw R, Scutt AM, Haycock JW. 2012, Integrated culture and purification of rat Schwann cells from freshly isolated adult tissue, *Nat Protoc*, **7**: 1996–2004.
170. Kajiwara K, Ogata S, Tanihara M. 2005, Promotion of neurite outgrowth from fetal hippocampal cells by TNF-alpha receptor 1-derived peptide, *Cell Transplant*, **14**: 665–672.
171. Kakinoki R, Nishijima N, Ueba Y, Oka M, Yamamuro T. 1995, Relationship between axonal regeneration and vascularity in tubulation--an experimental study in rats, *Neurosci Res*, **23**: 35–45.
172. Kakinoki R, Nishijima N, Ueba Y, Oka M, Yamamuro T, Nakamura T. 1997, Nerve regeneration over a 25 mm gap in rat sciatic nerves using tubes containing blood vessels: the possibility of clinical application, *Int Orthop*, **21**: 332–336.
173. Kalbermatten DF, Kingham PJ, Mahay D, Mantovani C, Pettersson J, Raffoul W, *et al.* 2008, Fibrin matrix for suspension of regenerative cells in an artificial nerve conduit, *J Plast Reconstr Aesthet Surg*, **61**: 669–675.
174. Kanaide H, Shainoff JR. 1975, Cross-linking of fibrinogen and fibrin by fibrin-stablizing factor (factor XIIIa), *J Lab Clin Med*, **85**: 574–597.
175. Kang SK, Shin MJ, Jung JS, Kim YG, Kim CH. 2006, Autologous adipose tissue-derived stromal cells for treatment of spinal cord injury, *Stem Cells Dev*, **15**: 583–594.
176. Kapur TA, Shoichet MS. 2004, Immobilized concentration gradients of nerve growth factor guide neurite outgrowth, *J Biomed Mater Res A*, **68**: 235–243.
177. Karki R, Mariani M, Andreoli M, He S, Scambia G, Shahabi S, *et al.* 2013, βIII-Tubulin: biomarker of taxane resistance or drug target?, *Expert Opin Ther Targets*, **17**: 461–472.
178. Katz JS, Burdick JA. 2009, Hydrogel mediated delivery of trophic factors for neural repair, *Wiley Interdiscip Rev Nanomed Nanobiotechnol*, **1**: 128-139
179. Keilhoff G, Wolf G, Fansa H. 2002, NOS-mediated differences in peripheral nerve graft revascularization and regeneration, *Neuroreport*, **13**: 1463–1468.
180. Kerschnitzki M, Wagermaier W, Roschger P, Seto J, Shahar R, Duda GN, *et al.* 2011, The organization of the osteocyte network mirrors the extracellular matrix orientation in bone, *J Struct Biol*, **173**: 303–311.

181. Kew JN, Sofroniew MV. 1997, Brain-derived neurotrophic factor, acidic and basic fibroblast growth factors, insulin-like growth factor-I, and various antioxidants do not prevent the apoptotic death of developing septal cholinergic neurons following nerve growth factor withdrawal *in vitro*, *Neuroscience*, **76**: 809–820.
182. Khalil S, Sun W. 2009, Bioprinting endothelial cells with alginate for 3D tissue constructs, *J Biomech Eng*, **131**: 111002.
183. Khanam N, Mikoryak C, Draper RK, Balkus KJ. 2007, Electrospun linear polyethyleneimine scaffolds for cell growth, *Acta Biomater*, **3**: 1050–1059.
184. Kilmartin PA, Gizdavic-Nikolaidis M, Zujovic Z, Travas-Sejdic J, Bowmaker GA, Cooney RP. 2005, Free radical scavenging and antioxidant properties of conducting polymers examined using EPR and NMR spectroscopies, *Synth Met*, **153**: 153–156.
185. Kim G, Ahn S, Yoon H, Kim Y, Chun W. 2009, A cryogenic direct-plotting system for fabrication of 3D collagen scaffolds for tissue engineering, *J Mater Chem*, **19**: 8817–8823.
186. Kim HJ, Hwang JJ, Behrens MM, Snider BJ, Choi DW, Koh JY. 2003, TrkB mediates BDNF-induced potentiation of neuronal necrosis in cortical culture, *Neurobiol Dis*, **14**: 110–119.
187. Kim K, Jeong CG, Hollister SJ. 2008, Non-invasive monitoring of tissue scaffold degradation using ultrasound elasticity imaging, *Acta Biomater*, **4**: 783–790.
188. Kim SH, Kiick KL. 2010, Cell-mediated Delivery and Targeted Erosion of Vascular Endothelial Growth Factor-Crosslinked Hydrogels, *Macromol Rapid Commun*, **31**: 1231–1240.
189. Kim J, Park J, Yang S, Baek J, Kim B, Lee SH, *et al.* 2007, Establishment of a fabrication method for a long-term actuated hybrid cell robot, *Lab Chip*, **7**: 1504–1508.
190. Kingery WS, Castellote JM, Maze M. 1999, Methylprednisolone prevents the development of autotomy and neuropathic edema in rats, but has no effect on nociceptive thresholds, *Pain*, **80**: 555–566.
191. Klein TJ, Rizzi SC, Schrobback K, Reichert JC, Jeon JE, Crawford RW, *et al.* 2010, Long-term effects of hydrogel properties on human chondrocyte behavior, *Soft Matter*, **6**: 5175.
192. Kleinman HK, Klebe RJ, Martin GR. 1981, Role of collagenous matrices in the adhesion and growth of cells, *J Cell Biol*, **88**: 473–485.
193. Kong HJ, Lee KY, Mooney DJ. 2002, Decoupling the dependence of rheological/mechanical properties of hydrogels from solids concentration, *Polymer*, **43**: 6239–6246.
194. Kong HJ, Mooney DJ. 2003, The effects of poly(ethyleneimine) (PEI) molecular weight on reinforcement of alginate hydrogels, *Cell Transplant*, **12**: 779–785.
195. Kong HJ, Smith MK, Mooney DJ. 2003, Designing alginate hydrogels to maintain viability of immobilized cells, *Biomaterials*, **24**: 4023–4029.
196. Koroleva A, Schlie S, Fadeeva E, Gittard SD, Miller P, Ovsianikov A, *et al.* 2010, Microreplication of laser-fabricated surface and three-dimensional structures, *J Opt*, **12**: 124009.
197. Kotz J. 1996, Polyelectrolyte Complexes (Overview). In: Salamone JC (ed) *Polymeric Materials Encyclopedia*, CRC Press: Boca Raton, FL, p 5762.
198. Krystosek A. 1984, Peripheral neurons and Schwann cells secrete plasminogen activator, *J Cell Biol*, **98**: 773–776.
199. Kunze A, Giugliano M, Valero A, Renaud P. 2011, Micropatterning neural cell cultures in 3D with a multi-layered scaffold, *Biomaterials*, **32**: 2088–2098.

200. Kuo YC, Ku IN. 2009, Application of polyethyleneimine-modified scaffolds to the regeneration of cartilaginous tissue, *Biotechnol Prog*, **25**: 1459–1467.
201. Kuo CK, Ma PX. 2001, Ionically crosslinked alginate hydrogels as scaffolds for tissue engineering: Part 1. Structure, gelation rate and mechanical properties, **22**: 511–521.
202. Lakard S, Herlem G, Propper A, Kastner A, Michel G, Vallès-Villarreal N, *et al.* 2004, Adhesion and proliferation of cells on new polymers modified biomaterials, *Bioelectrochemistry*, **62**: 19–27.
203. Landa N, Miller L, Feinberg MS, Holbova R, Shachar M, Freeman I, *et al.* 2008, Effect of injectable alginate implant on cardiac remodeling and function after recent and old infarcts in rat, *Circulation*, **117**: 1388–1396.
204. Landers R, Hübner U, Schmelzeisen R, Mülhaupt R. 2002, Rapid prototyping of scaffolds derived from thermoreversible hydrogels and tailored for applications in tissue engineering, *Biomaterials*, **23**: 4437–4447.
205. Landers R, Pfister A, John H. 2002, Fabrication of soft tissue engineering scaffolds by means of rapid prototyping techniques, *J Mat Sci*, **7**: 3107–3116.
206. Lee KY, Bouhadir KH, Mooney DJ. 2000, Degradation Behavior of Covalently Cross-Linked Poly(aldehyde guluronate) Hydrogels, *Macromolecules*, **33**: 97–101.
207. Lee W, Lee VK, Polio S, Fischer K, Lee JH, Park JK, *et al.* 2009, Three-dimensional cell-hydrogel printer using electromechanical microvalve for tissue engineering. In: *TRANSDUCERS 2009 - 2009 International Solid-State Sensors, Actuators and Microsystems Conference*, IEEE: Denver, CO, USA, pp 2230–2233.
208. Lee JY, Lee JW, Schmidt CE. 2009, Neuroactive conducting scaffolds: nerve growth factor conjugation on active ester-functionalized polypyrrole, *J R Soc Interface*, **6**: 801–810.
209. Lee SH, Moon JJ, West JL. 2008, Three-dimensional micropatterning of bioactive hydrogels via two-photon laser scanning photolithography for guided 3D cell migration, *Biomaterials*, **29**: 2962–2968.
210. Lee WR, Park JH, Kim KH, Kim SJ, Park DH, Chae MH, *et al.* 2009, The biological effects of topical alginate treatment in an animal model of skin wound healing, *Wound repair Regen*, **17**: 505–510.
211. Lee W, Pinckney J, Lee V, Lee JH, Fischer K, Polio S, *et al.* 2009, Three-dimensional bioprinting of rat embryonic neural cells, *Neuroreport*, **20**: 798–803.
212. Lee YB, Polio S, Lee W, Dai G, Menon L, Carroll RS, *et al.* 2010, Bio-printing of collagen and VEGF-releasing fibrin gel scaffolds for neural stem cell culture, *Exp Neurol*, **223**: 645–652.
213. Lee KY, Rowley JA, Eiselt P, Moy EM, Bouhadir KH, Mooney DJ. 2000, Controlling Mechanical and Swelling Properties of Alginate Hydrogels Independently by Cross-Linker Type and Cross-Linking Density, *Macromolecules*, **33**: 4291–4294.
214. Levett PA, Melchels FPW, Schrobback K, Hutmacher DW, Malda J, Klein TJ. 2014, A biomimetic extracellular matrix for cartilage tissue engineering centered on photocurable gelatin, hyaluronic acid and chondroitin sulfate, *Acta Biomater*, **10**: 214–223.
215. Li X, Dancausse H, Grijalva I, Oliveira M, Levi ADO. 2003, Labeling Schwann cells with CFSE—an in vitro and in vivo study, *J Neurosci Methods*, **125**: 83–91.
216. Li Y, Field PM, Raisman G. 1997, Repair of adult rat corticospinal tract by transplants of olfactory ensheathing cells, *Science*, **277**: 2000–2002.

217. Li MG, Tian XY, Chen XB. 2009, A brief review of dispensing-based rapid prototyping techniques in tissue scaffold fabrication: role of modeling on scaffold properties prediction, *Biofabrication*, **1**: 032001.
218. Li M, Tian X, Zhu N, Schreyer DJ, Chen X. 2010, Modeling process-induced cell damage in the biodispensing process, *Tissue Eng Part C Methods*, **16**: 533–542.
219. Li S, Yan Y, Xiong Z, Weng C, Zhang R. 2009, Gradient Hydrogel Construct Based on an Improved Cell Assembling System, *J Bioact Compat Polym*, **24**: 84–99.
220. Li M, Zhang P, Guo W, Li H, Gu X, Yao D. 2014, Protein expression profiling during wallerian degeneration after rat sciatic nerve injury, *Muscle Nerve*, **50**: 73–78.
221. Lietz M, Dreesmann L, Hoss M, Oberhoffner S, Schlosshauer B. 2006, Neuro tissue engineering of glial nerve guides and the impact of different cell types, *Biomaterials*, **27**: 1425–1436.
222. Lim F, Sun AM. 1980, Microencapsulated islets as bioartificial endocrine pancreas., *Science*, **210**: 908–910.
223. Lindenhayn K, Perka C, Spitzer R, Heilmann H, Pommerening K, Mennicke J, *et al.* 1999, Retention of hyaluronic acid in alginate beads: aspects for in vitro cartilage engineering, *J Biomed Mater Res*, **44**: 149–155.
224. Liu VA, Bhatia SN. 2002, Three-Dimensional Photopatterning of Hydrogels Containing Living Cells, *Biomed Microdevices*, **4**: 257–266.
225. Liu WQ, Martinez J, Durand J, Wildering W, Zochodne DW. 2009, RGD-mediated adhesive interactions are important for peripheral axon outgrowth in vivo, *Neurobiol Dis*, **34**: 11–22.
226. Liu CZ, Xia ZD, Han ZW, Hulley PA, Triffitt JT, Czernuszka JT. 2008, Novel 3D collagen scaffolds fabricated by indirect printing technique for tissue engineering, *J Biomed Mater Res B Appl Biomater*, **85**: 519–528.
227. Livnat N, Sarig-Nadir O, Seliktar D, Shoham S. 2009, Three-dimensional guidance of DRG neurite outgrowth using multi-photon photo-ablation, *2009 4th Int IEEE/EMBS Conf Neural Eng*, 116–119.
228. Lobsiger CS, Taylor V, Suter U. 2002, The early life of a Schwann cell, *Biol Chem*, **383**: 245–253.
229. Loebsack A, Greene K, Wyatt S, Culberson C, Austin C, Beiler R, *et al.* 2001, In vivo characterization of a porous hydrogel material for use as a tissue bulking agent, *J Biomed Mater Res*, **57**: 575–581.
230. Lorand L. 2006, Factor XIII: Structure, Activation, and Interactions with Fibrinogen and Fibrin, *Ann N Y Acad Sci*, **936**: 291–311.
231. Lu MC, Ho CY, Hsu SF, Lee HC, Lin JH, Yao CH, *et al.* 2011, Effects of electrical stimulation at different frequencies on regeneration of transected peripheral nerve, *Neurorehabil Neural Repair*, **22**: 367–373.
232. Lund LM, Machado VM, McQuarrie IG. 2002, Increased beta-actin and tubulin polymerization in regrowing axons: relationship to the conditioning lesion effect, *Exp Neurol*, **178**: 306–312.
233. Luo Y, Wu C, Lode A, Gelinsky M. 2013, Hierarchical mesoporous bioactive glass/alginate composite scaffolds fabricated by three-dimensional plotting for bone tissue engineering, *Biofabrication*, **5**: 015005.
234. Ma S, Peng C, Wu S, Wu D, Gao C. 2013, Sciatic nerve regeneration using a nerve growth factor-containing fibrin glue membrane, *Neural Regen Res*, **8**: 3416–3422.

235. Mackinnon SE, Doolabh VB, Novak CB, Trulock EP. 2001, Clinical outcome following nerve allograft transplantation, *Plast Reconstr Surg*, **107**: 1419–1429.
236. Maher PS, Keatch RP, Donnelly K, Mackay RE, Paxton JZ. 2009, Construction of 3D biological matrices using rapid prototyping technology, *Rapid Prototyp J*, **15**: 204–210.
237. Maher PS, Keatch RP, Donnelly K, Paxton JZ. 2009, Formed 3D Bio-Scaffolds via Rapid Prototyping Technology. In: Vander Sloten J, Verdonck P, Nyssen M, Haueisen J (eds) *4th European Conference of the International Federation for Medical and Biological Engineering*, IFMBE Proceedings. Springer Berlin Heidelberg: Berlin, Heidelberg Vol 22, pp 2200–2204.
238. Malda J, Visser J, Melchels FP, Jüngst T, Hennink WE, Dhert WJA, *et al.* 2013, 25th anniversary article: Engineering hydrogels for biofabrication, *Adv Mater*, **25**: 5011–5028.
239. Malinda KM, Kleinman HK. 1996, The laminins, *Int J Biochem Cell Biol*, **28**: 957–959.
240. Manning GS. 1972, Polyelectrolytes, *Annu Rev Phys Chem*, **23**: 117–140.
241. Marga F, Jakab K, Khatiwala C, Shephard B, Dorfman S, Forgacs G. 2012, Organ Printing: A Novel Tissue Engineering Paradigm. In: Jobbágy Á (ed) *5th European Conference of the International Federation for Medical and Biological Engineering*, IFMBE Proceedings. Springer Berlin Heidelberg Vol 37, pp 27–30.
242. Marga F, Jakab K, Khatiwala C, Shepherd B, Dorfman S, Hubbard B, *et al.* 2012, Toward engineering functional organ modules by additive manufacturing, *Biofabrication*, **4**: 22001.
243. Martini R, Xin Y, Schmitz B, Schachner M. 1992, The L2/HNK-1 Carbohydrate Epitope is Involved in the Preferential Outgrowth of Motor Neurons on Ventral Roots and Motor Nerves, *Eur J Neurosci*, **4**: 628–639.
244. Martins RS, Siqueira MG, Da Silva CF, Plese JPP. 2005, Overall assessment of regeneration in peripheral nerve lesion repair using fibrin glue, suture, or a combination of the 2 techniques in a rat model. Which is the ideal choice?, *Surg Neurol*, **64**: S10–S16.
245. Massia SP, Rao SS, Hubbell JA. 1993, Covalently immobilized laminin peptide Tyr-Ile-Gly-Ser-Arg (YIGSR) supports cell spreading and co-localization of the 67-kilodalton laminin receptor with alpha-actinin and vinculin., *J Biol Chem*, **268**: 8053–8059.
246. Matsumoto T, Sasaki JI, Alsberg E, Egusa H, Yatani H, Sohmura T. 2007, Three-Dimensional Cell and Tissue Patterning in a Strained Fibrin Gel System, *PLoS One*, **2**: e1211.
247. Matsuyama T, Mackay M, Midha R. 2000, Peripheral nerve repair and grafting techniques: a review, *Neurol Med Chir (Tokyo)*, **40**: 187–199.
248. Maysinger D, Krieglstein K, Filipovic-Grcic J, Sendtner M, Unsicker K, Richardson P. 1996, Microencapsulated ciliary neurotrophic factor: physical properties and biological activities, *Exp Neurol*, **138**: 177–188.
249. McConnell GC, Rees HD, Levey AI, Gutekunst CA, Gross RE, Bellamkonda RV. 2009, Implanted neural electrodes cause chronic, local inflammation that is correlated with local neurodegeneration, *J Neural Eng*, **6**: 056003.
250. McKay HA, Wiberg M, Terenghi G. 2003, Exogenous leukaemia inhibitory factor enhances nerve regeneration after late secondary repair using a bioartificial nerve conduit, *Br J Plast Surg*, **56**: 444–450.
251. McKeon KD, Lewis A, Freeman JW. 2010, Electrospun poly(D,L-lactide) and polyaniline scaffold characterization, *J Appl Polym Sci*, **115**: 1566–1572.
252. McQuarrie IG. 1985, Effect of conditioning lesion on axonal sprout formation at nodes of Ranvier, *J Comp Neurol*, **231**: 239–249.

253. Mecham RP. 1991a, Laminin receptors, *Annu Rev Cell Biol*, **7**: 71–91.
254. Mecham RP. 1991b, Receptors for laminin on mammalian cells, *FASEB J*, **5**: 2538–2546.
255. Meiners S, Mercado MLT. 2003, Functional peptide sequences derived from extracellular matrix glycoproteins and their receptors: strategies to improve neuronal regeneration, *Mol Neurobiol*, **27**: 177–196.
256. Mendonça AC, Barbieri CH, Mazzer N. 2003, Directly applied low intensity direct electric current enhances peripheral nerve regeneration in rats, *J Neurosci Methods*, **129**: 183–190.
257. Midha R. 2004, Nerve transfers for severe brachial plexus injuries: a review, *Neurosurg Focus*, **16**: E5.
258. Midha R, Munro CA, Dalton PD, Tator CH, Shoichet MS. 2003, Growth factor enhancement of peripheral nerve regeneration through a novel synthetic hydrogel tube, *J Neurosurg*, **99**: 555–65.
259. Milligan ED, Hinde JL, Mehmert KK, Maier SF, Watkins LR. 1999, A method for increasing the viability of the external portion of lumbar catheters placed in the spinal subarachnoid space of rats, *J Neurosci Methods*, **90**: 81–86.
260. Mironov V, Visconti RP, Kasyanov V, Forgacs G, Drake CJ, Markwald RR. 2009, Organ printing: tissue spheroids as building blocks, *Biomaterials*, **30**: 2164–2174.
261. Mogil JS. 2009, Animal models of pain: progress and challenges, *Nat Rev Neurosci*, **10**: 283–294.
262. Mohamed S, Salleh AB. 1982, Physical properties of polyethyleneimine-alginate gels, *Biotechnol Lett*, **4**: 611–614.
263. Monacelli G, Spagnoli AM, Valesini L, Rizzo MI, Pardi M, Irace S. 2007, Surgical treatment of painful amputation neuromas with hyaluronic acid gel. Preliminary study of six patients, *G Chir*, **28**: 25–28.
264. Monte-Raso VV, Barbieri CH, Mazzer N, Yamasita AC, Barbieri G. 2008, Is the Sciatic Functional Index always reliable and reproducible?, *J Neurosci Methods*, **170**: 255–261.
265. Moore AM, MacEwan M, Santosa KB, Chenard KE, Ray WZ, Hunter DA, *et al.* 2011, Acellular nerve allografts in peripheral nerve regeneration: a comparative study, *Muscle Nerve*, **44**: 221–234.
266. Moore K, MacSween M, Shoichet M. 2006, Immobilized concentration gradients of neurotrophic factors guide neurite outgrowth of primary neurons in macroporous scaffolds, *Tissue Eng*, **12**: 267–278.
267. Morimoto K, Nishikawa M, Kawakami S, Nakano T, Hattori Y, Fumoto S, *et al.* 2003, Molecular weight-dependent gene transfection activity of unmodified and galactosylated polyethyleneimine on hepatoma cells and mouse liver, *Mol Ther*, **7**: 254–261.
268. Mosahebi A, Fuller P, Wiberg M, Terenghi G. 2002, Effect of allogeneic Schwann cell transplantation on peripheral nerve regeneration, *Exp Neurol*, **173**: 213–223.
269. Mosahebi A, Simon M, Wiberg M, Terenghi G. 2001, A novel use of alginate hydrogel as Schwann cell matrix, *Tissue Eng*, **7**: 525–534.
270. Mosahebi A, Wiberg M, Terenghi G. 2003, Addition of fibronectin to alginate matrix improves peripheral nerve regeneration in tissue-engineered conduits, *Tissue Eng*, **9**: 209–218.
271. Mosahebi A, Woodward B, Green C, Martin R, Terenghi G. 2000, Long-term effect of vital labelling on mixed Schwann cell cultures, *Histochem J*, **32**: 337–343.
272. Mumper RJ, Huffman AS, Puolakkainen PA, Bouchard LS, Gombotz WR. 1994, Calcium-alginate beads for the oral delivery of transforming growth factor-β1: stabilization of TGF-

β1 by the addition of polyacrylic acid within acid-treated beads, *J Control Release*, **30**: 241–251.
273. Murovic JA. 2009, Upper-extremity peripheral nerve injuries: a Louisiana State University Health Sciences Center literature review with comparison of the operative outcomes of 1837 Louisiana State University Health Sciences Center median, radial, and ulnar nerve lesions, *Neurosurgery*, **65**: A11-17.
274. Murphy SV, Skardal A, Atala A. 2013, Evaluation of hydrogels for bio-printing applications, *J Biomed Mater Res A*, **101**: 272–284.
275. Nadeau JR, Wilson-Gerwing TD, Verge VMK. 2014, Induction of a reactive state in perineuronal satellite glial cells akin to that produced by nerve injury is linked to the level of p75NTR expression in adult sensory neurons, *Glia*, **62**: 763–777.
276. Nadim W, Anderson PN, Turmaine M. 1990, The role of Schwann cells and basal lamina tubes in the regeneration of axons through long lengths of freeze-killed nerve grafts, *Neuropathol Appl Neurobiol*, **16**: 411–421.
277. Nair K, Gandhi M, Khalil S, Yan KC, Marcolongo M, Barbee K, *et al.* 2009, Characterization of cell viability during bioprinting processes, *Biotechnol J*, **4**: 1168–1177.
278. Narakas AO, Hentz VR. 1988, Neurotization in brachial plexus injuries. Indication and results, *Clin Orthop Relat Res*, **237**: 43–56.
279. Nath RK, Mackinnon SE, Shenaq SM. 1997, New nerve transfers following peripheral nerve injuries, *Oper Tech Plast Reconstr Surg*, **4**: 2–11.
280. Neu M, Fischer D, Kissel T. 2005, Recent advances in rational gene transfer vector design based on poly(ethyleneimine) and its derivatives, *J Gene Med*, **7**: 992–1009.
281. Nguyen QT, Sanes JR, Lichtman JW. 2002, Pre-existing pathways promote precise projection patterns, *Nat Neurosci*, **5**: 861–867.
282. Nicodemus GD, Bryant SJ. 2008, Cell encapsulation in biodegradable hydrogels for tissue engineering applications, *Tissue Eng Part B Rev*, **14**: 149–165.
283. Nicosia RF, Nicosia SV, Smith M 1994, Vascular endothelial growth factor, platelet-derived growth factor, and insulin-like growth factor-1 promote rat aortic angiogenesis in vitro, *Am J Pathol*, **145**: 1023–1029.
284. Nikkhah M, Eshak N, Zorlutuna P, Annabi N, Castello M, Kim K, *et al.* 2012, Directed endothelial cell morphogenesis in micropatterned gelatin methacrylate hydrogels, *Biomaterials*, **33**: 9009–9018.
285. Nitz AJ, Dobner JJ, Kersey D. 1985, Nerve injury and Grades II and III ankle sprains, *Am J Sports Med*, **13**: 177–182.
286. Noble J, Munro CA, Prasad VS, Midha R. 1998, Analysis of upper and lower extremity peripheral nerve injuries in a population of patients with multiple injuries, *J Trauma*, **45**: 116–122.
287. Novikova LN, Mosahebi A, Wiberg M, Terenghi G, Kellerth J-O, Novikov LN. 2006, Alginate hydrogel and matrigel as potential cell carriers for neurotransplantation, *J Biomed Mater Res A*, **77**: 242–252.
288. Nukada H. 1988, Post-traumatic endoneurial neovascularization and nerve regeneration : a morphometric study, **49**: 89–96.
289. Nukada H, Dyck PJ. 1984, Microsphere embolization of nerve capillaries and fiber degeneration, *Am J Pathol*, **115**: 275–287.

290. Oerther S, Le Gall H, Payan E, Lapicque F, Presle N, Hubert P, *et al.* 1999, Hyaluronate-alginate gel as a novel biomaterial: mechanical properties and formation mechanism, *Biotechnol Bioeng*, **63**: 206–215.
291. Oerther S, Maurin AC, Payan E, Hubert P, Lapicque F, Presle N, *et al.* 2000, High interaction alginate-hyaluronate associations by hyaluronate deacetylation for the preparation of efficient biomaterials, *Biopolymers*, **54**: 273–281.
292. Ogata K, Naito M. 1986, Blood flow of peripheral nerve effects of dissection, stretching and compression, *J Hand Surg Am*, **11**: 10–14.
293. Orita S, Henry K, Mantuano E, Yamauchi K, De Corato A, Ishikawa T, *et al.* 2013, Schwann cell LRP1 regulates remak bundle ultrastructure and axonal interactions to prevent neuropathic pain, *J Neurosci*, **33**: 5590–5602.
294. Ortigüela ME, Wood MB, Cahill DR. 1987, Anatomy of the sural nerve complex, *J Hand Surg Am*, **12**: 1119–1123.
295. Otero TF, Cortés MT. 2003, A sensing muscle, *Sensors Actuators B Chem*, **96**: 152–156.
296. Othon CM, Wu X, Anders JJ, Ringeisen BR. 2008, Single-cell printing to form three-dimensional lines of olfactory ensheathing cells, *Biomed Mater*, **3**: 034101.
297. Owens CM, Marga F, Forgacs G, Heesch CM. 2013, Biofabrication and testing of a fully cellular nerve graft, *Biofabrication*, **5**: 45007.
298. Ozbolat IT, Yu Y. 2013, Bioprinting toward organ fabrication: challenges and future trends, *IEEE Trans Biomed Eng*, **60**: 691–699.
299. Ozgenel GY. 2003, Effects of hyaluronic acid on peripheral nerve scarring and regeneration in rats, *Microsurgery*, **23**: 575–581.
300. Pabari A, Lloyd-Hughes H, Seifalian AM, Mosahebi A. 2014, Nerve conduits for peripheral nerve surgery, *Plast Reconstr Surg*, **133**: 1420–1430.
301. Pannunzio ME, Jou I, Long A, Wind TC, Beck G, Balian G. 2005, A new method of selecting Schwann cells from adult mouse sciatic nerve, *J Neurosci Methods*, **149**: 74–81.
302. Papavasiliou G, Cheng M-H, Brey EM. 2010, Strategies for vascularization of polymer scaffolds., *J Investig Med*, **58**: 838–844.
303. Parish CR. 1999, Fluorescent dyes for lymphocyte migration and proliferation studies., *Immunol Cell Biol*, **77**: 499–508.
304. Park EC, Jou I, Gwag BJ. 1998, Nerve growth factor potentiates the oxidative necrosis of striatal cholinergic neurons, *Neuroreport*, **9**: 687–690.
305. Park S, Kim G, Jeon YC, Koh Y, Kim W. 2009, 3D polycaprolactone scaffolds with controlled pore structure using a rapid prototyping system, *J Mater Sci Mater Med*, **20**: 229–234.
306. Patnaik S, Aggarwal A, Nimesh S, Goel A, Ganguli M, Saini N, *et al.* 2006, PEI-alginate nanocomposites as efficient in vitro gene transfection agents, *J Control Release*, **114**: 398–409.
307. Pattison ST, Melrose J, Ghosh P, Taylor TK. 2001, Regulation of gelatinase-A (MMP-2) production by ovine intervertebral disc nucleus pulposus cells grown in alginate bead culture by Transforming Growth Factor-beta(1) and insulin like growth factor-I, *Cell Biol Int*, **25**: 679–689.
308. Paves H, Saarma M. 1997, Neurotrophins as in vitro growth cone guidance molecules for embryonic sensory neurons, *Cell Tissue Res*, **290**: 285–297.
309. Pellitteri R, Russo A, Stanzani S. 2006, Schwann cell: a source of neurotrophic activity on cortical glutamatergic neurons in culture, *Brain Res*, **1069**: 139–144.

310. Peltola SM, Melchels FPW, Grijpma DW, Kellomäki M. 2008, A review of rapid prototyping techniques for tissue engineering purposes, *Ann Med*, **40**: 268–280.
311. Penkert G, Bini W, Samii M. 1988, Revascularization of nerve grafts: an experimental study, *J Reconstr Microsurg*, **4**: 319–325.
312. Perry VH, Brown MC, Gordon S. 1987, The macrophage response to central and peripheral nerve injury. A possible role for macrophages in regeneration, *J Exp Med*, **165**: 1218–1223.
313. Pettingill LN, Minter RL, Shepherd RK. 2008, Schwann cells genetically modified to express neurotrophins promote spiral ganglion neuron survival *in vitro*, *Neuroscience*, **152**: 821–828.
314. Pfister LA, Alther E, Papaloizos M, Merkle HP, Gander B. 2008, Controlled nerve growth factor release from multi-ply alginate/chitosan-based nerve conduits, *Eur J Pharm Biopharm*, **69**: 563–572.
315. Pfister A, Landers R, Laib A, Hubner U, Schmelzeisen R, Mulhaupt R. 2004, Biofunctional rapid prototyping for tissue-engineering applications: 3D bioplotting versus 3D printing, *J Polym Sci Part A Polym Chem*, **42**: 624–638.
316. Philipp B, Dautzenberg H, Linow KJ, Kötz J, Dawydoff W. 1989, Polyelectrolyte complexes - recent developments and open problems, *Prog Polym Sci*, **14**: 91–172.
317. Piotrowicz A, Shoichet MS. 2006, Nerve guidance channels as drug delivery vehicles, *Biomaterials*, **27**: 2018–2027.
318. Podhajsky RJ, Myers RR. 1993, The vascular response to nerve crush: relationship to Wallerian degeneration and regeneration, *Brain Res*, **623**: 117–123.
319. Potts JR, Campbell ID. 1996, Structure and function of fibronectin modules, *Matrix Biol*, **15**: 313–320.
320. Quan D, Bird SJ. 1999, Nerve conduction studies and electromyography in the evaluation of peripheral nerve injuries, *Univ Pennsylvania Orthop J*, **12**: 45–51.
321. Radtke C, Aizer A, Agulian SK, Lankford KL, Vogt PM, Kocsis JD. 2009, Transplantation of olfactory ensheathing cells enhances peripheral nerve regeneration after microsurgical nerve repair, *Brain Res*, **1254**: 10–17.
322. Rajaram A, Schreyer D, Chen D. 2014, Bioplotting Alginate/Hyaluronic Acid Hydrogel Scaffolds with Structural Integrity and Preserved Schwann Cell Viability, *3D Print Addit Manuf*, **1**: 194–203.
323. Rajnicek AM, Robinson KR, McCaig CD. 1998, The direction of neurite growth in a weak DC electric field depends on the substratum: contributions of adhesivity and net surface charge, *Dev Biol*, **203**: 412–423.
324. Ramón-Cueto A, Avila J. 1998, Olfactory ensheathing glia: properties and function, *Brain Res Bull*, **46**: 175–187.
325. Ramón-Cueto A, Plant GW, Avila J, Bunge MB 1998, Long-distance axonal regeneration in the transected adult rat spinal cord is promoted by olfactory ensheathing glia transplants, *J Neurosci*, **18**: 3803–3815.
326. Raof NA, Schiele NR, Xie Y, Chrisey DB, Corr DT. 2011, The maintenance of pluripotency following laser direct-write of mouse embryonic stem cells, *Biomaterials*, **32**: 1802–1808.
327. Raps SP, Lai JCK, Hertz L, Cooper AJL. 1989, Glutathione is present in high concentrations in cultured astrocytes but not in cultured neurons, *Brain Res*, **493**: 398–401.

328. Ravichandran R, Sundarrajan S, Venugopal JR, Mukherjee S, Ramakrishna S. 2010, Applications of conducting polymers and their issues in biomedical engineering, *J R Soc Interface*, **7 Suppl 5**: S559–S579.
329. Ribeiro-Resende VT, Koenig B, Nichterwitz S, Oberhoffner S, Schlosshauer B. 2009, Strategies for inducing the formation of bands of Büngner in peripheral nerve regeneration, *Biomaterials*, **30**: 5251–5259.
330. Ringeisen BR, Othon CM, Wu X, Krizman DB, Darfler MM, Anders JJ, *et al.* 2010, *Cell and Organ Printing* (BR Ringeisen, BJ Spargo, and PK Wu, Eds.). Springer Netherlands: Dordrecht.
331. Rizzo M, Bayo J, Piccioni F, Malvicini M, Fiore E, Peixoto E, *et al.* 2014, Low molecular weight hyaluronan-pulsed human dendritic cells showed increased migration capacity and induced resistance to tumor chemoattraction, *PLoS One*, **9**: e107944.
332. Robinson LR. 2000, Traumatic injury to peripheral nerves, *Muscle Nerve*, **23**: 863–873.
333. Robinson GA, Madison RD. 2004, Motor neurons can preferentially reinnervate cutaneous pathways, *Exp Neurol*, **190**: 407–413.
334. Rodríguez FJ, Verdú E, Ceballos D, Navarro X. 2000, Nerve guides seeded with autologous schwann cells improve nerve regeneration, *Exp Neurol*, **161**: 571–584.
335. Rogério F, de Souza Queiroz L, Teixeira S, Oliveira AL, de Nucci G, Langone F. 2002, Neuroprotective action of melatonin on neonatal rat motoneurons after sciatic nerve transection, *Brain Res*, **926**: 33–41.
336. Roth EA, Xu T, Das M, Gregory C, Hickman JJ, Boland T. 2004, Inkjet printing for high-throughput cell patterning, *Biomaterials*, **25**: 3707–3715.
337. Rowley JA, Madlambayan G, Mooney DJ. 1999, Alginate hydrogels as synthetic extracellular matrix materials, *Biomaterials*, **20**: 45–53.
338. Rowshan K, Jones NF, Gupta R. 2004, Current surgical techniques of peripheral nerve repair, *Oper Tech Orthop*, **14**: 163–170.
339. De Ruiter GCW, Malessy MJA, Yaszemski MJ, Windebank AJ, Spinner RJ. 2009, Designing ideal conduits for peripheral nerve repair, *Neurosurg Focus*, **26**: E5.
340. De Ruiter GCW, Spinner RJ, Verhaagen J, Malessy MJA. 2014, Misdirection and guidance of regenerating axons after experimental nerve injury and repair, *J Neurosurg*, **120**: 493–501.
341. Sachlos E. 2003, Novel collagen scaffolds with predefined internal morphology made by solid freeform fabrication, *Biomaterials*, **24**: 1487–1497.
342. Saheb-Al-Zamani M, Yan Y, Farber SJ, Hunter DA, Newton P, Wood MD, *et al.* 2013, Limited regeneration in long acellular nerve allografts is associated with increased Schwann cell senescence, *Exp Neurol*, **247**: 165–177.
343. Sahiner N, Jha AK, Nguyen D, Jia X. 2008, Fabrication and characterization of cross-linkable hydrogel particles based on hyaluronic acid: potential application in vocal fold regeneration, *J Biomater Sci Polym Ed*, **19**: 223–243.
344. Sakiyama-Elbert SE, Hubbell JA. 2000, Controlled release of nerve growth factor from a heparin-containing fibrin-based cell ingrowth matrix, *J Control Release*, **69**: 149–158.
345. Salzer JL. 2012, Axonal regulation of Schwann cell ensheathment and myelination, *J Peripher Nerv Syst*, **17 Suppl 3**: 14–19.
346. Sanders FK. 1948, The Thickness of the Myelin Sheaths of Normal and Regenerating Peripheral Nerve Fibres, *Proc R Soc B Biol Sci*, **135**: 323–357.

347. Sang L, Luo D, Xu S, Wang X, Li X. 2011, Fabrication and evaluation of biomimetic scaffolds by using collagen–alginate fibrillar gels for potential tissue engineering applications, *Mater Sci Eng C*, **31**: 262–271.
348. Sarig-Nadir O, Livnat N, Zajdman R, Shoham S, Seliktar D. 2009, Laser photoablation of guidance microchannels into hydrogels directs cell growth in three dimensions, *Biophys J*, **96**: 4743–4752.
349. Saringer W, Nöbauer-Huhmann I, Knosp E. 2002, Cranioplasty with individual carbon fibre reinforced polymere (CFRP) medical grade implants based on CAD/CAM technique, *Acta Neurochir (Wien)*, **144**: 1193–1203.
350. Schade R, Weiss T, Berg A, Schnabelrauch M, Liefeith K. 2010, Two-photon techniques in tissue engineering, *Int J Artif Organs*, **33**: 219–227.
351. Schmalenberg KE, Uhrich KE. 2005, Micropatterned polymer substrates control alignment of proliferating Schwann cells to direct neuronal regeneration, *Biomaterials*, **26**: 1423–1430.
352. Schmidt CE, Shastri VR, Vacanti JP, Langer R. 1997, Stimulation of neurite outgrowth using an electrically conducting polymer, *Proc Natl Acad Sci U S A*, **94**: 8948–8953.
353. Schuurman W, Khristov V, Pot MW, van Weeren PR, Dhert WJ, Malda J. 2011, Bioprinting of hybrid tissue constructs with tailorable mechanical properties, *Biofabrication*, **3**: 021001.
354. Seddon HJ. 1943, Three types of nerve injury, *Brain*, **66**: 237–288.
355. Seggio AM, Narayanaswamy A, Roysam B, Thompson DM. 2010, Self-aligned Schwann cell monolayers demonstrate an inherent ability to direct neurite outgrowth, *J Neural Eng*, **7**: 046001.
356. Seidlits SK, Khaing ZZ, Petersen RR, Nickels JD, Vanscoy JE, Shear JB, *et al.* 2010, The effects of hyaluronic acid hydrogels with tunable mechanical properties on neural progenitor cell differentiation, *Biomaterials*, **31**: 3930–3940.
357. Seltzer Z, Tal M, Sharav Y. 1989, Autotomy behavior in rats following peripheral deafferentation is suppressed by daily injections of amitriptyline, diazepam and saline, *Pain*, **37**: 245–50.
358. Semmling B, Nagel S, Sternberg K, Weitschies W, Seidlitz A. 2013, Long-term stable hydrogels for biorelevant dissolution testing of drug-eluting stents, *J Pharm Technol Drug Res*, **2**: 19.
359. Setty CM, Sahoo SS, Sa B. 2005, Alginate-coated alginate-polyethyleneimine beads for prolonged release of furosemide in simulated intestinal fluid, *Drug Dev Ind Pharm*, **31**: 435–446.
360. Shen Y, Fan Y, Dai H, Fu Q, Hu W, Chen Z. 2007, Neuroprotective effect of carnosine on necrotic cell death in PC12 cells, *Neurosci Lett*, **414**: 145–149.
361. Shen Y, Mani S, Donovan SL, Schwob JE, Meiri KF. 2002, Growth-associated protein-43 is required for commissural axon guidance in the developing vertebrate nervous system, *J Neurosci*, **22**: 239–247.
362. Shen H, Shen ZL, Zhang PH, Chen NL, Wang YC, Zhang ZF, *et al.* 2010, Ciliary neurotrophic factor-coated polylactic-polyglycolic acid chitosan nerve conduit promotes peripheral nerve regeneration in canine tibial nerve defect repair, *J Biomed Mater Res B Appl Biomater*, **95**: 161–170.

363. Shimizu K, Fujita H, Nagamori E. 2009, Alignment of skeletal muscle myoblasts and myotubes using linear micropatterned surfaces ground with abrasives, *Biotechnol Bioeng*, **103**: 631–638.
364. Shteyer E, Ben Ya'acov A, Zolotaryova L, Sinai A, Lichtenstein Y, Pappo O, *et al.* 2014, Reduced liver cell death using an alginate scaffold bandage: A novel approach for liver reconstruction after extended partial hepatectomy, *Acta Biomater*, **10**: 3209–3216.
365. Siemionow M, Brzezicki G. 2009, Current techniques and concepts in peripheral nerve repair, *Int Rev Neurobiol*, **87**: 141–172.
366. Siemionow M, Sonmez E. 2007, Nerve allograft transplantation: a review, *J Reconstr Microsurg*, **23**: 511–520.
367. Sikorski P, Mo F, Skjak-Braek G, Stokke BT. 2007, Evidence for egg-box-compatible interactions in calcium-alginate gels from fiber X-ray diffraction, *Biomacromolecules*, **8**: 2098–2103.
368. Silva DS, Wallace DB, Cooley PW, Radulescu D, Hayes DJ. 2007, An InkJet Printing Station for Neuroregenerative Tissue Engineering, Engineering in Medicine and Biology Workshop, 2007 IEEE, Dallas, 71–73.
369. Sinis N, Schaller HE, Schulte-Eversum C, Schlosshauer B, Doser M, Dietz K, *et al.* 2005, Nerve regeneration across a 2-cm gap in the rat median nerve using a resorbable nerve conduit filled with Schwann cells, *J Neurosurg*, **103**: 1067–1076.
370. Skene JH. 1989, Axonal growth-associated proteins, *Annu Rev Neurosci*, **12**: 127–156.
371. Skene JH, Willard M. 1981, Axonally transported proteins associated with axon growth in rabbit central and peripheral nervous systems, *J Cell Biol*, **89**: 96–103.
372. Sketelj J, Bresjanac M, Popović M. 1989, Rapid growth of regenerating axons across the segments of sciatic nerve devoid of Schwann cells, *J Neurosci Res*, **24**: 153–162.
373. Smausz T, Hopp B, Kecskeméti G, Bor Z. 2006, Study on metal microparticle content of the material transferred with Absorbing Film Assisted Laser Induced Forward Transfer when using silver absorbing layer, *Appl Surf Sci*, **252**: 4738–4742.
374. Smidsrød O. 1973, The relative extension of alginates having different chemical composition, *Carbohydr Res*, **27**: 107–118.
375. Smidsrød O, Skjak-Braek G. 1990, Alginate as immobilization matrix for cells, *Trends Biotechnol*, **8**: 71–78.
376. Son YJ, Thompson WJ. 1995, Schwann cell processes guide regeneration of peripheral axons, *Neuron*, **14**: 125–132.
377. Son YJ, Yoon IS, Sung JH, Cho HJ, Chung SJ, Shim CK, *et al.* 2013, Porous hyaluronic acid/sodium alginate composite scaffolds for human adipose-derived stem cells delivery, *Int J Biol Macromol*, **61**: 175–181.
378. Song SJ, Choi J, Park YD, Hong S, Lee JJ, Ahn CB, *et al.* 2011, Sodium alginate hydrogel-based bioprinting using a novel multinozzle bioprinting system, *Artif Organs*, **35**: 1132–1136.
379. Staniforth P, Fisher TR. 1978, The effects of sural nerve excision in autogenous nerve grafting, *Hand*, **10**: 187–190.
380. Stevens MM, Qanadilo HF, Langer R, Prasad SV. 2004, A rapid-curing alginate gel system: utility in periosteum-derived cartilage tissue engineering, *Biomaterials*, **25**: 887–894.

381. Stoll G, Griffin JW, Li CY, Trapp BD. 1989, Wallerian degeneration in the peripheral nervous system: participation of both Schwann cells and macrophages in myelin degradation, *J Neurocytol*, **18**: 671–683.
382. Stoll G, Müller HW. 2006, Nerve Injury, Axonal Degeneration and Neural Regeneration: Basic Insights, *Brain Pathol*, **9**: 313–325.
383. Struzyna LA, Katiyar K, Cullen DK. 2014, Living scaffolds for neuroregeneration, *Curr Opin Solid State Mater Sci*, **18**: 308–318.
384. Sufan W, Suzuki Y, Tanihara M, Ohnishi K, Suzuki K, Endo K, *et al.* 2001, Sciatic nerve regeneration through alginate with tubulation or nontubulation repair in cat, *J Neurotrauma*, **18**: 329–338.
385. Sun HB, Kawata S. 2004, Two-Photon Photopolymerization and 3D Lithographic Microfabrication. In: *NMR, 3D Analysis, Photopolymerization*, Apvances in Polymer Science. Springer Berlin Heidelberg Vol 170, pp 169–273.
386. Sunderland S. 1978, *Nerves and Nerve Injuries*, Second ed. Churchill Livingstone: Edinburgh.
387. Suri S, Schmidt CE. 2010, Cell-laden hydrogel constructs of hyaluronic acid, collagen, and laminin for neural tissue engineering, *Tissue Eng Part A*, **16**: 1703–1716.
388. Suzuki Y, Tanihara M, Ohnishi K, Suzuki K, Endo K, Nishimura Y. 1999, Cat peripheral nerve regeneration across 50 mm gap repaired with a novel nerve guide composed of freeze-dried alginate gel, *Neurosci Lett*, **259**: 75–78.
389. Svensson WE, Amiras D. 2006, Ultrasound elasticity imaging, *Breast Cancer Online*, **9**: e24.
390. Szarek D. 2012, Influence of Alginates on Tube Nerve Grafts of Different Elasticity - Preliminary *in Vivo* Study, *J Biomater Nanobiotechnol*, **03**: 20–30.
391. Szynkaruk M, Kemp SWP, Wood MD, Gordon T, Borschel GH. 2013, Experimental and clinical evidence for use of decellularized nerve allografts in peripheral nerve gap reconstruction, *Tissue Eng Part B Rev*, **19**: 83–96.
392. Taniuchi M, Clark HB, Johnson EM. 1986, Induction of nerve growth factor receptor in Schwann cells after axotomy, *Proc Natl Acad Sci USA*, **83**: 4094–4098.
393. Tapia C, Escobar Z, Costa E, Sapag-Hagar J, Valenzuela F, Basualto C, *et al.* 2004, Comparative studies on polyelectrolyte complexes and mixtures of chitosan-alginate and chitosan-carrageenan as prolonged diltiazem clorhydrate release systems, *Eur J Pharm Biopharm*, **57**: 65–75.
394. Tashiro K, Sephel GC, Greatorex D, Sasaki M, Shirashi N, Martin GR, *et al.* 1991, The RGD containing site of the mouse laminin A chain is active for cell attachment, spreading, migration and neurite outgrowth, *J Cell Physiol*, **146**: 451–459.
395. Tashiro K, Sephel GC, Weeks B, Sasaki M, Martin GR, Kleinman HK, *et al.* 1989, A synthetic peptide containing the IKVAV sequence from the A chain of laminin mediates cell attachment, migration, and neurite outgrowth, *J Biol Chem*, **264**: 16174–16182.
396. Taylor CA, Braza D, Rice JB, Dillingham T. 2008, The incidence of peripheral nerve injury in extremity trauma., *Am J Phys Med Rehabil*, **87**: 381–385.
397. Teare GF, Horan PK, Slezak SE, Smith C, Hay JB. 1991, Long-term tracking of lymphocytes in vivo: the migration of PKH-labeled lymphocytes, *Cell Immunol*, **134**: 157–170.

398. Tesco G, Latorraca S, Piersanti P, Piacentini S, Amaducci L, Sorbi S. 1992, Protection from oxygen radical damage in human diploid fibroblasts by acetyl-L-carnitine, *Dement Geriatr Cogn Disord*, **3**: 58–60.
399. Thomas PK, Olsson Y. 1984, Microscopic anatomy and function of the connective tissue components of peripheral nerve. In: Dyck PJ, Thomas PK, Lambert EH, Bunge RP (eds) *Peripheral Neuropathy Vol I*, Saunders: Philadelphia/London/ Toronto, pp 97–120.
400. Thompson DM, Buettner HM. 2004, Oriented Schwann cell monolayers for directed neurite outgrowth, *Ann Biomed Eng*, **32**: 1120–1130.
401. Thompson DM, Buettner HM. 2006, Neurite outgrowth is directed by schwann cell alignment in the absence of other guidance cues, *Ann Biomed Eng*, **34**: 161–168.
402. Thu B, Smidsrød O, Skjak-Brӕk G. 1996, Alginate gels—Some structure-function correlations relevant to their use as immobilization matrix for cells. In: *Progress in Biotechnology*, Progress in Biotechnology. Elsevier Vol 11, pp 19–30.
403. Toke ER, Lorincz O, Somogyi E, Lisziewicz J. 2010, Rational development of a stable liquid formulation for nanomedicine products, *Int J Pharm*, **392**: 261–267.
404. Toole BP. 2004, Hyaluronan: from extracellular glue to pericellular cue, *Nat Rev Cancer*, **4**: 528–539.
405. Torigoe K, Tanaka HF, Takahashi A, Awaya A, Hashimoto K. 1996, Basic behavior of migratory Schwann cells in peripheral nerve regeneration, *Exp Neurol*, **137**: 301–308.
406. Vandenbossche GM, Remon JP. 1993, Influence of the sterilization process on alginate dispersions, *J Pharm Pharmacol*, **45**: 484–486.
407. Varejão ASP, Cabrita AM, Meek MF, Bulas-Cruz J, Filipe VM, Gabriel RC, *et al.* 2003, Ankle kinematics to evaluate functional recovery in crushed rat sciatic nerve, *Muscle Nerve*, **27**: 706–714.
408. Vasudevan S, Huang J, Botterman B, Matloub HS, Keefer E, Cheng J. 2014, Detergent-free Decellularized Nerve Grafts for Long-gap Peripheral Nerve Reconstruction, *Plast Reconstr Surgery Glob Open*, **2**: e201.
409. Verdu E, Navarro X, Gudino-Cabrera G, Rodriguez FJ, Ceballos D, Valero A, *et al.* 1999, Olfactory bulb ensheathing cells enhance peripheral nerve regeneration, *Neuroreport*, **10**: 1097–1101.
410. Vleggeert-Lankamp CL, Pêgo AP, Lakke EA, Deenen M, Marani E, Thomeer RT. 2004, Adhesion and proliferation of human Schwann cells on adhesive coatings, *Biomaterials*, **25**: 2741–2751.
411. Vu LT, Jain G, Veres BD, Rajagopalan P. 2015, Cell Migration on Planar and 3D Matrices: A Hydrogel-Based Perspective, *Tissue Eng Part B Rev*, **21**:67–74.
412. Waikakul S, Wongtragul S, Vanadurongwan V. 1999, Restoration of elbow flexion in brachial plexus avulsion injury: comparing spinal accessory nerve transfer with intercostal nerve transfer, *J Hand Surg Am*, **24**: 571–577.
413. Waitayawinyu T, Parisi DM, Miller B, Luria S, Morton HJ, Chin SH, *et al.* 2007, A comparison of polyglycolic acid versus type 1 collagen bioabsorbable nerve conduits in a rat model: an alternative to autografting, *J Hand Surg Am*, **32**: 1521–1529.
414. Wall PD, Devor M, Inbal R, Scadding JW, Schonfeld D, Seltzer Z, *et al.* 1979, Autotomy following peripheral nerve lesions: experimental anesthesia dolorosa, *Pain*, **7**: 103–113.
415. Wang XQ, Duan XM, Liu LH, Fang YQ, Tan Y. 2005, Carboxyfluorescein Diacetate Succinimidyl Ester Fluorescent Dye for Cell Labeling, *Acta Biochim Biophys Sin (Shanghai)*, **37**: 379–385.

416. Wang Y, Teng HL, Huang Z. 2012, Intrinsic Migratory Properties of Cultured Schwann Cells Based on Single-Cell Migration Assay, *PLoS One*, **7**: e51824.
417. Wang CC, Yang KC, Lin KH, Liu YL, Liu HC, Lin FH. 2012, Cartilage regeneration in SCID mice using a highly organized three-dimensional alginate scaffold, *Biomaterials*, **33**: 120–127.
418. Wang MD, Zhai P, Schreyer DJ, Zheng RS, Sun XD, Cui FZ, *et al.* 2013, Novel crosslinked alginate/hyaluronic acid hydrogels for nerve tissue engineering, *Front Mater Sci*, **7**: 269–284.
419. Weber RA, Proctor WH, Warner MR, Verheyden CN 1993, Autotomy and the sciatic functional index, *Microsurgery*, **14**: 323–327.
420. Wee SF, Gombotz WR, Fanslow WC. 1995, Evaluation of alginate microbeads for intranasal delivery of ovalbumin. In: *Proceedings of the Controlled Release Society*, pp 566–567.
421. Weisel JW. 2005, Fibrinogen and fibrin, *Adv Protein Chem*, **70**: 247–299.
422. Whitlock EL, Tuffaha SH, Luciano JP, Yan Y, Hunter DA, Magill CK, *et al.* 2009, Processed allografts and type I collagen conduits for repair of peripheral nerve gaps, *Muscle Nerve*, **39**: 787–799.
423. Whittlesey KJ, Shea LD. 2006, Nerve growth factor expression by PLG-mediated lipofection, *Biomaterials*, **27**: 2477–2486.
424. Wilkinson CD., Riehle M, Wood M, Gallagher J, Curtis AS. 2002, The use of materials patterned on a nano- and micro-metric scale in cellular engineering, *Mater Sci Eng C*, **19**: 263–269.
425. Williams LR. 1987, Exogenous fibrin matrix precursors stimulate the temporal progress of nerve regeneration within a silicone chamber, *Neurochem Res*, **12**: 851–860.
426. Willie BM, Petersen A, Schmidt-Bleek K, Cipitria A, Mehta M, Strube P, *et al.* 2010, Designing biomimetic scaffolds for bone regeneration: why aim for a copy of mature tissue properties if nature uses a different approach?, *Soft Matter*, **6**: 4976.
427. Wilson ADH, Hart A, Brännström T, Wiberg M, Terenghi G. 2007, Delayed acetyl-L-carnitine administration and its effect on sensory neuronal rescue after peripheral nerve injury, *J Plast Reconstr Aesthet Surg*, **60**: 114–118.
428. Winter JO, Schmidt CE. 2002, Biomimetic strategies and applications in the nervous system. In: Dillow AK, Lowman AM (eds) *Biomimetic Materials and Design: Biointerfacial Strategies, Tissue Engineering, and Targeted Drug Delivery*, Marcel Dekker: New York, NY, pp 375–415.
429. Witkowska E, Oriowska A, Izdebski J, Salwa J, Wietrzyk J, Opolski A. 2004, New analogues of laminin active fragment YIGSR: synthesis and biological activity *in vitro* and *in vivo*, *J Pept Sci*, **10**: 285–290.
430. Wittmer CR, Phelps JA, Saltzman WM, Van Tassel PR. 2007, Fibronectin terminated multilayer films: protein adsorption and cell attachment studies, *Biomaterials*, **28**: 851–860.
431. Won SJ, Park EC, Ryu BR, Ko HW, Sohn S, Kwon HJ, *et al.* 2000, NT-4/5 exacerbates free radical-induced neuronal necrosis in vitro and in vivo, *Neurobiol Dis*, **7**: 251–259.
432. Woodhoo A, Sahni V, Gilson J, Setzu A, Franklin RJM, Blakemore WF, *et al.* 2007, Schwann cell precursors: a favourable cell for myelin repair in the Central Nervous System, *Brain*, **130**: 2175–2185.

433. Wu PK, Ringeisen BR, Krizman DB, Frondoza CG, Brooks M, Bubb DM, *et al.* 2003, Laser transfer of biomaterials: Matrix-assisted pulsed laser evaporation (MAPLE) and MAPLE Direct Write, *Rev Sci Instrum*, **74**: 2546–2557.
434. Wu S, Suzuki Y, Tanihara M, Ohnishi K, Endo K, Nishimura Y. 2002, Repair of facial nerve with alginate sponge without suturing: an experimental study in cats., *Scand J Plast Reconstr Surg Hand Surg*, **36**: 135–140.
435. Xu T, Gregory CA, Molnar P, Cui X, Jalota S, Bhaduri SB, *et al.* 2006, Viability and electrophysiology of neural cell structures generated by the inkjet printing method, *Biomaterials*, **27**: 3580–3588.
436. Yamada Y, Hozumi K, Katagiri F, Kikkawa Y, Nomizu M. 2010, Biological activity of laminin peptide-conjugated alginate and chitosan matrices, *Biopolymers*, **94**: 711–720.
437. Yang F, Murugan R, Wang S, Ramakrishna S. 2005, Electrospinning of nano/micro scale poly(L-lactic acid) aligned fibers and their potential in neural tissue engineering, *Biomaterials*, **26**: 2603–2610.
438. Yao Y, Wang Y. 2013, ATDC5: an excellent in vitro model cell line for skeletal development, *J Cell Biochem*, **114**: 1223–1229.
439. Yeh CC, Lin YC, Tsai FJ, Huang CY, Yao CH, Chen YS. 2010, Timing of applying electrical stimulation is an important factor deciding the success rate and maturity of regenerating rat sciatic nerves, *Neurorehabil Neural Repair*, **24**: 730–735.
440. Yeo M, Kim G. 2014, Cell-printed hierarchical scaffolds consisting of micro-sized polycaprolactone (PCL) and electrospun PCL nanofibers/cell-laden alginate struts for tissue regeneration, *J Mater Chem B*, **2**: 314–324.
441. Yu X, Bellamkonda RV. 2003, Tissue-engineered scaffolds are effective alternatives to autografts for bridging peripheral nerve gaps, *Tissue Eng*, **9**: 421–430.
442. Yu TT, Shoichet MS. 2005, Guided cell adhesion and outgrowth in peptide-modified channels for neural tissue engineering, *Biomaterials*, **26**: 1507–1514.
443. Zeltser R, Beilin B-Z, Zaslansky R, Seltzer Z. 2000, Comparison of autotomy behavior induced in rats by various clinically-used neurectomy methods, *Pain*, **89**: 19–24.
444. Zhao Q, Qian J, An Q, Zhu M, Yin M, Sun Z. 2009, Poly(vinyl alcohol)/polyelectrolyte complex blend membrane for pervaporation dehydration of isopropanol, *J Memb Sci*, **343**: 53–61.
445. Zhu H, Ji J, Shen J. 2004, Construction of multilayer coating onto poly-(DL-lactide) to promote cytocompatibility, *Biomaterials*, **25**: 109–117.
446. Zhu N, Li MG, Guan YJ, Schreyer DJ, Chen XB. 2010, Effects of laminin blended with chitosan on axon guidance on patterned substrates, *Biofabrication*, **2**: 045002.
447. Zigmond SH. 1981, Consequences of chemotactic peptide receptor modulation for leukocyte orientation, *J Cell Biol*, **88**: 644–647.
448. Zor F, Deveci M, Kilic A, Ozdag MF, Kurt B, Sengezer M, *et al.* 2014, Effect of VEGF gene therapy and hyaluronic acid film sheath on peripheral nerve regeneration, *Microsurgery*, **34**: 209–216.
449. Zouani O, Chollet C, Lesage S, Chanseau C, Guillemot F, Durrieu M. 2009, RGD Peptides Grafting onto Polyethylene Terephthalate Surfaces by Biological Laser Printing. In: *2nd Chinese-European Symposium on Biomaterials in Regenerative Medicine*, Barcelona, Spain.